TECHNISCHE
UNIVERSITÄT
WIEN

VIENNA
UNIVERSITY OF
TECHNOLOGY

DISSERTATION

The Interaction of Bi Cluster Ions with Ionic Liquids

ausgeführt zum Zwecke der Erlangung des akademischen Grades eines
Doktors der technischen Wissenschaften unter der Leitung von

ao.Univ.-Prof. Dipl.-Ing. Dr.techn. Herbert Hutter

eingereicht an der Technischen Universität Wien
bei der Fakultät für Chemie

von

Dipl.-Ing. Markus Holzweber
Matrikelnummer: 9725888
Hießgasse 11/9
1030 Wien

Wien, im Dezember 2011

for my parents Elisabeth und Johann (†1991)

"To boldly go where no man has gone before"
JAMES T. KIRK

Abstract

Ionic liquids are currently in the focus of scientific research. Applications of ionic liquids can be found in numerous chemical domains like synthetic chemistry, electrochemical storage media, tribosystems, chemical analysis and many more. However, little is known on the intermolecular ion-ion interaction, mostly discussed in terms of polarity. This work presents a secondary ion mass spectrometric approach to the interactions of primary ions with ionic liquids. The capabilities of the new generation of the bismuth liquid metal ion gun (LMIG), emitting primary Bi-ion cluster Bi_{1-7}^+ and $Bi_{1,3,5,7}^{++}$, for the investigation of ionic liquids has been demonstrated by means of static time-of-flight secondary-ion-mass-sectrometry (ToF-SIMS). The influence of primary ion bombardment conditions on the emission of molecular secondary ions from ionic liquids is systematically carried out for the first time on liquid surfaces. The data were evaluated by calculating secondary ion yields (including the yield enhancement), damage cross section and ion formation efficieny upon variation of the size and charge of the primary particle. Furthermore, the static SIMS limit is investigated on a liquid organic-inorganic surface. The generally accepted donor-acceptor approach for solvent and ions in solution has been extended to ionic liquids. Therefore, ionic liquids are considered as cations solvated by anions and anions solvated by cations. The solvatochromic shift of metal-complex based indicators is used to calculate donor and acceptor numbers for ionic liquids, which are on the same scale as used for common solvents. The results indicate a new solvent system which is not comparable to conventional solvents. It has been successfully proven that donor-acceptor properties correlate with the mass spectrometric studies in this work.

Deutsche Kurzfassung

Die Anwendungen von ionischen Flüssigkeiten lassen sich in zahlreichen chemischen Bereichen wie synthetische Chemie, elektrochemische Speichermedien, Tribosystemen, chemische Analysen und viele mehr finden. Ionische Flüssigkeiten sind daher derzeit im Fokus der wissenschaftlichen Forschung. Jedoch ist wenig über die intermolekulare Ion-Ion Wechselwirkung bekannt, vor allem in Bezug auf Lösungsmittelpolarität. Die vorliegende Arbeit stellt einen massenspektrometrischen (SIMS) Ansatz vor, um die Wechselwirkungen von Primärionen mit ionischen Flüssigkeiten zu bestimmen. Mittels der neuen Generation der Flüssigmetall-Ionenkanonen (LMIG), welche Bi_{1-7}^{+} und $Bi_{1,3,5,7}^{++}$ Bi-Primärionencluster emittieren können, wurde die Untersuchung von ionischen Flüssigkeiten mit Hilfe der statischen Flugzeit-Sekundärionen-Massenspektrometrie (ToF-SIMS) durchgeführt. Der Einfluss der Bedingungen des primären Ionenbeschusses auf die Emission von molekularen Sekundärionen wurde systematisch an ionischen Flüssigkeiten und zum ersten Mal auf flüssigen Oberflächen durchgeführt. Die Daten wurden durch die Berechnung der Sekundärionenausbeuten (einschlieślich der Ausbeutensteigerung),des Schadensquerschnittes und der Ionenbildungseffizienz unter Variation der Gröse und Ladung der primären Partikel ausgewertet. Darüber hinaus wurde das statische SIMS-Limit auf flüssigen organischen-anorganischen Oberflächen untersucht. Der allgemein bekannte Donor-Akzeptor-Ansatz für Lösungsmittel und Ionen in Lösung wurde auf ionischer Flüssigkeiten ausgeweitet. Dafür werden ionische Flüssigkeiten als Kationen solvatisiert von Anionen und Anionen solvatisiert von Kationen betrachtet. Die solvatochrome Verschiebung von Metallkomplex-Indikatoren wurde verwendet, um Donor- und Akzeptorzahlen für ionische Flüssigkeiten zu berechnen. Die Ergebnisse deuten auf ein neues Lösungsmittelsystem hin, das nicht mit herkömmlichen Lösungsmitteln vergleichbar ist. Es konnte gezeigt werden, dass Donor-Akzeptor-Eigenschaften mit den massenspektrometrischen Untersuchungen korrelieren.

Acknowledgements

During my years at Vienna University of Technology, I have been helped and encouraged by a number people whom I would like to recognize.

I am very grateful to ao.Univ.-Prof. Dipl.-Ing. Dr.techn. Herbert Hutter for the opportunity to perform my PhD thesis in his research group. His patience with me at the beginning and the end of my graduate career and his support both in scientific as well as in private matters is truly appreciated. Especially the numerous hours we spent drinking a "drammie" and discussing on university policy, on World War II and its influence on the Austrian politics, and countless topics about life itself has strongly influenced my way thinking.

My thanks also go to the Head of the "Institute of Chemical Technologies and Analytics" Univ.-Prof. Dipl.-Ing. Dr.techn. Herbert Danninger who financially supported me during the PhD thesis by working on small side projects in steel analytics after the pristine project was canceled due to the global financial crisis.

I would also thank the group members Georg, Kathi, Silvia, Michi, Sabrina and Flo and the former group members Johnny, Stefan 1, Stefan 2, Klaus, Arno, Roman and Christoph of the workgroup "Physical Analysis" for fruitful discussions on SIMS and their friendship. Especially, I am deeply indepted to Christoph for his help and his encouraging words during the difficult beginning. My gratitude also goes to Till from the "Solid State Ionics and Electroceramics" group for thought-provoking impulses and discussion on "Ionic Liquids" and to Ernst from the "Bio and Polymer Analysis" group for his help in the interpretation of organic mass spectra and for proofreading of this thesis.

Thanks to my predecessors and my colleagues from the representative body for PhD studies at the Vienna University of Technology. In the past four years we could achieve better terms and conditions for the doctoral students. We had a lot of work and difficult negotiations but also a lot of fun. Thanks Andi, Ed, Chruss, Peter, Nici, Philipp, Edgar and David for the community service and memorable seminars and evening sessions in the

wirlpool or at the "Heurigen".

Special thanks to all my friends with which I boozed countless nights away till dawn during my PhD thesis.

Last but not least I want to thank my familiy which supported me on the home front and never stopped believing in me.

Contents

Chapter 1

Introduction

1.1 Time of Flight Secondary Ion Mass Spectrometry

The following description on the technique used meets the essence and is therefore resumed without significant alterations: *

"Secondary ion mass spectrometry (SIMS) [1] is a technique used in materials science and surface science to analyze the composition of surfaces and thin films by sputtering the surface of the specimen with a focused primary ion beam and collecting and analyzing ejected secondary ions. These secondary ions are measured with a mass spectrometer to determine the elemental, isotopic, or molecular composition of the surface. SIMS is the most sensitive surface analysis technique, being able to detect all elements present up to the ppb range.

Time-of-flight mass spectrometry (ToF-SIMS) [2] is a combination of the analytical technique SIMS with a special type of mass analyser in which ions mass-to-charge ratio is determined via a time measurement. Ions are accelerated by an electric field of known strength. This acceleration results in an ion having the same kinetic energy as any other ion that has the same charge. The velocity of the ion depends on the mass-to-charge ratio. The time that it subsequently takes for the charged species to reach a detector at

---

*taken from www.qwiki.com

1

a known distance is measured. This time will depend on the mass-to-charge ratio of the particle. From this time and the known experimental parameters one can find the mass-to-charge ratio of the ion." In the following a few basics on SIMS and ToF-SIMS shall be treated. Far a deeper understanding of the technique the reader is refered to [1, 2, 3] and to the SIMS proceedings volumes.

In principal the instrumentation for a SIMS experiment can be divided into three parts:

- Primary ion generation

- Secondary ion generation

- Mass analysis and detection

In the following sections the basic concepts behind the above mentioned parts will be highlighted.

1.2 Primary Ion Generation

The upcoming of commercially available cluster ion sources has led to a breaktrough in organic secondary ion mass spectrometry. Currently, SF_5, [4, 5] Au, [6] Bi, [7, 8] C_{60} [9, 10] and recently Ar-cluster [11, 12] guns are in use. however it has to be distiguished between analysis guns (e.g. Bi) and sputter guns (e.g. Ar-cluster). A remarkable property of a cluster ion source is due to an enhanced secondary ion yield [7, 13, 14, 15, 16] which is generally more pronounced for complex molecular ions than for smaller fragments. Especially the so called liquid metal ion guns (LMIG) are of importance due to a high brightness and can consequently be focused to a small area with high current density. [17] LMIGs allow also a fast switching between monoatomic and polyatomic primary ions (e.g. Bi_1^+, Bi_2^+, ..., Bi_7^+) and are therefore well suited for elemental and molecular surface analysis. This makes LMIG sources currently the workhorses for modern ToF-SIMS surface analysis.

1.2.1 Liquid Metal Ion Guns

The most commonly used ion sources for modern ToF-SIMS systems are the liquid metal ion guns. Due to favorable flow properties in liquid state, an outstanding beam stability and the low melting point Ga emitters [18] were the standard for ToF-SIMS analysis for several decades. With the knowledge of higher secondary ion yields for heavy primary ions and the need of better focusing abilities gold emitters were introduced as analysis guns. [6, 19] The capability to form also Au-cluster ions and therfore a large nonlinear yield enhancement upon changing to gold clusters proved to be very favorable for organic and imaging SIMS. [20, 21] The higher mass of bismuth, the relatively higher primary ion current and the ability to form even doubly charged cluster [7] ions replaced the gold emitters.
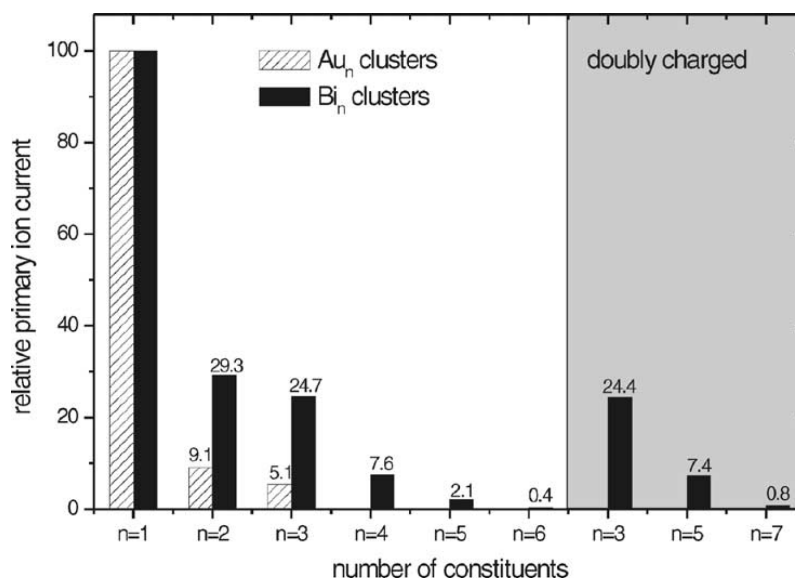
Figure 1.1: *Normalised primary ion currents for Au and Bi clusters as a function of cluster size and charge. Au and Bi_1^+ currents are normalised to 100%.*

Assembling of the Bi Liquid Metal Ion Gun

Figure 1.2 shows the principal design of the Bi-LMIG. It consists of a needle and a reservoir (filled with an Bi alloy) welded together and held on support

legs. These are connected to a power supply and serve also as electrical contact to provide an adjustable heating current. The emitter needle may thus be held at a temperature at which the bismuth remains molten and moistens the needle. If a high voltage between the needle tip and the extractor plate is applied, a sharp so called "Taylor-cone" of molten bismuth is formed. Following the formation of a Taylor-cone an emission can start and provides a constant flow of ions from the tip. These ions are guided trough an ion optical system to form the primary ion beam.

Figure 1.2: *The bismuth liquid metal ion gun.*

This ion source possess a very small virtual source and a high degree of angular intensity. This allows the LMIG to be accurately focused down to approx. 7 nm for a relatively high beam flow. [8] The Bi-LMIG pocesses several advantages:

- The ability to form cluster primary ions up to 7 Bi atoms in one cluster.

- The ability to emit singly and doubly charged primary ions and cluster ions (Bi_{1-7}^{+} and $Bi_{1,3,5,7}^{++}$).

- High primary ion currents compared to other LMIGs.

- High brightness and consequently a small focus with high current density and thus giving a high lateral resolution.

- High acquisition rates and measurement speed.

- High sensitivity and lateral resolution with cluster primary ions.

- Strong yield enhancements of secondary ions.

Mass Filter

The DC ion beam produced from a Bi-LMIG contains many different single charged (Bi_{1-7}^+) and double charged ($Bi_{1,3,5,7}^{++}$) cluster ion species. Newer LMIG emitters (G-TIP) also contain Mn^+ and Bi_nMn^+ cluster ions. To separate these different ions the LMIG column is equipped with an electro-dynamic mass filter consisting of two pulsing systems. The first one is the so-called pre-chopper the second one the chopper (see Figure 1.3)
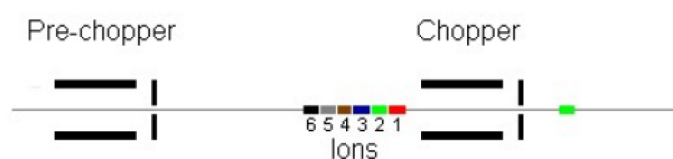
Figure 1.3: *Electrodynamic mass filter of the LMIG.*

During operation the pre-chopper is cutting a short ion package, containing all different ions, out of the DC ion beam. All ions have the same energy, but due to their difference in mass the ions become separated while they are travelling down the column. The second pulsing system (chopper) ensures that only one of the primary ion packages is transmitted. All other packages are blocked.[†]

Modes of Operation

The LMIG can be operated at several modes, depending mainly on the analytical question. For surface spectroscopy high mass resolution is usually required. The gun is the operated in the so called "high curren bunched mode". For surface imaging, where high lateral resolution is required, the gun is operated in the "burst alignment mode" or "collimated mode". However these two modes are at the expense of the mass resolution which is henceforth only nominal (unity mass resolution). A trade-off between mass resolution and lateral resolution is the "burst mode".[‡] [22] In this work, the high current bunched mode was mainly used, so the principle will be described briefly.

[†]From SurfaceLab 6 help file

[‡]See also SurfaceLab 6 help file

High Current Bunched Mode
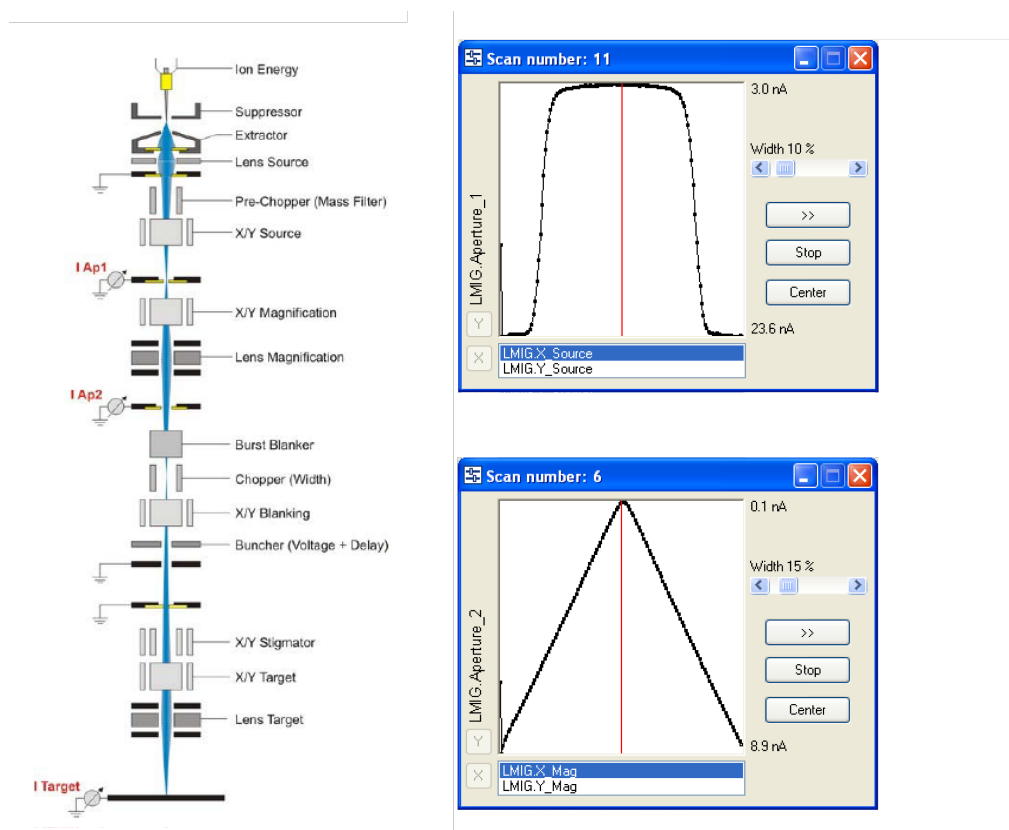
Figure 1.4: *Schematic illustration of the buncher. The enlargement shows the effect of the chromatic abberation on the beam focus*

The high current bunched mode has two crossovers inside in the ion beam path (Figure 1.4) and is mainly used for ultimate mass resolution, mass resolved spectra and depth profiles. A DC ion beam leaves the LMIG and passes the prechopper. The prechopper cuts out an ion package containing all ion and cluster ion species by deflecting the beam out of the center. For a clear blanking a crossover in aperture 1 is needed. The rectangular profile of the oscilloscope in aperture 1 is due to a smaller beam diameter than the aperture diameter, so the ion package is either guided completely trough the aperture or completely blanked out (Figure 1.4). The ion package then passes aperture 2 whose diameter is smaller than the beam diameter. The triangular shape is now due to the a high intensity in centreline which diminishesout of

the centreline (Figure 1.4). For a clear blanking of a particular ion cluster (e.g. Bi_3^+) a second crossover is needed in the chopper. For ultimate mass resolution the ion cluster package has to be bunched from a pulse width of 20-40 ns (depending on the ion cluster species) to a sub-nanometer pulse (0.5-1.2 ns, depending on the ion cluster species). This is carried out in the buncher (see Figure1.5). The ion package (all ions in the package have the
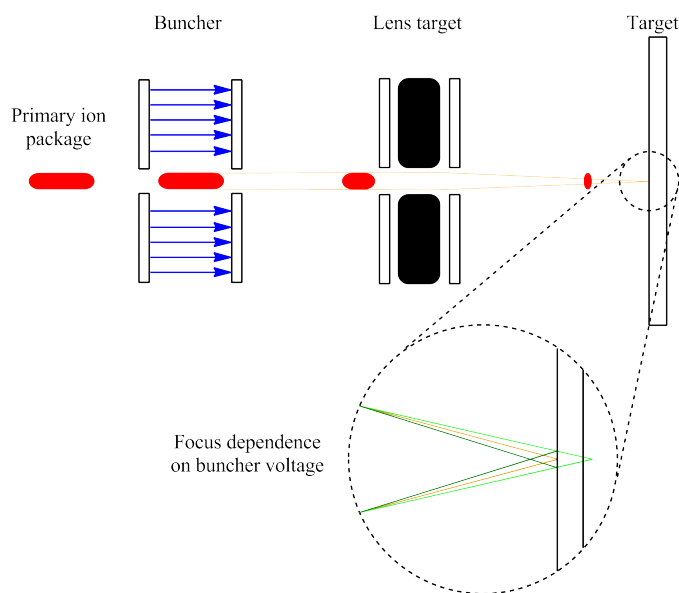
Figure 1.5: *Schematic illustration of the ion beam path in the high current bunched mode. The right side shows the signal on aperture 1 (top) and aperture 2 (bottom)*

same kinetic energy) arriving in the buncher are accelerated by are short high voltage pulse. The ions in the back are thus subject to a longer acceleration time than the ions in the front. This causes on one hand a sub-nanometer pulse but on the other hand a change in kinetic energy of the ions. This change in kinetic energy induces a chromatic aberration in the "lens target" whereby the focus of the ion beam (i.e. the ion beam diameter) on the target is restricted to 1-3 micron.

1.3 Secondary Ion Generation

Ion formation in SIMS is a complex phenomenon. The concept of the method involves the interaction of a high energy ion beam (25 keV or 30 keV for newer ion guns) with the surface of a condensed phase (liquid or solid). The energy of the impinging primary ion is transferred to the atoms of the sample by a collisional process, the so-called collisional cascade (See Figure 1.6).
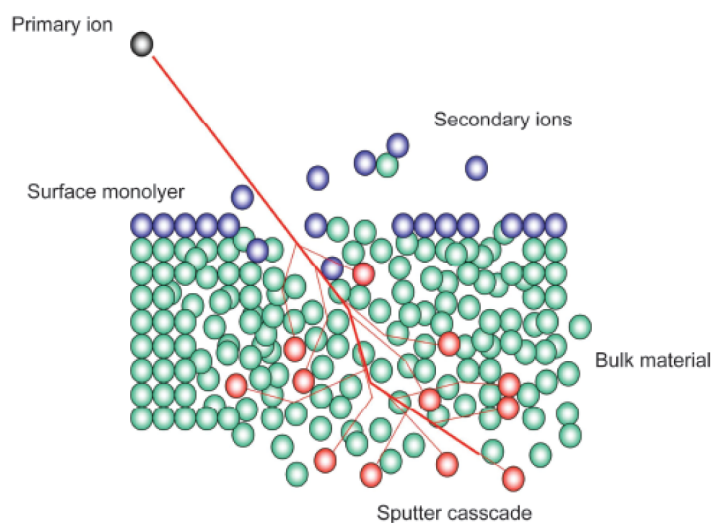
Figure 1.6: *Fundamental principle of the sputter process and secondary ion generation*[§]

1.3.1 Sputtering

A primary ion entering the surface is slowed down by striking the surface and subsurface atoms until it has lost its kinetic energy. The impact of the primary particle leads to a sputter cascade whereby an energy and momentum transfer occurs to a limited area around the point of impact. Various collisions of the primary ion displace the target atoms, as well as alter the initial linear trajectory. Recoiling target atoms strike other atoms in the lattice and the so called collisional cascade proceeds until the energy is consumed. The primary recoils are low in number but have high energy that damages the sample even in deep layers tough they do not cause emission

of particles. This results in a change of the lattice structure. During the cascade some atoms are directed towards the surface and if the energy is higher than the surface binding energy, the atom will be emitted from the surface (See Figure 1.6). These secondary recoils are large in number and carry most of the cascade energy which leads to emission of surface particles and sample damage at the surface. These secondary particles are related to the chemical composition of surface. Sigmund's formulation of this model provides a quantitative basis for many of the listed observations [23, 24, 25] and gives a good match for many experimental results under typical experimental conditions. [26, 27] Surfaces with high binding energy will be more difficult to sputter than those with low binding energies. [28]

1.3.2 Nascent Ion-Molecule Model

The basic concepts of the nascent ion-molecule model [29, 2] have their origin in the sputtering of atomic and molecular species. It was proposed from Gerhard and Plog [30] to reproduce the strong mass dependence of Me^+ ions from metal oxides on their secondary ion yield. Charged particles in the surface near regions are neutralised due to rapid electronic transitions before they can escape the surface. For instance, electronic transitions rates in metals are so fast (10^{-14}s - 10^{-16}s), that deexcitation of sputtered ions occurs (10-13s) before they can leave the surface. Since secondary ions are still detected during sputtering, they have to be formed some distance away from the metal surface. Ions are therefore formed by the non-adiabatic dissociation of nascent ion molecules (neutral molecules). Based on these assumptions the bond breaking model [3] was developed. A molecule AB (salt, partly polarised oxide) exists in a solid as A^+ and B^-. The molecule will be sputtered as neutral, originating from the direct emission of ion pairs, or as ions, due to high internal energy to dissociate into their constituents, depending on the internuclear distance at which the lowest potential energy level switches from the ionic to the neutral state (Figure 1.7).

This model has been extended to the emission of polyatomic molecules leaving the surface as neutrals (ion pairs). The ions are formed if the nascent

---

§Figure taken from ION-TOF GmbH internal documents
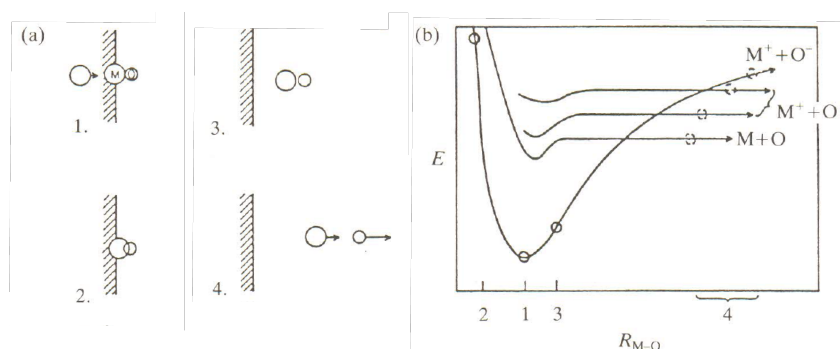
Figure 1.7: *Schematic diagram of a) the sputtering of a transient M-O molecule and b) the possible level-crossing process during dissociation of this entity.*

ion pairs have enough internal energy to ionise by minimal fragmentation or by breaking up into smaller ionised fragments. This approach had empirically success as it was used to describe the formation of secondary ion clusters from metal oxides [31] and as the energy distributions of monoatomic singly charged cations were fitted into existing models [32]. The emission of diatomic species with subsequent bond cleavage seemed to be the more likely explanation for the detected ions.

1.3.3 Precursor Model

The precursor model was first formulated by Benninghoven [33] as he investigated organic compounds with SIMS. [34, 35] The emission of large unfragmented organic molecules was unexpected since the sputter process was regarded to be highly destructive, especially for organic surfaces. In this model he depicts a view of energy distribution of the collision cascade energy at the surface induced by a keV particle bombardment and its relation with the ejection of intact and fragmented molecule. The energy curve around the impact is described as a bell shape (Figure 1.8).

In the central area, where the energy introduced into this part is high, the precursor molecules in the surface fragment. Additional fragments may occur due to decomposition of larger excited molecules after their separation from the surface. At the boundaries of the excited zone the recoil energy is to low to break intermolecular forces in the surface layer and no emis-
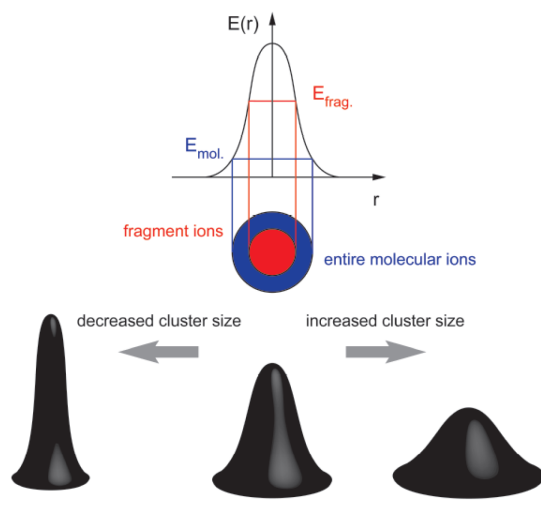
Figure 1.8: *Parent-like ion formation of large organic molecules during sputtering. The energy distribution E(r) represents the average energy which is transferred by an impact cascade to a surface atom at a distance r from the point of primary ion impact (r = 0).*

sion occurs. Between these two extremes there is a region where sufficient energy is imparted to eject unfragmented precursor molecules. In the case of molecular solids with direct bonds the energy will be transferred through vibrations. Thus, in a ploymer violent fragmentation occurs in the impact zone of the primary ion. [36] As the energy dissipates into vibrations in the polymer chain, larger lower energy fragments are emitted. Farther away from the impact point, in the monomer region, ejection of monomers and minimal rearranged species is predominant (Figure 1.9). [2, 29, 33]

1.3.4 Desorption Ionisation Model

It has been suggested that, particularily for organic materials, vibrational excitation may be important for the emission of molecular and cluster ions. Cooks and Busch [37] introduced a desorption-ionisation model schematized in (Figure 1.10). It is basically assumed that the desorption and the ionisation processes are considered separately (except for preformed ion from, e.g.
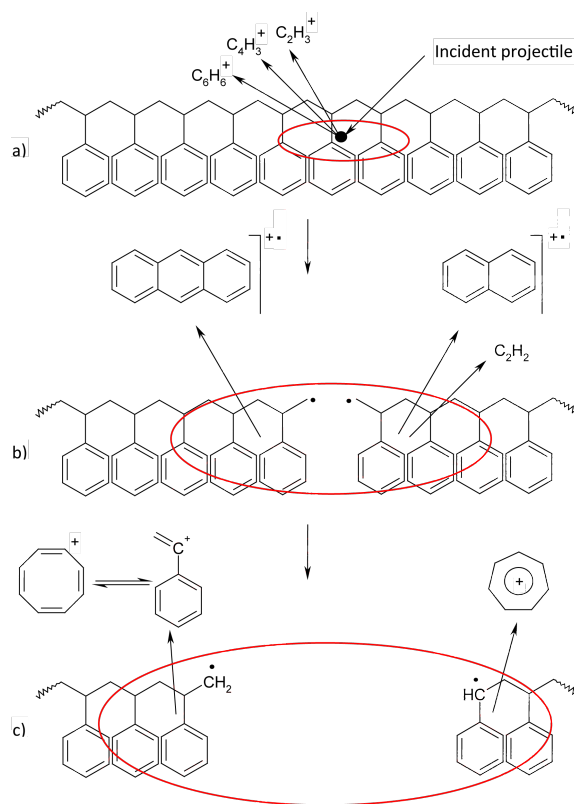
Figure 1.9: *Precursor model of sputtering of a polymer: a) violent fragmentation in primary impact region, b) unzipping to give large fragments, c) Low energy fragmentation in monomer region.*

salts) and that the initial energy is transformed into thermal and vibrational motion as far as the molecules are concerned. Desorption of preformed ions (from salts) no ionisation step is required and these ions traverse the uppermost layers, called the selvedge, unperturbed and are thus detected with high yields.

It is assumed that most of the ions desorb with low internal energy (or are unlikely to be energised by subsequent collision) and thus fragmentation is minimised. Neutral molecules desorb in high yield, but to be detected, they have to undergo an ionisation process such as cationisation. To generate other ions, the model suggest, that desorption is followed by two types of chemical reaction:

- in the selvedge or top surface layers fast ion/molecule reactions or electron ionisation can occur.
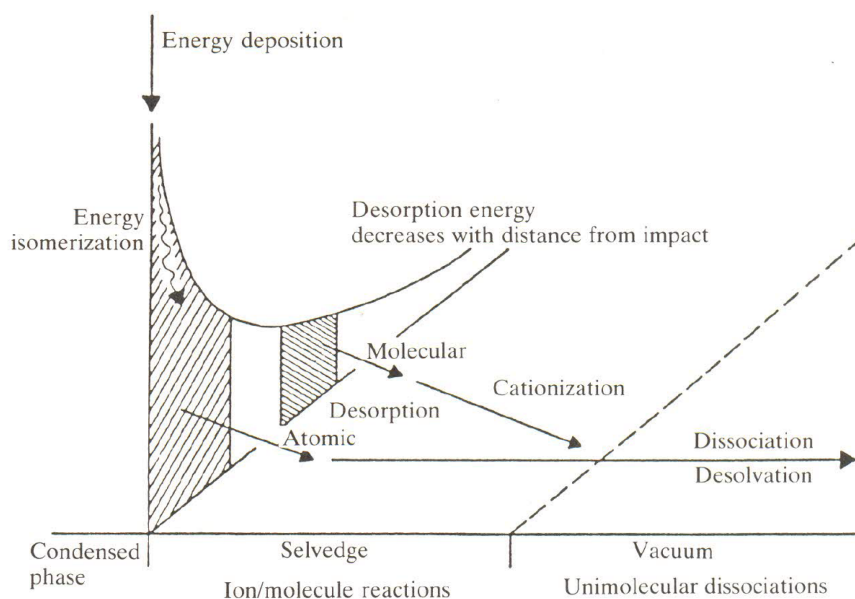
Figure 1.10: *Summary of the process tought to occur during desorption-ionisation in static SIMS.*

- in the free vacuum unimolecular fragmentation may occur, governed by the internal energy of the parent ion giving rise to fragment ions.

According to these ideas the desorption process is of relatively low energy. The linear cascade ideas are not wholly appropriate when dealing with molecular solids. Energy is being transferred to the vibrational modes of the molecule thus leading to fragmentation and ionisation. This is consistent with the fact that static SIMS is a relatively soft ionisation process where little low-mass fragmentation and large yields for molecular ions are observed. [2, 29, 3]

1.4 Mass Analysis and Detection

In a ToF-SIMS experiment a time of flight mass analyser of the reflectron design is widely used. Together with a microchannel plate detector it provides the mass analysis and detection system for the desorbed secondary ions.

1.4.1   Mass Analysis System

A scheme of a reflectron ToF is displayedn in Figure 1.11. The secondary ions
generated on the target surface are accelerated by an electrostatic extraction
pulse (2 kV) and enter a the field-free drift region. A subsequent 3 electrode
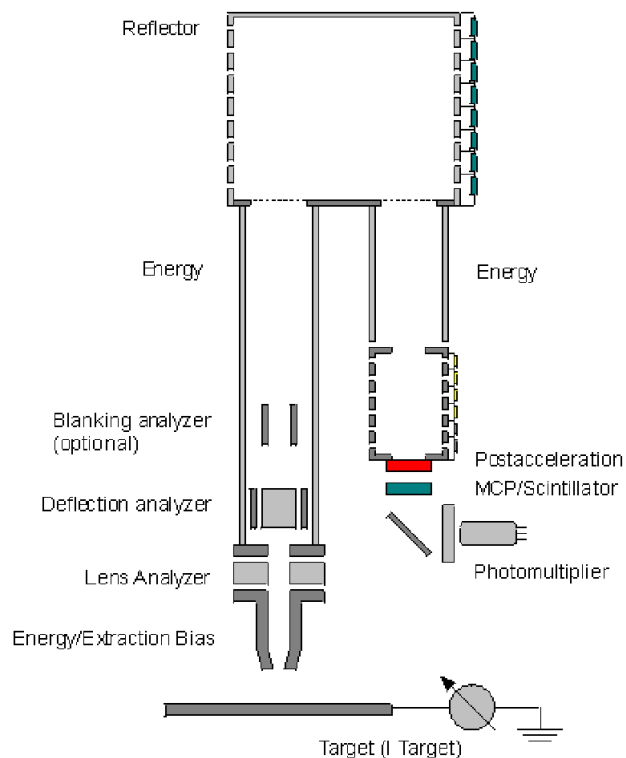
Figure 1.11: *Schematic view of a reflectron type ToF analyser.*

lens focuses the secondary ion beam onto the detector. On their way to the
detector the ions pass the analyser deflection unit, enter and leave the reflec-
tron (ion mirror) and finally enter the post acceleration unit before hitting
the multichannelplate of the detector. As a consequence of ion bombardment
secondary ions with slightly different energy are desorbed. This energy dis-
tribution leads to a decrease in mass resolution. This can be compensated
in the analyser by using a reflectron which consists of a combination of drift
regions with an ion mirror which acts as an energy focussing device. Those
secondary ions with higher energy will therefore have a longer flight path

than those with slightly less energy since the former penetrate deeper into the retarding field of the reflectron. After the secondary ions have left the reflectron they all have their initial kinetic energy and will hit the detector at the same time thus increasing the mass resolution [¶][2, 17]. Since a very well defined start time is required for the flight time measurement, the primary ion gun is operated in a pulsed mode, which provides the start signal for the time measurement. All secondary ions of a given polarity (positive or negative) are then accelerated to the same nominal kinetic energy qU ($q =$ ion charge, $U =$ applied voltage), and the time t of an ion to reach the detector after traveling along a field-free path of a given length s is measured according to [17]:

$$E_{kin} \ = \ qU \ = \ ms^2/2t^2 \tag{1.1}$$

which can be rearranged to:

$$t^2 \ = \ ms^2/2qU \ = \ m/q \tag{1.2}$$

The mass-to-charge ratio m/q can then be calculated from the flight time. The main features of a ToF analyser are

- quasi-simultaneous detection of all masses of a given polarity,

- high geometrical transmission,

- high mass resolution and

- no movable parts.

ToF analyser offer therefore excellent sensitivity and a high mass accuracy and have become the analyser of choice for organic analysis and screening purposes [17].

1.4.2   Detection System

The detection system for the secondary ions consists of a microchannel plate (MCP) and a scintillation counter. A MCP is an array of miniature electron multipliers oriented parallel to each other (Figure 1.12) and usually biased

---

[¶]ION-TOF GmbH SurfaceLab 6 help file
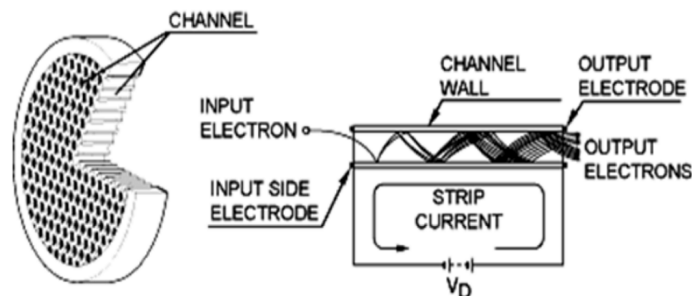
Figure 1.12: *Schematic view of a microchannel plate.*

at a small angle of approx. 8°. Each channel works as a continous dynode electron multiplier in which the multiplication takes place under the presence of a strong electric field. A particle (e.g. secondary ion) enters a channel and hits the wall of the channel. The impact starts a cascade of electrons that
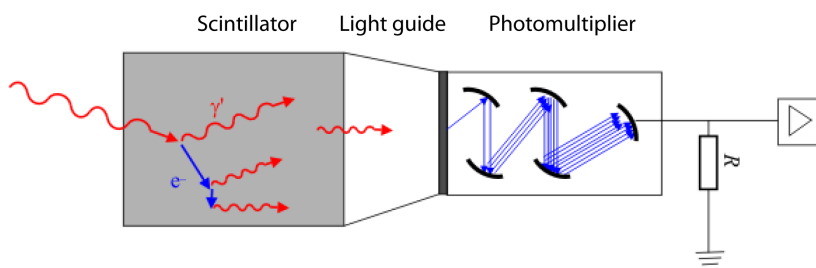
Figure 1.13: *Schematic view of a scintillation counter.*

propagates through the channel. The original signal is amplified by several orders of magnitude depending on the electric field strength and the geometry of the microchannel plate [38]. The electrons exit the channels on the opposite side where they are detected by a scintillation counter (Figure 1.13). The electrons strike a phosphor which emitts a flash of light. The scintillations are detected by the light-sensitive cathode of a photomultiplier tube and are converted by the succession of electrodes in the tube into a stream of electrons which are collected and recorded [39].

---

from wikipedia - microchannel plate detector

1.5 Important ToF-SIMS Parameters

To compare spectra or the performance of primary ion particles on substances or substance classes it is necessary to evaluate certain parameters. In the following, the parameters used in this work will be defined.

1.5.1 Ion Yields

The total ion yield Y_{tot} as well as the secondary ion yield Y_i for a cetrain species (atoms, clusters or molecules) X_i can be derived from the measurement data (see equation 1.3 and 1.4),

$$Y_i \;=\; N_{SI,i}/N_{PI} \tag{1.3}$$

$$Y_{tot} \;=\; \sum Y_i \;=\; \sum N_{SI,i}/N_{PI} \tag{1.4}$$

where N_{SI} are the number of detected secondary ions and N_{PI} the number of primary ions [1].

1.5.2 Fragmentation

The fragmentation F is defined as the ratio of the summarised fragment ion yields to a quasi-molecular ion yield (usually $[M+H]^+$ or $[M-H]^-$) of the substance in question (see equation 1.5 and 1.6) [40].

$$F^+ \;=\; \sum Y_i^+ / Y_{C^+} \tag{1.5}$$

$$F^- \;=\; \sum Y_i^- / Y_{A^-} \tag{1.6}$$

In the analysis of ionic liquids it is more convenient to use the cation yield Y_{C^+} or anion yield Y_{A^-} (as quasi-molecular ion yield). Thus high values for F correspond to a high degree of fragmentation and vice versa.

1.5.3 Dissappearance Cross Section

For a secondary ion i with a measured intensity I_i and a primary ion flux ϕ, the dissapearence cross section σ_i can be expressed as:

$$I_i(\phi) \;=\; I_{i,0} \; exp(-\sigma_i \phi) \tag{1.7}$$

This expression assumes that the degradation of the surface molecules follows an exponential decay law. The dissapearance cross section can easily be derived from a logarithmic description of equation 1.7 as the slope of the straight line [2].

1.6 Ionic Liquids

The beginning of ionic liquids dates back to 1914 when Walden reported on the physical properties of ethylammonium nitrate [41] (mp $13-14\,°C$) which was formed upon neutralisation of ethylamine with concentrated nitric acid. He investigated several anhydrous ammonium salts which melt at relatively low temperatures, approximately down to $100\,°C$. Since such low melting temperatures reduce the degree of thermolysis they allowed the reproducibility of the observation of melts of anhydrous mineral salts at low temperatures previously only feasible at high temperatures. However, his discovery of a new class of liquid and the possible chemical reactions in such solvents did not prompt any significant interest until 1951 when the first organic chloroaluminates [42] were mentioned. These are nowadays considered as the first generation of ionic liquids. Disregarded for decades, the class of ionic liquids has regained a great interest over the last years and the number of publications increased exponentially (Figure 1.14).

To answer the question what ionic liquids are, there is a commonly used definition today [43, 44]: *"Ionic liquids are defined as molten salts that are composed of cations and anions whose melting point is below* $100\,°C$*."* This temperature does not have any chemical or physical significance, but is has persisted until the present day; it is only now that it is being queried.
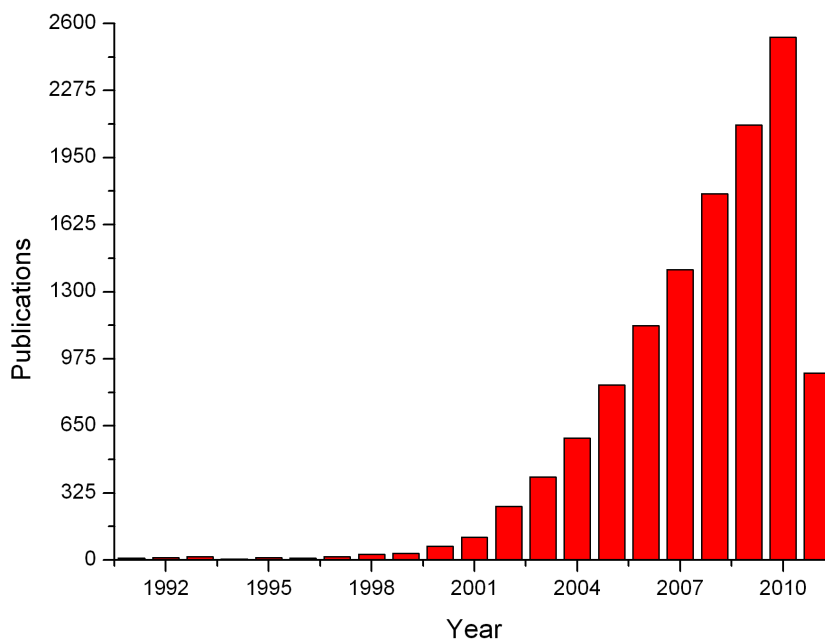
Figure 1.14: *Publications on ionic liquids in the past 20 years*

1.6.1   Ionic Liquids as Solvents

A general interest in ionic liquids is to use them as solvent for different applications such as synthesis [44, 45] (including asymmetric synthesis), embalming fluid [46], ion drives for space travel [47], lubricants [48], liquid crystals for displays [49], chemical analysis [50], sample preparation [51], energy storage [52], electroplating [53], new ion beams for secondary ion mass spectrometry (SIMS) [54] and many more. This enhanced interest is due to the extraordinary physical and chemical properties like low vapour pressure, which makes them useful as so called "green solvents". Since they are composed of ions and each ion contributes to a specific property it is of course self-evident to create tailor-made (or task specific) [55] ionic liquids with different physical and chemical properties. Comparing the around 600 conventional solvents used in industry to the at least one million simple ionic liquids that can easily prepared in the laboratory (several hundreds are commercialised) one can imagine the many opportunities yet undiscovered in composing the ions of ionic liquids. Combining all currently known ionic liquid cations and anions

Plechkova and Seddon [43] estimated 10^6 simple systems, 10^{12} binary systems and at least 10^{18} ternary systems possible. Unraveling the mystery of the influence of the ions on the physical and chemical properties is a challenging task but opens up to undreamt opportunities in solvent chemistry and chemistry in ionic liquids.

1.6.2 Properties of Ionic Liquids

The physical and chemical properties of ionic liquids are numerous and many excellent reviews [44, 56, 57, 58, 59, 60] on this topic are available in the literature. For convenience only the properties relevant for this work shall be discussed briefly.

Vapour Pressure

The vapour pressure of ionic liquids is very low and are comparable to those of Zn and Na at 400 °C [61], allowing the analysis of ionic liquids with UHV techniques such as ToF-SIMS (time of flight secondary ion mass spectrometry) [62, 63, 16], PES (photoelectron spectroscopy) [62, 61, 64], LEIS (low energy ion scattering) [65] and NICISS (neutral impact collision ion scattering spectroscopy) [64]. This negligible vapour pressure at ambient temperature results in very high boiling temperature (approx. 900 °C) exceeding the decomposition temperature by far. Nevertheless it is reported that ionic liquids are distillable [66, 67] at strongly reduced pressure thus openig the study of ionic liquid vapor [68, 69, 70].

Melting Point

A key property for all ionic liquids is the melting point. The variation of the cation and anion in ionic liquids influences their characteristic properties in particular the melting point and liquidus range. This two properties are mainly influenced by anion species [71], cation structure [72], ion symmetry [73], side chain length [74] and branching [75, 76] (if applicable for both) in a given cation class (e.g. imidazolium ILs)(see Table 1.1). An increase in anion size leads in principle to a reduction of the melting points by reducing

Table 1.1: *Glass transition temperature and melting point in dependence on the anion size, cation size and side chain length*

Cation	Anion	T_g	T_m
$C_4C_1im^+$	$(C_2F_5SO_2)_2N^-$	-84	-
$C_4C_1im^+$	NTf_2^-	-87	-3
$C_4C_1im^+$	$CF_3SO_3^-$	-	17
$C_4C_1im^+$	PF_6^-	-77	10
$C_4C_1im^+$	CF_3COO^-	-78	-
$C_4C_1im^+$	BF_4^-	-83	-
$C_4C_1im^+$	NTf_2^-	-87	-3
C_4py^+	NTf_2^-	-76	26
$N_{1,1,1,4}^+$	NTf_2^-	-74	19
$C_1C_1im^+$	NTf_2^-	-	26
$C_2C_1im^+$	NTf_2^-	-87	-18
$C_4C_1im^+$	NTf_2^-	-87	-3
$C_6C_1im^+$	NTf_2^-	-81	-6
$C_8C_1im^+$	NTf_2^-	-80	-

the Coulombic attraction force. However, large, near spherical anions with highly delocalised charge distribution have low melting points, but are higher than anticipated based on a model solely comparing anion size [77]. Aromatic π-π stacking like in tetraphenylborate [78] as well as induced dipoles trough hydrogen bonding [79] can also lead to higher melting points. The size of the cation in ionic liquids controls the melting point due to a reduction of the Coulombic attraction force and disruption of packing efficiency. Simply said, a large cation like tetraalkylammonium and tetraalkylphosphonium reduces the melting point by alkyl-shielding of the charge. However the cation symmetry has also to be taken into consideration; increasing the symmetry increases the melting point due to a more efficient ion-ion packing [44]. An increase in side chain length, e.g. in imidazolium based ionic liquids, leads to lower melting points when going from methyl to hexyl side chains. This can be attributed to a destabilisation of Coulombic packing. Further extending of the side chain (from octyl upwards) leads to increased van der

Waals forces between the hydrocarbon chains and increased structural ordering which is expressed in increasing melting points [44, 74]. Increasing the degree of branching increases also the melting point as the free rotation volume decreases and the atomic density increases [75, 76]. Generally the following effects on the melting point can be concluded [80]:

- The size of the anion.

- Number and strength of interactions.

- The conformational flexibility.

- The packing efficiency.

- The symmetry of the ions.

- The length and conformation of alkyl chains.

- Hydrogen bonding.

- The addition of functional groups (mainly cations) [81, 82, 83].

- Charge delocalisation.

- The number of possible conformations of flexible substituents and chiral centers.

Polarity

Almost all modern interpretations of solvent effects rely on the concept of solvent polarity. This property is the sum of all possible, specific and non-specific, intermolecular interactions between a solute and solvent, excluding such interactions leading to definite chemical alteration (reaction) of the solute [84, 44]. The most common measure of polarity used is the dielectric constant which considers the solvent as a continous dielectric medium. However, ionic liquids do not even approximate to continous dielectric media [44]. Several other polarity scales are proposed, whereas the Kamlet-Abboud-Taft [85] and the Dimroth-Reichardt [86] scales are currently the most common for ionic liquids. In this work, we extend the also widely acknowledged donor-acceptor approach [87] to ionic liquids (see section 1.7).

1.7 Sovent Polarity

The selection of an appropriate solvent or solvent mixture to perform chemical reactions or to separate mixtures of reactants and products is crucial in many chemical processes [88]. Also physical properties like the frequencies and intensities of transitions in IR, UV-visible, fluorescence, NMR and ESR spectroscopies are also known to be affected by solvents. It is customary to state that these effects reflect the influence of "solvent polarity" [89]. A common method to classify solvent systems (including ionic liquids as solvents) and therefore choosing an appropriate solvent is their polarity. Polarity is a general term that refers to all interaction forces between molecules, both specific and nonspecific, excluding such interactions leading to definite chemical alterations of the ions or molecules of the solute [84]. For better understanding of polarity it is important to describe the interactions between the solute and solvent on molecular level. The most common measure of polarity used by chemists is that of dielectric constant ϵ. Due to the often observed inadequacies of the dielectric approach another one is needed. To solve this problem empirical solvent parameters have been applied. The basic concept of such an approach is that a particular reaction rate, equilibrium or spectral effect is suitable to serve as a model for other reactions [90]. Several polarity scales [89] exist, but the donor-acceptor approach developed by Gutmann [91] precedes all other polarity scales and plays a seminal role in solution chemistry [92, 93]. In this approach, the donor number (DN) is a quantitative measure of Lewis basicity and the acceptor number (AN) a quantitative measure of Lewis acidity, respectively.

1.7.1 The Donor-Acceptor Approach

An intermolecular interaction leads to a charge density rearrangement within the system. This causes variations in bond length due to a charge transfer between an electron donor and an electron acceptor. Thus the structure of a molecule is not rigid but rather adaptable to the environment. To get a measure for the ability of a molecule to act as a donor or acceptor respectively, the donor number (DN) and the acceptor number (AN) were introduced. Donor numbers measure the ability of solvents to give shares in electron pairs

to suitable acceptors (to "donate" electrons) and have been defined as the negative of the enthalpy of adduct formation between the reference acid $SbCl_5$ and a solvent molecule in high dilute 1,2-dichloroethane solutions. Acceptor numbers measure the ability of the solvents to take shares in electron pairs from suitable donors (to "accept" electrons). They are derived from NMR chemical shifts of phosphorus by transfer of Et_3PO through solvents [87, 90]. Using these two model systems DN and AN for solvents were determined which correlate well with other polarity scales. Linear relationship have been found between the donor number and the Lewis basicity parameter B [94, 95] ,DN and the standard free energies of transfer of the potassium cation $\Delta G_{tr}(K^+)$ [96], DN and the ^{19}F chemical shifts of trifluoroiodomethane. [97] Linear trends are also found between the acceptor number and the Dimroth-Reichardt E_T [98], AN and the Kosower Z values [99] and AN and the free energy of solvation of the chloride ion $\Delta G_{tr}(Cl^-)$. [96]

1.7.2 Solvatochromic Indicators

Nowadays, AN and DN were determined by spectroscopic methods (UV/VIS) using solvatochromic indicators. Solvatochromism [100] describes the changes in spectra of dissolved species depending of the media. Such effects are used to visualize solvent properties; however different indicator species may measure different aspects of solvent solute interactions. This can be overcome in some extent using multiparameter correlations. Soukup and Schmid proposed metal complexes as excellent color indicators for both the σ-donor (nucleophilic, basic, cation-solvating) and σ-acceptor (electrophilic, acidic, anion-solvating) abilities of solvent [101]. Figure 1.15 shows the solvatochromic indicators $Fe(phen)_2(CN)_2$ for AN and $Cu(acac)(tmen)^+$ for DN that were proposed and successfully applied for the estimation of donor and acceptor properties of solvents, of ions in non-aqueous solvent [102, 103] and of active surfaces [104].

The effect of acceptor properties on the electronic structure of $Fe(phen)_2(CN)_2$ can be well explained as shown in Figure 1.16. The solvatochromism arises from the coordination of acceptor species to the free electron pair(s) of the N-atom from the -CN ligands (see Figure 1.15a). The
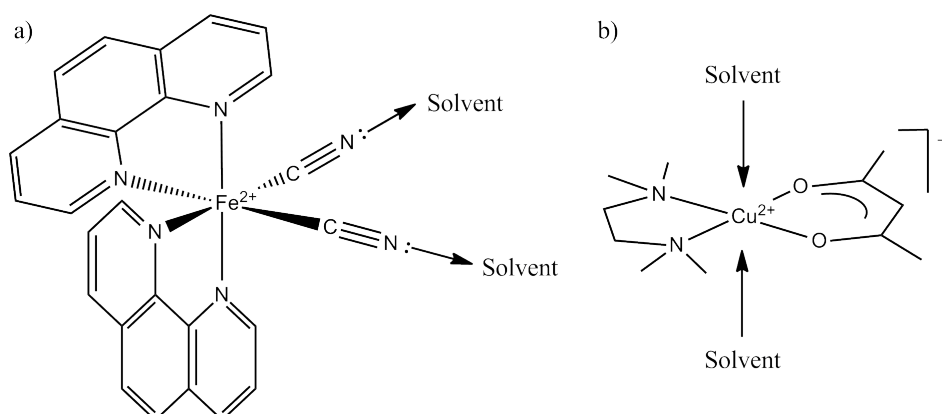
Figure 1.15: *Solvatochromic indicators a) $Fe(phen)_2(CN)_2$ and b) $Cu(acac)(tmen)^+$*

electronic spectrum of the iron(II) complex shows two broad bands, whereas ν_2, observed at lower transition energy, is significantly stronger affected by Lewis acids. However, both are "metal to ligand charge transfer" bands, i.e. from the iron coordination center to the $\pi*$ orbitals of the phenatroline ligands. Electronic withdrawal due to interactions with acceptor species leads changes in the σ bonding MOs, including the e_g levels of the iron. This in turn leads to deformations of the iron complex and the concomitant p orbitals, including the split of the t_{2g} levels of the coordination centre, which then influences the energy level of the antibinding $\pi*$ ligand orbital. [104, 101, 103]

The effect of donor properties on the electronic structure of $Cu(acac)(tmen)^+$ can be well explained by simple molecular orbital theory as shown in Figure 1.17. The chelate complex is axially attacked by donor species so that the original square planar complex is transformed to a tetragonal and eventually to an octahedral configuration (see Figure 1.15b). The former configuration is mainly governed by the coordination of anions (usually in low concentration) to the complex, the latter by coordination of solvent molecules to the complex. Both coordination forms lead to significant changes in the d-d transitions and therefore to a strong change in color of the complex in solution. Starting from the square planar complex the change in d orbital splitting is a result of the ligands moving in on the z axies and
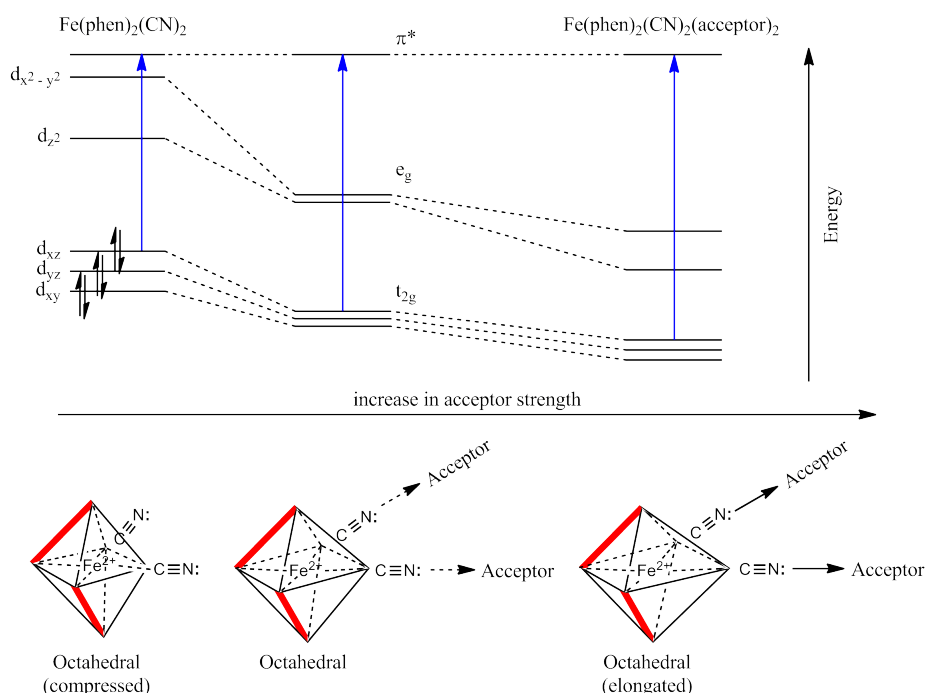
Figure 1.16: *Simplified schematic orbital arrangement of $Fe(phen)_2(CN)_2$ adjusted to constant $\pi*$ level. Therefore the center of gravity of the d levels varies with the ligand field strenght. The blue full arrow shows the relevant charge transfer transition. The bold red line in the configurational changes of the iron complex schematises the chelating ligands.*

those moving out. The interaction with the orbitals having a z component (i.e. d_{z^2}, d_{xz} and d_{yz}) are increasing, thus raising the energy. The interactions with the ligands in the x,y plane are decreasing whereupon those orbitals are energetically stabilised. The highest energy transition $d_{xz}, d_{yz} \rightarrow d_{x^2-y^2}$ can be assumed to be the most important and an increase in z ligand basicity leads consequently to a blue shift as the energy difference become gradually shorter. This effect is found experimentally. [104, 101, 102]

1.7.3 Ions in Non-Aqueous Solvents

The determination of donor and acceptor numbers of solvents by solvatochromic indicators is quite straight forward. By contrast the determination of donor and acceptor numbers for ions in non-aqueous solvents is more com-
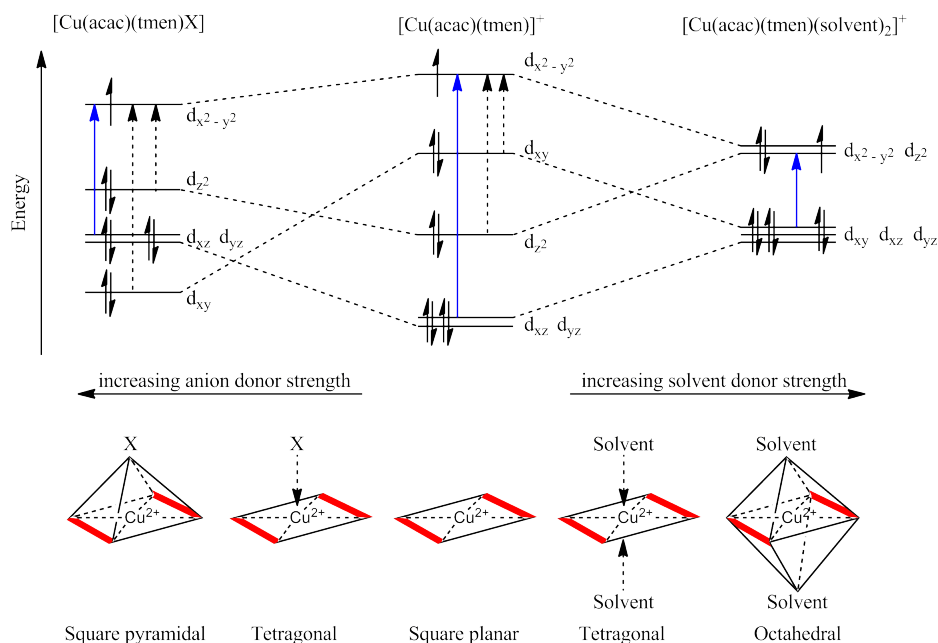
Figure 1.17: *Relative orbital energy levels and d-d transitions (blue full arrow) for $Cu(acac)(tmen)^+$ in square planar, tetragonal and octahedral environment. Teh configurational changes include a lengthening of the original bonds accompanying the increase in coordination number. The bold red line in the configurational changes of the copper complex schematises the chelating ligands.*

plex. The ability of anions (cations) to act as an electron pair donor (an electron pair acceptor) influences the donor and acceptor properties of a solvent.

Therefore anions for example such as perchlorates and tetraphenylborates were often used as counter ions as they are assumed to have a low basicity and thus not influencing the donor and acceptor properties of solvents significantly. [105, 106] The first estimation of donor numbers for anions was based on the measurement of the free energies (i.e. equilibrium constant) of the reaction $[VO(acac)_2(MeCN)] + D \rightleftarrows [VO(acac)_2D] + MeCN$ where D was either an anion or a solvent of comparable donor strength and acac = acetylacetonate. This was then further improved for anions and cations using the above mentioned indicators. [102, 103] The behaviour of the absorption maxima of $Cu(acac)(tmen)^+$ in various solvents in the presence of anions

Table 1.2: *Absorption maxima* 10^{-3} $\tilde{\nu}_{max}(solv)$ *in* $[cm^{-1}]$ *for* $Cu(acac)(tmen)^+$ *dissolved in different solvents in the presence of various anions.*

Anion	DCE_s	DCE_l	MeNO2	MeCN	Me2CO	H2O	MeOH	EtOH	DMF	DMSO
$BPh_4{}^-$	20.0	20.0	23.5	17.5	17.7	-	17.1	17.1	16.6	16.5
$BF_4{}^-$	18.9	19.0	-	-	-	-	17.0	-	-	-
$ClO_4{}^-$	18.6	18.6	19.0	17.3	17.5	-	16.9	17.1	16.6	16.5
$CO_3{}^{2-}$	17.5	17.8	-	-	-	-	-	-	-	-
$CF_3SO_3{}^-$	17.2	17.2	-	-	-	-	-	-	-	-
$NO_3{}^-$	16.5	16.5	-	-	16.5	-	16.9	16.9	-	-
CN^-	-	15.5	-	-	-	-	-	-	-	-
I^-	15.2	15.2	19.0	17.1	16.9	16.9	16.8	16.5	16.3	-
$MeCO_2{}^-$	-	15.1	18.9	-	-	-	-	-	-	-
SCN^-	14.8	14.7	18.8	15.7	14.8	16.9	16.8	16.3	16.2	16.2
Br^-	14.5	14.4	18.8	15.6	14.4	16.9	16.8	16.7	16.2	16.2
$N_3{}^-$	14.4	14.3	18.7	15.0	14.1	16.9	16.8	16.3	15.3	16.1
OH^-	-	14.2	18.7	-	-	-	-	-	-	-
Cl^-	14.1	14.0	18.6	14.5	13.8	16.9	16.9	16.7	14.7	15.7
NCO^-	13.4	13.3	18.4	13.7	13.3	16.9	16.9	15.9	14.0	14.8

can be explained as follows. The interaction of the anions with the copper indicator depends on both the donor and acceptor properties of the solvent. If the donor strength of the solvent is higher than that of the anion the solvent coordinates preferably with the copper complex, however if the acceptor strenght of the solvent is too high it will compete with the indicator for the coordination of the anion and no change in the absorption maximum is found (solvent dependent part). If the donor strenght of the anion exceeds the donor strenght of the solvent a shift of the absorption maximum can be observed (ion dependent part). For strong acceptor solvents like water and methanol even strong donating anions cannot coordinate to the copper complex as they are preferentially solvated by such solvents (see Table 1.2 and Figure 1.18). The ascending part of the curves depend therefore on both the acceptor and donor number of the respective solvent. The following relationship can therefore be expressed as

$$\tilde{\nu}_{max}(solv) = \tilde{\nu}_{max}(DCE) + a(DN_{solv} - DN_{DCE}) + b(AN_{solv} - AN_{DCE}) \qquad (1.8)$$
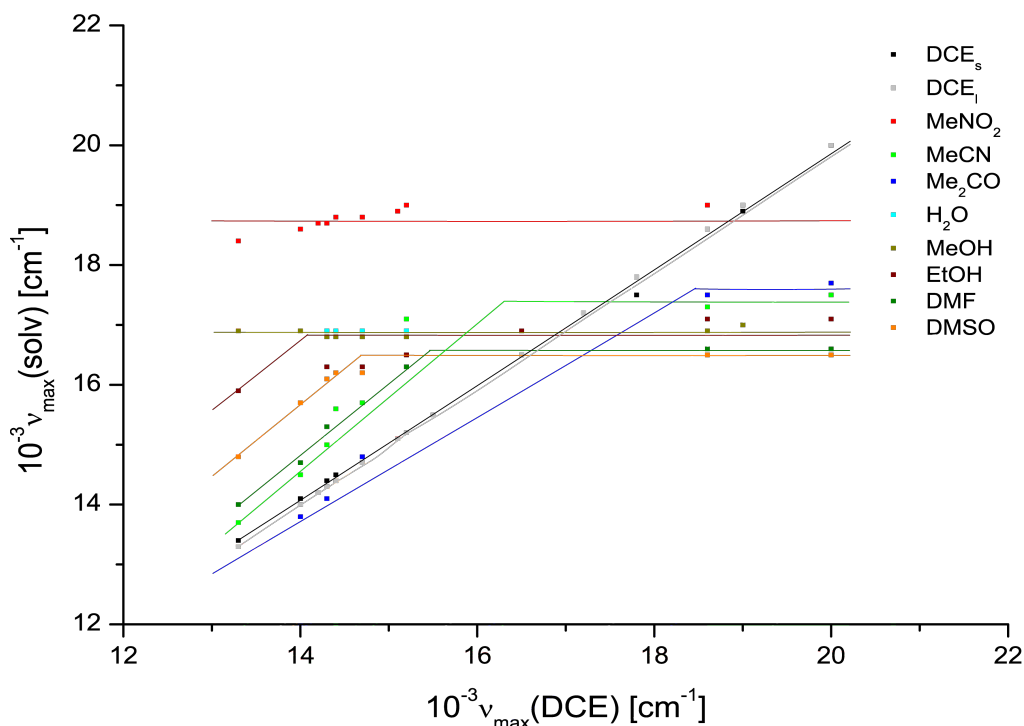
Figure 1.18: *Absorption maxima of $Cu(acac)(tmen)^+$ in various solvents in the presence of anions versus the absorption maximum observed in DCE solutions.*

in which donor and acceptor number for dichloroethane (DCE) (DN = 0, AN = 16.7) is known. A multiple regression analysis of the data yields for a = 63 and for b = 91 (r = 0.986). Measuring the absorption maximum of $Cu(acac)(tmen)^+$ for a large number of solvents a linear correlation with solvent donor numbers is found leading to the expression

$$10^{-3}\,\tilde{\nu}_{max} \;=\; 20 \;-\; 0.103\;DN_{solv} \tag{1.9}$$

Equalising both expressions gives the condition for the intersection of the curve in Figure 1.18. At this intersection point both the donor properties of the solvent and those of the anion are equal and the donor number thus obtained is defined as the donor number of the anion dissolved in that particular solvent ($DN_{X,solv}$).

$$DN_{X,solv} \;=\; 129.6 \;-\; 0.548\;AN_{solv} \;-\; 0.00602\;\tilde{\nu}_{max}(DCE) \tag{1.10}$$

Table 1.3: *Absorption maxima* 10^{-3} $\tilde{\nu}_{max}(solv)$ *in* $[cm^{-1}]$ *for* $Fe(phen)_2(CN)_2$ *dissolved in different solvents in the presence of various metal cations added as perchlorate salts.*

Cation	NM	NE	PC	EtOH	DMF	DMSO	HMPA	AC	AcOH
K^+	16.95	16.53	-	17.89	16.34	16.56	-	16.23	19.34
Na^+	17.86	17.64	-	17.89	16.34	16.56	16.75	17.27	19.23
Li^+	18.62	18.48	17.95	17.80	16.34	16.56	16.18	17.86	19.19
Ba^{2+}	19.12	18.87	-	17.89	16.34	16.56	16.67	16.29	18.98
Mg^{2+}	19.42	19.42	18.79	18.55	16.34	16.56	17.18	18.66	19.34
Ni^{2+}	19.65	19.57	19.16	18.66	17.89	-	18.52	18.94	19.61
Mn^{2+}	20.08	19.96	19.53	18.80	17.89	16.56	17.54	19.28	19.88
Ce^{3+}	20.16	20.00	19.30	18.98	16.37	16.58	17.54	19.46	21.83
Co^{2+}	20.41	20.28	20.00	18.76	17.89	16.58	17.86	19.76	19.34
Cu^{2+}	20.79	20.58	20.33	19.80	19.96	18.32	19.46	20.16	20.53
Zn^{2+}	21.51	21.10	21.01	20.88	18.32	16.57	-	20.92	-
Fe^{2+}	20.62	20.83	20.20	18.8	17.86	16.61	-	21.28	-

The same concept can be applied to determine the acceptor number of cations in solution [103]. Figure 1.19 depicts the absorption maxima of $Fe(phen)_2(CN)_2$ in the presence of a cation in a solvent versus the absorption maxima under the same conditions using nitromethane as solvent. A similar behaviour is found for cations as it was observed for anions. If the solvent is a stronger Lewis acid than the cation, the solvent interacts solely with the indicator, or the solvent is a Lewis base strong enough to solvate the cations making an interaction between indicator and cation impossible (see Table 1.3). In these two cases no significant change in the absorption maximum is found as the influence of the dissolved cation is negligible (solvent dependent part). An increase of Lewis acidity and therefore an increase of acceptor properties of the cation leads to a shift of the absorption maximum to lower energies (ion dependent part). This part depends on the acceptor and donor properties of the respective solvent and can be, using nitromethane as reference solvent (DN = 2.7, AN = 20.5), expressed as

$$\tilde{\nu}_{max}(solv) = \tilde{\nu}_{max}(NM) + A(DN_{solv} - DN_{NM}) + B(AN_{solv} - AN_{NM}) \qquad (1.11)$$

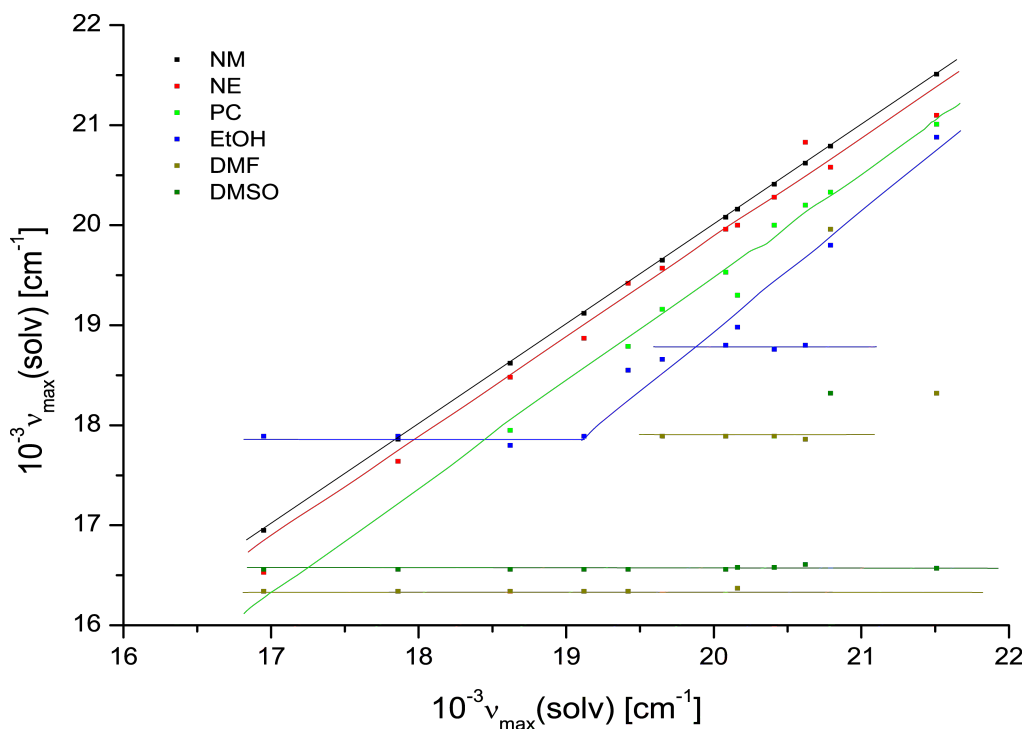A multiple regression analysis of the data yields for A = -48.7 and for B = -

Figure 1.19: *Absorption maxima of $Fe(phen)_2(CN)_2$ in various solvents in the presence of cations versus the absorption maximum observed in NM solutions.***

5.62 (r = 0.960). Measuring the absorption maximum of $Fe(phen)_2(CN)_2$ for a large number of solvents a linear correlation with solvent donor numbers [107] is found leading to the expression

$$10^{-3}\, \tilde{\nu}_{max} \;=\; 15.08 \;+\; 0.076\; AN_{solv} \tag{1.12}$$

Equalising both expressions gives the condition for the intersection of the curve in Figure 1.19. At this intersection point both the acceptor properties of the solvent and those of the cation are equal and the acceptor number thus obtained is defined as the acceptor number of the cation dissolved in that particular solvent ($AN_{M,solv}$).

$$AN_{M,solv} \;=\; -181 \;-\; 0.595\; DN_{solv} \;+\; 0.0122\; \tilde{\nu}_{max}(NM) \tag{1.13}$$

The validity of the approach for donor and acceptor numbers for ions in

nonaqueous solvents is given in several examples. The solvatochromism of
the analogous complex $Ru(phen)_2(CN)_2$ is linearely related to the absorp-
tion maxima obtained with $Fe(phen)_2(CN)_2$. [103, 104] The logarithm of
formation constants of metal ion - EDTA-complexes in aqueos solutions is
found to be related to the apparent AN of metal ions in the respective sol-
vent. [103] By transferring a given ion from one solvent to another the free
energy of transfer can be considered as a characteristic parameter for the
solvation of ions. Thus a linear relationship was found for the free energy
of transfer from water to various solvents and the solvent dependent donor
numbers of anions. [104] The logarithm of the rate constants for the reaction
of $Ni^{2+} + X^- + terpy \rightarrow [NiX(terpy)]^+$ in acetonitrile is found to correlate
with the DN of the anions in the respective solvent [102].

1.7.4   Application to Ionic Liquids

The same concept for ions in nonaqeous solutions shall be applied for the
determination of donor and acceptor numbers of ionic liquids. As stated
above cations and anions influence the donor and acceptor properties of a
solvent thus shifting the absorption maximum af a solvatochromic dye. In
the case of ionic liquids the assumption is made that cations are solvated
by anions and vice versa. The anions therefore are acting as solvent for the
cations and the cations as solvent for the anions. Therefore there is again
a mutual influence of the ions on their donating and accepting ability. A
system of equations can be estabished in order to reflect the ionic influence.

$$\tilde{\nu}_{max,Cu(IL)} - \tilde{\nu}_{max,Cu(DCE)} = a(DN_{IL} - DN_{DCE}) + b(AN_{IL} - AN_{DCE}) \qquad (1.14)$$

$$\tilde{\nu}_{max,Fe(IL)} - \tilde{\nu}_{max,Fe(NM)} = A(DN_{IL} - DN_{NM}) + B(AN_{IL} - AN_{NM}) \qquad (1.15)$$

By solving this system of equations, using the previously determined
constants (a, b and A, B), donor and acceptor numbers for neat ionic liquids
can be obtained. Using again dichloroethane and nitromethane as reference

---

**In the case of some transition metal ions in a given solvent (EtOH, DMF and DMSO)
an apparent constant displacement can be observed. In these cases the solvated species are
coordinated to the indicator by an outer sphere mechanism, i.e. the cations are separated
from the indicator by a solvent molecule.

solvents the DN and AN are on the same scale as Gutmann's DN and AN for solvents [87].

Chapter 2

Results and Discussion

2.1 Emission of Molecular Secondary Ions from Ionic Liquids

2.1.1 Introduction

A systematic study of the influence of the primary ion size and charge (Bi_{1-7}^{+} and $Bi_{1,3,5,7}^{++}$) was carried out on liquid organic-inorganic surfaces. As model sample the ionic liquids $[C_4C_1im][Ac]$ and $[C_4C_1im][PF_6]$ were used. The data were evaluated by calculating secondary ion yields, static SIMS limit, dissapearing cross section, ion formation efficiency and fragmentation.

2.1.2 Signal Enhancement

The secondary ion yield of the ionic liquids $[C_4C_1im][Ac]$ and $[C_4C_1im][PF_6]$ were calculated from their mass spectra using the intensity from the FWHM-area of the respective ions. The secondary ion yields are presented as a function of the kinetic energy per atom in the primary cluster ion beam (see Figure 2.1). The open symbols correspond to the doubly charged cluster $Bi_{1,3,5,7}^{++}$ (doubly charged primary ions are accelerated with 50 keV towards the surface, therefore the energy per incident ion is 50 keV divided by the number of Bi atoms in the primary ion). Doubly charged primary ion cluster generally result in higher yield than the single charged, except for Bi_1^{++}. The

yield rises exponentially for both examined ionic liquids, for both ion modes and all primary ions (non-linear yield enhancement). The left side of Figure 2.1 depicts the enhancement of the intact cation not only in dependence of the energy deposition on the surface but also in dependence on the anion. Since the cation remains constant in all measured samples, the right side of Figure 2.1 shows the yield enhancement for the different anions only as a function of the energy per atom in the Bi cluster. It can be seen, that the secondary anion yield for the ionic liquid with weak ion-ion interactions is significantly higher than that for the strong interactions, especially with large primary ion cluster (i.e. Bi_6^+ and Bi_7^+). To examine this behaviour in more detail more ionic liquids with the same cation but different anion and hence varying ion-ion interactions (i.e. $[C_4C_1im][NO_3]$, $[C_4C_1im][I]$ and $[C_4C_1im][NTf_2]$), are investigated using Bi_7^+. The left side of Figure 2.2 shows three different groups, which can in principal be explained using solvent parameters [16], which shows a linear correlation with the anion yield (right side of Figure 2.2). Briefly summarised, the greater enhancement for PF_6^- and NTf_2^- can be readily explained by their intermolecular interaction (hydrogen bonding, electrostatic (coulomb) and Van der Vaals interactions) towards the cation. Weaker interactions cannot hold the anions in the supramolecular network as it is in the case of the strong coordinating acetate.
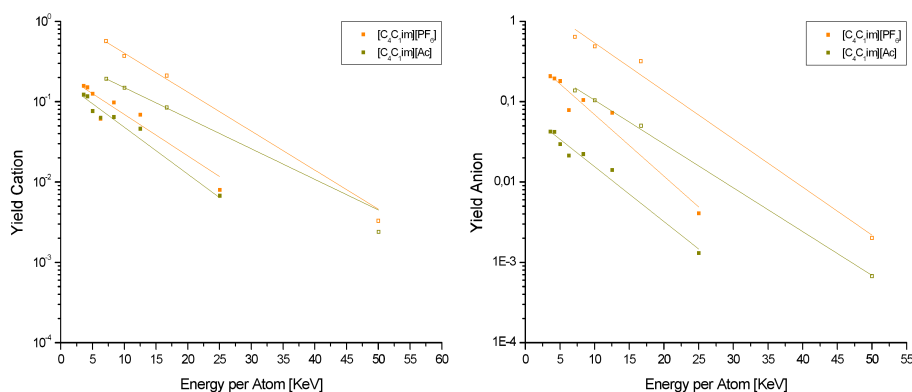

Figure 2.1: *Yield enhancement of the cation $C_4C_1im^+$ (left) and the anions PF_6^- and Ac^- (right).*

Upon analysing the available data on Irganox 1010 [40, 7], Seah [108, 109]

showed, that the yield of the deprotonated molecular ion depend on the total ion yield squared and assumend a proportional correlation of the total ion yield with the sputtering yield (see equation 2.1), where n = 2.

$$Y(M - H)^- \ \propto \ Y^n \tag{2.1}$$

To compare the effect of the different primary ions on ionic liquids with the data on Irganox 1010 a similar graph for the cations and anions is generated (see Figure 2.3) using the intensities instead of yields (yields are the intensities normalised to the primary ions). A proportionality is also found. The dashed lines in Figure 2.3 show Equation 2.1, but n = 0.9 for the cations and n = 1.2 for the anions of the two studied ionic liquids is found. It is assumed, that the power of 2 is reduced towards 1, if with high total yields is dealt. Further, at high total yields, the molecular ion yield $(M-H)^{\pm}$ becomes a significant fraction of the total ion yield [109]. In fact, in the SIMS anaylsis of ionic liquids, where ionisation for the intact cation or anion is needless, the yield of these ions contribute to a significant amount to the total ion yield (2 to 20 %).
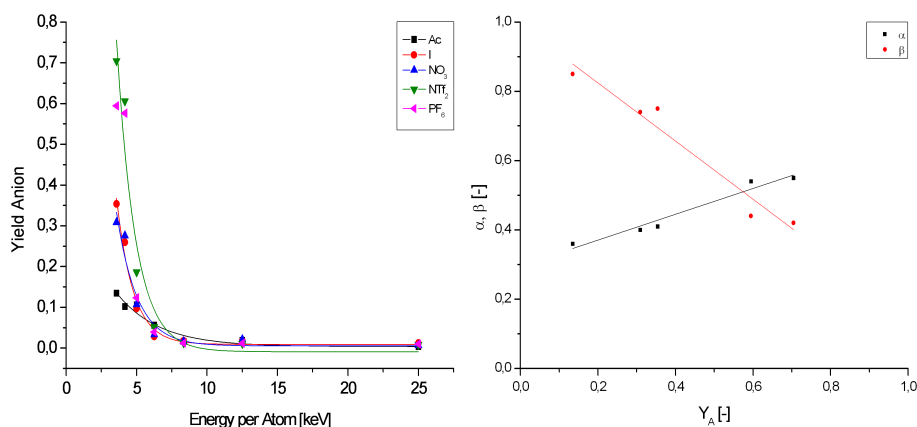

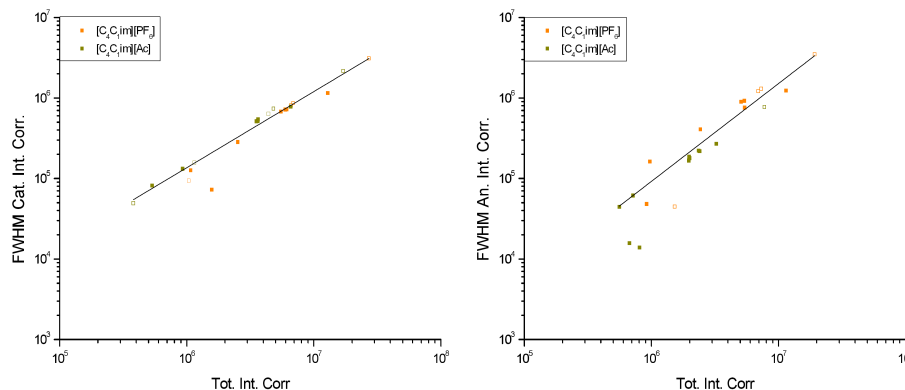Figure 2.2: *Yield dependence of the anions and correlation with Kamlet-Taft solvent parameters.*

Figure 2.3: *Cation yield (left) and anion yield (right) dependence on the total ion yield.*

2.1.3 Static Limit

It is generally known and accepted, that the intensity of organic compounds is decreasing with increasing primary ion dose density (PIDD) [1] due to a damage accumulation in the organic layer (exceptions occur using C_{60}^+ or massive argon clusters, e.q. Ar_{1000}^+).

This limits the measuring time and hence the detection limit of high molecular organic compounds. To increase the measuring time of an organic substance, the sample could be deposited into a liquid like glycerol [1]. Although using glycerol in modern ToF-SIMS instruments (reachable vacuum in the range of 10^{-10}mbar) considerably worsens the ultra-high vacuum (UHV). Using instead ionic liquids (thoroughly dried), which have a nearly non measurable vapour pressure, this problem can be solved and liquid surfaces can be studied at ambient temperatures. Ionic liquids also have the advantage of simple, well defined mass spectra. Inorganic liquid surfaces could also be studied using galinstan, an eutectic alloy consisting of gallium, indium, and tin, which is liquid at room temperature (mp $= -19\,^{\circ}$C, vapour pressure $= < 10^{-8}$ Torr at $500\,^{\circ}$C *). The static SIMS limit of liquid surfaces has not been examined so far. Figure 2.4 and 2.5 clearly show, that the intensity of atomic and molecular species does not decrease with an exponential
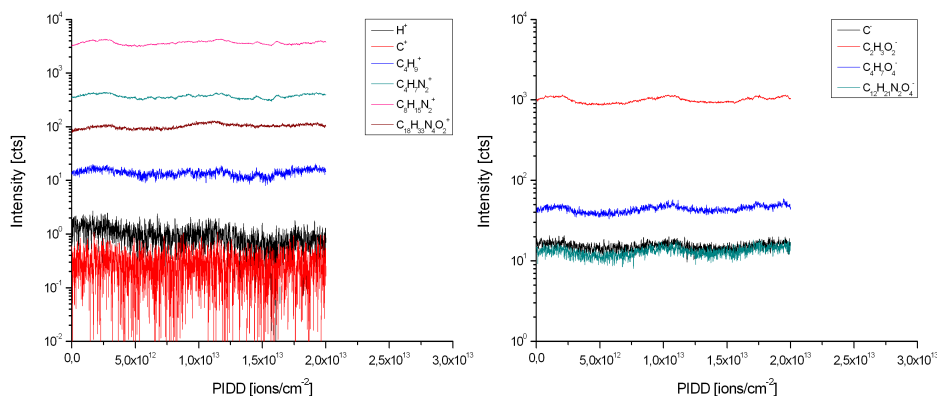
---

*values taken from wikipedia.

Figure 2.4: *Logarithm of the intensity of elemental and molecular secondary ions plotted vs. the primary ion dose (PIDD) from bulk [C$_4$C$_1$im][Ac] ionic liquid measured with Bi$_3$$^+$. Left: positive ion mode; right: negative ion mode.*

function, as usually observed for organic layers. The surface seems to regenerate by self diffusion. This effect could be used for MS/MS experiments of ionic liquids or substances dissolved in ionic liquids (if they accumulate at the liquid-vacuum interface). In a recent study, the molecular ion intensities (and hence the detection limits) are enhanced and the fragmentation is reduced, if ionic liquids are used as matrix. It is concluded that the ionization is promoted by proton transfer from or to the matrix [110].

2.1.4   Efficiency

An established parameter to compare primary ion bombardment conditions is the efficiency. To calculate this characteristic value, the dissapearance cross section σ, determined from the exponential decay of the molecular secondary ion intensitiy, is needed. As seen before, the atomic and molecular intensities of ionic liquid mother and daugther ions are not reduced (or icreased for atomic secondary ion species) by increasing the primary ion dose density (PIDD) beyond the static limit. Therefore σ cannot be evaluated and another approach is used. In this approximation the cross sectional area of the bismuth ion and cluster ions, determined from densitiy functional theory
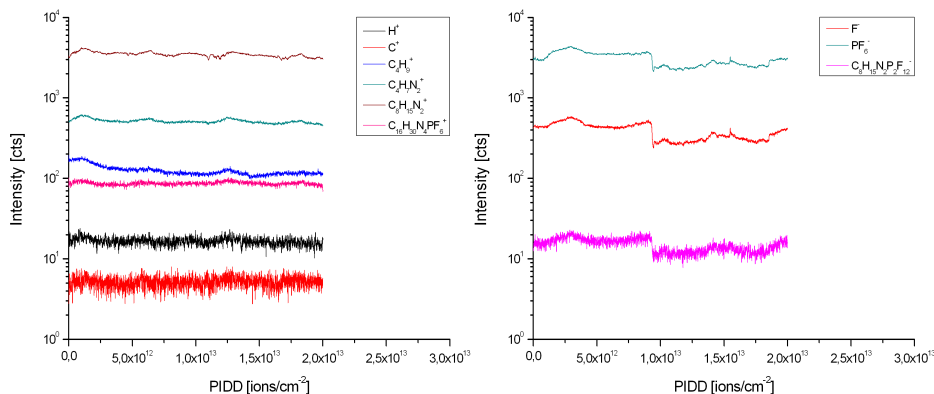
Figure 2.5: *Logarithm of the intensity of elemental and molecular secondary ions plotted vs. the primary ion dose (PIDD) from bulk [C$_4$C$_1$im][PF$_6$] ionic liquid measured with Bi$_3^+$. Left: positive ion mode; right: negative ion mode.*

(DFT) geometry optimisation calculations, were used [14]. Further, the cross sectional area for Bi$_7^+$ was obtained from a linear regression analysis of the Bi$_{1-6}^+$ values, and the same cross sectional areas were used for the doubly charged primary ions (being well aware, that σ is greater). The results from this approximation can be seen in Figure 2.6. The efficiency rises for approx. one order of magnitude upon changing from monoatomic primary ions to primary cluster ions and reaches a more or less constant value as soon as cluster ions are used. Upon changing from singly charged to doubly charged primary cluster ions an efficiency gain of a factor of 2 or 7 is observed, respectively, depending on the ionic liquid ([C$_4$C$_1$im][Ac] or [C$_4$C$_1$im][PF$_6$]). Only for the monoatomic primary ion the contrary is found. This is in contrast to the data available for Irganox 1010 from Kersting *et al.* [40], Kollmer [7] and [14], where a steady increase of efficiency is noticed (see Figure 2.7) upon increasing the primary particle (Au$_{1-3}^+$ and Bi$_{1-6}^+$).

2.1.5 Fragmentation

The fragmentation indicates the magnitude of decomposition of a certain substance under primary ion bombardment. This is dependent on the size
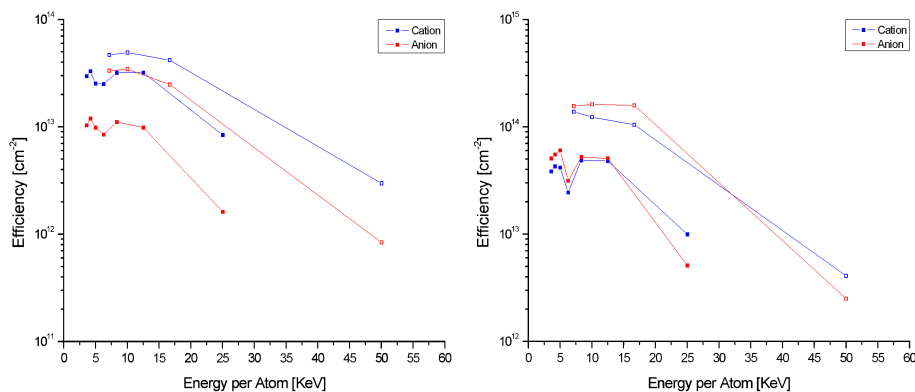
Figure 2.6: *Efficiency of the ionic liquids [C$_4$C$_1$im][Ac] (left) and [C$_4$C$_1$im][PF$_6$] (right) in dependence of the primary energy per incident atom in the primary ion cluster.*

of the primary particle and the primary energy deposited on the surface. Thus, primary cluster ions decrease the introduction of energy per atom in the cluster, considering a constant acceleration of 25 keV, a typical value in modern SIMS. To optimise the results with regard to enhanced signal intensity and simplified mass spectra (especially organic SIMS spectra) the knowledge of the fragmentation is important. The fragmentaion of ionic liquids is investigated using an ionic liquid with strong (i.e. [C$_4$C$_1$im][Ac]) and weak (i.e. [C$_4$C$_1$im][PF$_6$]) ion-ion interactions. These two substances also differ considerably in melting point and density (mp $=$ $-20\,°$C and $6.5\,°$C, d $=$ 1.06 and 1.37). Figure 2.8 shows the fragmentation of [C$_4$C$_1$im][Ac] (left) and [C$_4$C$_1$im][PF$_6$] (right) in dependence of the primary energy per incident atom in the primary ion cluster. The open symbols indicate the data for the doubly charged priamry ion clusters. It can be seen that the fragmentation generally decreases upon changing from primary monoatomic ions to primary cluster ions for singly and doubly charged species. Using primary cluster ions the fragmentation reaches a quite constant value, even though the surface near energy deposition increases [111, 14]. It has to be mentioned, that Bi$_3{}^+$ is slightly deviating from the other clusters. The probability for multiple collision cascades is higher using primary cluster ions causing a collisional spike event [111, 14]. These multiple cascades might have a maximum
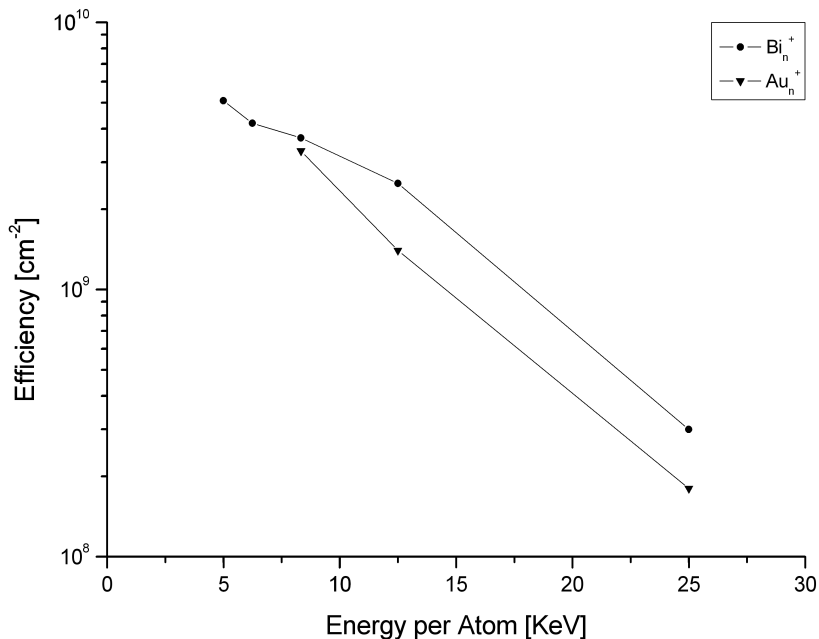
Figure 2.7: *Efficiency of Irganox 1010 in dependence of the primary energy per incident atom in the primary ion clusters Au_{1-3}^{+} and Bi_{1-6}^{+} at 25 keV primary energy.*

superposition using Bi_3^+ primary ions, a potential evidence for a collisional spike event in cluster SIMS.

2.1.6 Conclusion

Depending on which literature is read three basic approaches are mainly considered to discuss the results of cluster SIMS. These are the thermal spike model [112, 113, 109], the collisional spike model [19, 111, 14, 13] and Benninghovens precursor model [34, 1, 40]. The increase in yield can be explained by all three models, whereas the fragmentation and efficiency do not follow the usual observations for organic compounds. The sligthly increased fragmentation for Bi_3^+ might be the result of a collisional spike event. The deviation from the results for Irganox 1010 (the most intensely studied organic substance in SIMS) can be attributed on the one hand to the liquid state and
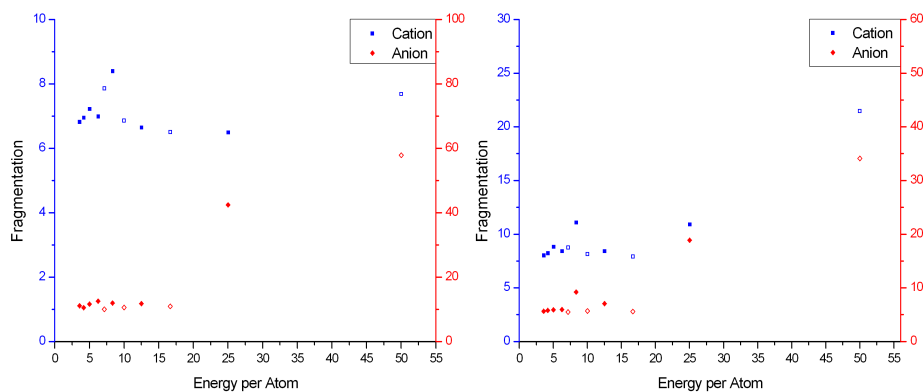
Figure 2.8: *Fragmentation of the ionic liquids [C$_4$C$_1$im][Ac] (left) and [C$_4$C$_1$im][PF$_6$] (right) in dependence of the primary energy per incident atom in the primary ion cluster.*

the ionic nature of the ionic liquids. In the liquid state the energy deposited on the surface can easily dissipated to vibrational energy and/or thermal energy without further fragmentation. The ionic nature nullifies a dependence of the ionisation probability as far as the unfragmented secondary anions and cations as well as the trimolecular secondary cluster ions, usually observed for SIMS analysis of ionic liquids [62, 15, 16]. Desortpion, fragmentation and occurence of larger secondary ion cluster can also be explained by Cooks and Busch desorption-ionisation model [37] as well as by the so called "Bubble Chamber Model" [114], which would support a thermal spike event.

2.2 Solvatochromism of Ionic Liquids

2.2.1 Introduction

Solute properties are known to be influenced by solvent molecules due to solvation. This is called a mutual interaction. The present work is based on the idea that ionic liquids are cations solvated by anions and anions solvated by cations. To show this (in this case pronounced) interaction the long time established donor-acceptor concept for solvents by Viktor Gutman is used. Neglection of this mutual influence leads to a number of solvent parameters for ionic liquids. It is shown how strong such parameters vary when the influence is taken into account.

2.2.2 Solvatochromism

Ionic liquids definitely have complex mutual interactions between the anionic and the cationic part of their composition with solutes. This gives these materials the potential to behave very differently when used as solvents compared to conventional molecular liquids. Even the simplest ionic liquids are significantly different from simple molten salts, with both the cation and anion often being polyatomic, asymmetric, organic or inorganic ions.

Each solvent ion is surrounded by a sphere of oppositely charged other solvent ions with complete dissociation, because an imaginary ion pair lacks stability as the electrostatic attractive forces between the ions of ion pair is nullified by the equal attraction of an ion with all its surrounding ions [115]. A particular property of solvents in case of ionic liquids has to be taken into account: the composition of the solute solvation shell can differ from that of the bulk solvent. This observation is called preferential solvation and leads to molecular-microscopic solute induced local inhomogeneities in multi-component solvent systems [88]. The solvent polarity expressed by the Dimroth-Reichardt scale $E_T(30)$, showed large changes for small amounts of ILs in organic solvents, indicating (as expected) that ionic liquids preferentially solvate polar molecules. This is due to a result of the competition between cation/anion and solvent/ionic liquid interactions [116]. For a full description different types of probes expressing different types of solute-

solvent interactions are needed. The widespread Dimroth-Reichardt $E_T(30)$ scale is based on betaine dyes, which are most strongly influenced by the hydrogen donor ability of a solvent, but it is not a good probe of the hydrogen bond acceptor ability, or nucleophilicity of ionic liquids.

The second solvatochromic system is based on metal complexes. The solvatochromic shift of $[Cu(acac)(tmen)][X]$ (acac - acetylacetonate, tmen - tetramethylethylenediamine, X = $[BPh_4]^-$ or $[ClO_4]^-$) is related to the donor number of a solvent and can be used as a measure of Lewis-base properties [102], whereas $[Fe(phen)_2(CN)_2]$ (phen - phenantroline) is related to the acceptor number of a solvent and is therefore useful as a measure of Lewis-acid properties [103].

In the discussion on Reichardt dye solvatochromic shifts for ionic liquids Welton pointed on the complicated cross-referenced systems [44]. It can be seen that the values are dominated by the nature of the cation. This is consistent with the expected hydrogen bond donor properties of these cations. The role of the anion is not so evident. Hence, it is clear that the effect of changing the anion depends on the nature of the cation. There is a competition between the anion and the betaine dye for the proton. Thus, the E_T values of the ionic liquids are controlled by the ability of the liquid to act as a hydrogen donor (cation effect) moderated by its hydrogen bond acceptor ability (anion effect). Hence, the difference made by changing the anion should depend on the hydrogen bond acidity of the cation. This leads to the conclusion that both, donor and acceptor numbers, must be related to the contrary attribute and that internally consistent scales using only one parameter (i.e. an invariant order) can only be obtained when contrary attribute can safely be disregarded or can be taken as a constant or low value, respectively. Using these complexes in salt solutions and considering the competition between solvent molecule and anion or cation for coordination to metal complex in solution, it is possible to determine the donor numbers of anions and acceptor numbers of cations by correlation analysis. Formally, ionic liquids can be considered as a salt solution in certain solvent. Therefore, acceptor and donor number measurements for ionic liquids must involve measurements with two different indicators and with two different reference solvents; a very weak acceptor for acceptor number measurement with $Fe(phen)_2(CN)_2$, usually

nitromethane, and very weak donor for donor number measurement with $Cu(acac)(tmen)^+$, usually dichloroethane. Solving equations 1.14 and 1.15 and inserting parameters, acceptor and donor numbers for neat ionic liquids can easily be determined:

$$AN_{IL} = \frac{A}{Ab - Ba} \left(\Delta\tilde{\nu}_{max,Cu} + \frac{a}{A} \Delta\tilde{\nu}_{max,Fe} + 1200.56 \right) \qquad (2.2)$$

$$DN_{IL} = \frac{B}{aB - bA} \left(\Delta\tilde{\nu}_{max,Cu} + \frac{b}{B} \Delta\tilde{\nu}_{max,Fe} - 2474.91 \right) \qquad (2.3)$$

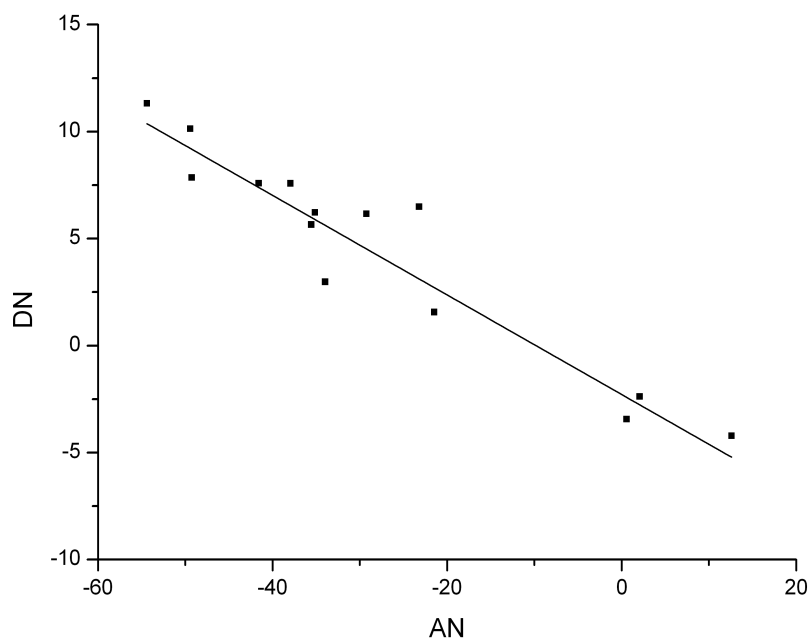### 2.2.3 Variation of the Anion

Figure 2.9: *Linear correlation of DN with AN for $[C_4C_1im][X]$, where X is the variation of the anion.*

In case of ionic liquids both the anions and the cations influence the absorption spectra of the indicator, and the summary effect can be seen. Table 2.1 summarises the absorption band maxima of the complexes and the

Table 2.1: *Absorption maxima of the solvatochromic indicators and calcu-lated donor and acceptor numbers for 1-butyl-3-methylimidazolium based neat ionic liquids.*

Cation	Anion	λ_{max}(Fe) [a]	λ_{max}(Cu)	AN	DN	δ_{H_2} [a]
		nm	nm			ppm
$C_4C_1im^+$	Cl^-	593.1		-	-	10.31
$C_4C_1im^+$	CH_3COO^-	590.0	702.0	-54.38	11.32	10.27
$C_4C_1im^+$	Br^-	590.0		-	-	9.94
$C_4C_1im^+$	CF_3COO^-	585.1	638.0 [b]	-35.15	6.23	9.74
$C_4C_1im^+$	NO_2^-	588.9	684.0	-49.44	10.14	9.68
$C_4C_1im^+$	I^-	586.2	659.0	-41.58	7.59	9.68
$C_4C_1im^+$	NO_3^-	586.9	645.0	-37.96	7.58	9.57
$C_4C_1im^+$	$n\text{-}C_8H_{18}SO_4^-$	586.2	617.0	-29.24	6.16	9.32
$C_4C_1im^+$	$CH_3SO_4^-$	587.9	596.0	-23.20	6.49	9.21
$C_4C_1im^+$	SCN^-	585.1	690.0 [c]	-49.26	7.86	9.15
$C_4C_1im^+$	$(CN)_2N^-$	584.1	641.0 [c]	-35.56	5.66	8.96
$C_4C_1im^+$	$CF_3SO_3^-$	580.0	601.5 [d]	-21.47	1.57	8.91
$C_4C_1im^+$	BF_4^-	578.0	540.0 [b]	2.07	-2.38	8.64
$C_4C_1im^+$	NTf_2^-	576.0	546.0	0.56	-3.44	8.56
$C_4C_1im^+$	PF_6^-	577.0	516.5 [e]	12.59	-4.21	8.38

[a] values from reference [117]; [b] values from reference [118]; [c] values from reference [119]; [d] values from reference [120]; [e] values from reference [121]

obtained donor and acceptor numbers in neat $C_4C_1im^+$ based ionic liquids. Figure 2.9 shows a linear dependence of the donor and acceptor number. In conventional solvents where a solvent molecule can act as donor and/or as acceptor, e.g. methanol is a strong acceptor but can also donate electrons from the lone pairs of the oxygen, and no such correlation can be found. In contrast, in ionic liquids the cation is only acting as acceptor and the anion only as donor. The negative AN (DN) might imply, that the cation (the anion) is actually a donor, but this seems to be a matter of referencing. In the donor-acceptor approach an arbitrarily referencing system is used. DN represents the negative ΔH value of the reaction of $SbCl_5$ with a solvent molecule L to the adduct $SbCl_5 \cdot L$ in high dilution of DCE. Here DCE has been defined as reference solvent with DN = 0 (despite the fact that it itself shows very low donor ability, which was neglected). For commonly used solvents this reaction is exotherm so that ΔH turns out to be positive and usual values are in the range between 0 (DN) and 100. AN on the contrary is defined as the NMR chemical shift of the ^{31}P nucleous in Et_3PO in the respective solvent (undiluted). To obtain comparable values with the DN scale this NMR shifts (measured in ppm) have been re-normated to become 100 for the (DN-important) probe $SbCl_5$. Negative AN (DN) just means, that the ionic liquid in question is a weaker acceptor (donor) than nitromethane (dichloroethane). For example, in acetone (AN = 12.5) Cl^- is as strong donor (DN = 38.5); upon changing to a solvent with a higher AN the donicity of Cl^- shrinks (DN in methanol is only 22.6). In $[C_4C_1im][Cl]$ the solvation shell consists of $C_4C_1im^+$ cations which are accepting most of the electrons from Cl^- and the cation is therefore a very weak acceptor and the Cl^- is a weaker donor than in acetone or methanol. $[BF_4]^-$ exhibits in acetone a donor strength of 8.33 and in methanol -7.56; in $C_4C_1im^+$ the DN is -4.18, having approximately the same donicity as $[CF_3SO_3]^-$ in water (DN = 4.0) [102].

Correlation of DN with NMR Shifts

It has been shown that the solvent parameter β is linearly correlated to the H-2 proton NMR shift δ_{H_2} of $C_4C_1im^+$ based ionic liquids [117]. In our con-

sideration the DN value should also be correlated linearly. Figure 2.10 shows such a behaviour. The electronic environment of the "theoretically isolated" cation $C_4C_1im^+$ is fixed. Any alteration on the electron density is therefore dependent on the nature of the anion. As there is no additional NMR
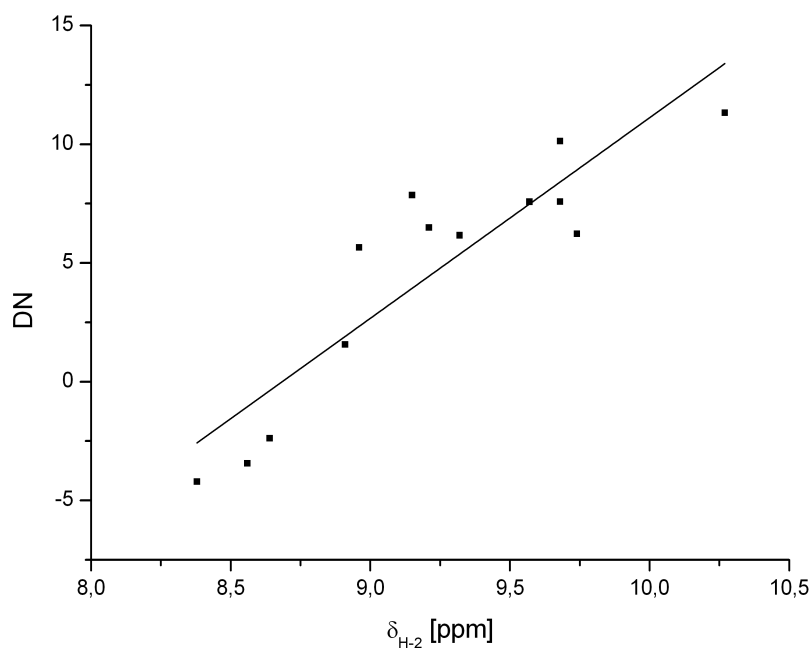

Figure 2.10: *Linear correlation of DN with δ_{H-2} for [C_4C_1im][X], where X is the variation of the anion.*

sensitive probe molecule in the ionic liquid (the shift of a NMR probe like triethylphosphine oxide should be dependent on donor and acceptor properties as do the solvatochromic indicators) the donor properties of the anion can be screened solely by the shift of H-2. From a linear correlation of δ_{H_2} with DN and a linear correlation of AN with DN, it is possible to determine donor and acceptor numbers for (in this case) $C_4C_1im^+$ based ionic liquids where a solvatochromic approach is not feasible (e.g. high melting, colored or hydrolysis sensitive ionic liquids):

$$DN \; = \; k_1 \; * \; \delta_{H_2} \; + \; d_1 \qquad (2.4)$$

Table 2.2: *Calculated donor and acceptor numbers for 1-butyl-3-methylimidazolium based neat ionic liquids based on the correlation of δ_{H_2} with DN and AN with DN.*

Cation	Anion	X_{AlCl_3}	δ_{H_2} [a]	AN	DN
			ppm		
$C_4C_1im^+$	$SnCl_3^-$		9.24	-28.29	4.52
$C_4C_1im^+$	BBr_4^-		9.04	-21.34	2.83
$C_4C_1im^+$	$TiCl_5^-$		8.99	-19.61	2.41
$C_4C_1im^+$	$SbCl_6^-$		8.68	-8.83	-0.22
$C_4C_1im^+$	I_3^-		8.66	-8.14	-0.39
$C_4C_1im^+$	$SnCl_5^-$		8.59	-5.71	-0.98
$C_4C_1im^+$	WCl_7^-		8.50	-2.58	-1.74
$C_4C_1im^+$	$MoCl_6^-$		8.06	12.71	-5.47
$C_4C_1im^+$	I_5^-		5.52	100.98	-26.97
$C_4C_1im^+$	$AlCl_4^-$	0.2	10.29	-64.78	13.41
$C_4C_1im^+$	$AlCl_4^-$	0.4	10.05	-56.44	11.38
$C_4C_1im^+$	$AlCl_4^-$	0.6	9.62	-41.50	7.74
$C_4C_1im^+$	$AlCl_4^-$	0.8	9.06	-22.04	3.00
$C_4C_1im^+$	$AlCl_4^-$	1	8.39	1.24	-2.67
$C_4C_1im^+$	$Al_2Cl_7^-$	1.2	8.37	1.94	-2.84
$C_4C_1im^+$	$Al_2Cl_7^-$	1.4	8.34	2.98	-3.10
$C_4C_1im^+$	$Al_2Cl_7^-$	1.6	8.30	4.37	-3.44
$C_4C_1im^+$	$Al_2Cl_7^-$	1.8	8.27	5.41	-3.69
$C_4C_1im^+$	$Al_2Cl_7^-$	2	8.23	6.80	-4.03

[a] values from reference [122]

$$AN = k_2 * DN + d_2 \qquad (2.5)$$

with $k_1 = 8.4667$, $d_1 = $ -73.7101, $k_2 = $ -4.1043 and $d_2 = $ -9.7339. Table 2.2 summarises the results calculated from the NMR shift. These are in agreement with the results for the anion variation of $C_4C_1im^+$ ionic liquids determined by solvatochromic indicators. In the series of chloroaluminate anions it can be seen, that an ionic liquid with a low mole fraction of $AlCl_3$ exhibits strong donating abilities, whereas the donor properties are reduced as the mole fraction rises (i.e. the "basicity" of the anion decreases by increasing the amount of the Lewis acid $AlCl_3$).

2.2.4 Variation of the Cation

Table 2.3: *Absorption maxima of the solvatochromic indicators and calculated donor and acceptor numbers for bis(trifluoromethylsulfonyl)imide based neat ionic liquids.*

Cation	Anion	λ_{max}(Fe)	λ_{max}(Cu)	AN	DN
		nm	nm		
$N_{1,1,1,4}^+$	NTf_2^-	573.2	546.0 [a]	1.89	-5.35
$S_{2,2,2}^+$	NTf_2^-	585.9	591.3	-4.00	3.09
C_4py^+	NTf_2^-	587.8	548.0 [a]	-5.60	4.41
$C_1C_4pyrr^+$	NTf_2^-	586.1	545.0 [b]	-3.64	3.17
C_8thiaz^+	NTf_2^-	580.6	573.7	4.60	-1.10
$P_{6,6,6,14}^+$	NTf_2^-	597.3	669.2	-32.55	13.08
$chol^+$	NTf_2^-	553.0	535.8	32.61	-21.98

[a] values from reference [118]; [b] values from reference [123]

Figure 2.11 shows for the variation of the cation two different correlations. Less steric demanding cations ($N_{1,1,1,4}^+$, $S_{2,2,2}^+$, C_4py^+, $C_1C_4pyrr^+$, $C_2C_1im^+$, $C_4C_1im^+$, $C_6C_1im^+$ and $C_8C_1im^+$) give a steeper slope than cations with a high steric demand ($P_{6,6,6,14}^+$, C_8thiaz^+). Altough choline is not steric demanding it do not correlate with the other less steric demanding cations. The reason for this coud be the functional group OH^- which gives an additional

possibility of interaction (e.q. hydrogen bridge bonding, interaction of the free electron pairs of the oxygen) with a given anion. The current state of knowledge from the available data allows the conclusion that the influence of the cation is driven by steric hindrance and the nature (and the number of) additional functional groups.
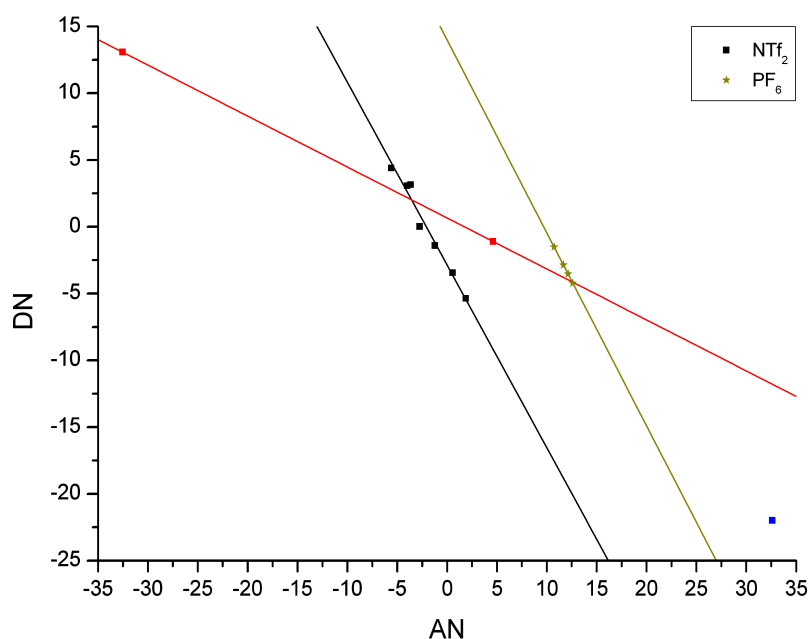

Figure 2.11: *Linear correlation of DN with AN for [C][NTf$_2$] (squares) and [C][PF$_6$] (stars), where C is the variation of the cation.*

2.2.5 Variation of the Side Chain Length

The interpretation of the influence of the side chain length is not straight forward. Considering a virtual, from anions unaffected C$_n$mim cation, a linear decrease of AN would be expected due to the increasing inductive effect of a longer side chain. From the available data the results show local minima and maxima respectively for DN and AN in dependence of the chain length. The DN and AN values are still linearly correlated but not in the
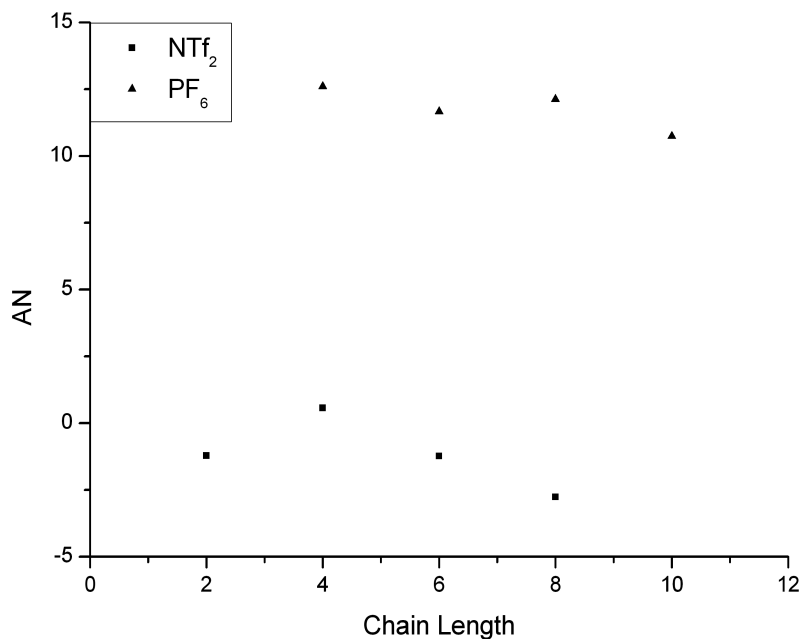
Figure 2.12: *Dependence of the side chain length in $[C_nC_1im][NTf_2]$ and $[C_nC_1im][PF_6]$ on AN.*

order as it would be expected from the increasing inductive effect (see Figure 2.12). Despite the different anion size and donor strength from PF_6^- and NTf_2^- a parallel displacement of the linear correlation can be observed. Influences from sterical hindrance of the side chain or the size of the anion $(r_{PF_6} \geq r_{NTf_2^-})$ and an ordering effect from side chain stacking must be taken into account. More data for different anions and especially for the structure of ionic liquids in the liquid state is needed for a correct interpretation.

Acceptor numbers determined from Kamlet-Taft parameters [117], Raman spectroscopy [124] and ^{31}P-NMR [125, 126] were already reported for ionic liquids. Table 2.5 compiles some values for AN from literature. The apparent donor and acceptor numbers established by our approach do not resemble the previously reported values for ionic liquids. The main difference lies in the mutual influence of cations and anions, which are not taken into account by the other authors. Calculating acceptor numbers without considering the

Table 2.4: *Absorption maxima of the solvatochromic indicators and calculated donor and acceptor numbers for imidazolium based neat ionic liquids with fixed anion.*

Cation	Anion	λ_{max}(Fe)	λ_{max}(Cu)	AN	DN
		nm	nm		
$C_4C_1im^+$	PF_6^-	577.0	516.5	12.61	-4.23
$C_6C_1im^+$	PF_6^-	579.0	516.5	11.66	-2.87
$C_8C_1im^+$	PF_6^-	578.0	516.5	12.13	-3.54
$C_{10}C_1im^+$	PF_6^-	581.1	516.5	10.74	-1.53
$C_2C_1im^+$	NTf_2^-	579.0	547.0	-1.21	-1.41
$C_4C_1im^+$	NTf_2^-	576.0	546.0	0.58	-3.46
$C_6C_1im^+$	NTf_2^-	579.0	547.0	-1.23	-1.38
$C_8C_1im^+$	NTf_2^-	581.1	548.5	-2.75	0.03

influence of the counter ion (using equation 1.12) AN's comparable to values determined by other methods are obtained. Polarity scales like Kamlet-Abboud-Taft and Reichardt's E_T do not consider this ionic interaction. The same is true for the calculation of AN for ionic liquids by ^{31}P-NMR. Any probe molecule dissolved in an ionic liquid is dependent on the donor and acceptor properties of the ionic liquid. Therefore the chemical shift (δ_P) of the probe triethylphosphine oxide is dependent on the solvent used. Using conventional solvents the donor property of a solvent is negligible, but not in ionic liquids, were the solvation shell of the probe molecule coordinated to the cation (Lewis acid) consists of anions (Lewis base). Therefore all previously reported acceptor numbers are to high since the lowering effect of the anion is not considered. To visualize the importance of mutual interactions to acid-base considerations, one might compare AN and DN (representing Lewis acidities and basicities) with "simple" Brønsted relations. Taking H_3BO_3 for example, which is a very weak acid an aqueous solutions (i.e. its grade of deprotonation is very low) becomes strongly deprotonated in liquid ammonia and is acting in reactions accordingly in such media. On the other hand, strong bases will loose their basicity in liquid ammonia. The situation ob-

Table 2.5: *Comparison of AN values determined by different approaches*

Cation	Anion	AN ref. [126]	AN ref. [117]	AN calc. eq. 1.12	AN ref. [124]	AN calc. eq. 2.2
$C_4C_1im^+$	NTf_2^-		30.05	25.99	25.20	2.37
$C_4C_1im^+$	BF_4^-		29.26	28.77	26.90	4.55
$C_4C_1im^+$	PF_6^-		29.66	29.18	27.70	12.37
$C_4C_1im^+$	Cl^-		23.41	AN	26.9	AN
$C_8C_1im^+$	$Cl\text{-}AlCl_3^-$	91.81				
$C_8C_1im^+$	$Cl\text{-}GaCl_3^-$	45.85				
$C_8C_1im^+$	$Cl\text{-}InCl_3^-$	57.11				

viously becomes reversed using acidic media like water-free acetic acid as solvents.

These results indicate, that ionic liquid cations and anions cannot be discussed separetely; the mutual influence of the counter ion has to be considered. That means, that the acceptor (donor) properties are not only a function of the cation (anion), as it is usually suggested for the Kamlet-Taft parameters α and β, but also a function on the anion (cation). Increasing the basicity, e.g. from $[BF_4]^-$ to $[Cl]^-$ the accepting ability is reduced. Increasing the acidity, e.g. from $[S_{2,2,2}]^+$ to $[chol]^+$ the donating abilitiy of $[NTf_2]^-$ is reduced.

2.2.6 Conclusion

DN and AN of cations and anions are influenced by the solvent [103, 102] Based on this fact and considering ionic liquids as cations (anions) solvated by anions (cations) a simple concept of mutual interactions was developed. For solvent describing scales this has not been taken into account (as for most reactions this can be neglected), however, it leads to the fact that basicity and acidity related scales are usually not in a simple relationship. For example, without this mutual interaction DN and AN are not simply related (for example linearly dependent) to each other like pK_A and corresponding pK_B values are ($pK_A + pK_B = pK_{Solvent}$ (i.e. the negative log of the ion-product)

for protic solvents. Frequently the polarity of ionic liquids is described to behave like conventional solvents [127] (depending on the ion combination) e.g. $C_4C_1im^+$ based ionic liquids are usually compared to lower alcohols [123]. Here we have to disagree with the literature, as our results clearly show that ionic liquids cannot be considered to behave like conventional solvents, they have to be regarded as a unique class of solvents. It has been shown, that Kamlet-Taft solvent descriptors do not offer a correlation with the Eyring activation parameters [128]. Recently in a study of salts (Kosover's salt) in ionic liquids contradictory results arose [129]; it has been indicated from measurements of absorption maxima that ionic liquids are of moderate polarity whereas absorptivity studies of the same ionic liquids show that they are highly polar. It was stated, that these results will require new models of solvation and polarity. The proposed donor-acceptor approach to ionic liquids might give some new insights for a better understanding of ionic liquids and chemistry carried out in ionic liquids.

2.3 SIMS Fragmentation of Ionic Liquids

2.3.1 Introduction

A systematic study with different room temperature ionic liquids (variation of the anion, variation of the cation and variation of the side chain length) was carried out by means of time-of-flight secondary-ion-mass-spectrometry in positive and negative ion mode. Thereby a variation of the anion in 1-butyl-3-methylimidazolium based ionic liquids, a variation of the cation, including a variation of the side chain length, in bis(trifluoromethylsulfonyl)imide based ionic liquids was taken into account. The compounds were measured under bismuth cluster ion (Bi_7^+) bombardment, and spectral information and general rules for the fragmentation pattern are presented. Evidence for cation-anion interactions (e.g. hydrogen bonding), due to high molecular secondary cluster ions, could be found. The interaction strength could be estimated by ToF-SIMS *via* correlation of the secondary anion intensity to secondary cluster ion intensity ratio with solvent parameters.

2.3.2 Mass Spectra - Fragmentation Pattern

Table 2.6 gives an overview of the measured samples and their abbreviations used. Figure 2.13 shows SIMS spectra of $[C_4C_1im][NTf_2]$ recorded in positive and negative ion mode. Each spectrum displays the mass range of interest containing the main ions of interest. The insets emphasise high molecular mass clusters with low relative intensities. The positive spectrum is dominated by RTIL related peaks, whereas the most intensive positive ion peak is that of the intact 1-butyl-3-methylimidazolium cation. All peaks in the positive spectrum of $[C_4C_1im][NTf_2]$ in the range up to m/z = 68 correspond to alkyl fragments resulting from a cleavage of the alkyl groups and the imidazolium ring. The peaks in the range from m/z = 69 to m/z = 140 can be assigned to the heterocyclic ring showing fragment cascades resulting from loss of C_xH_y. The peak at m/z 558 corresponds to the trimolecular cluster $[(CA)C]^+$, where C corresponds in general to the unfragmented cation and A to the unfragmented anion.

Table 2.6: *Ionic liquids used and abbreviation thereof.*

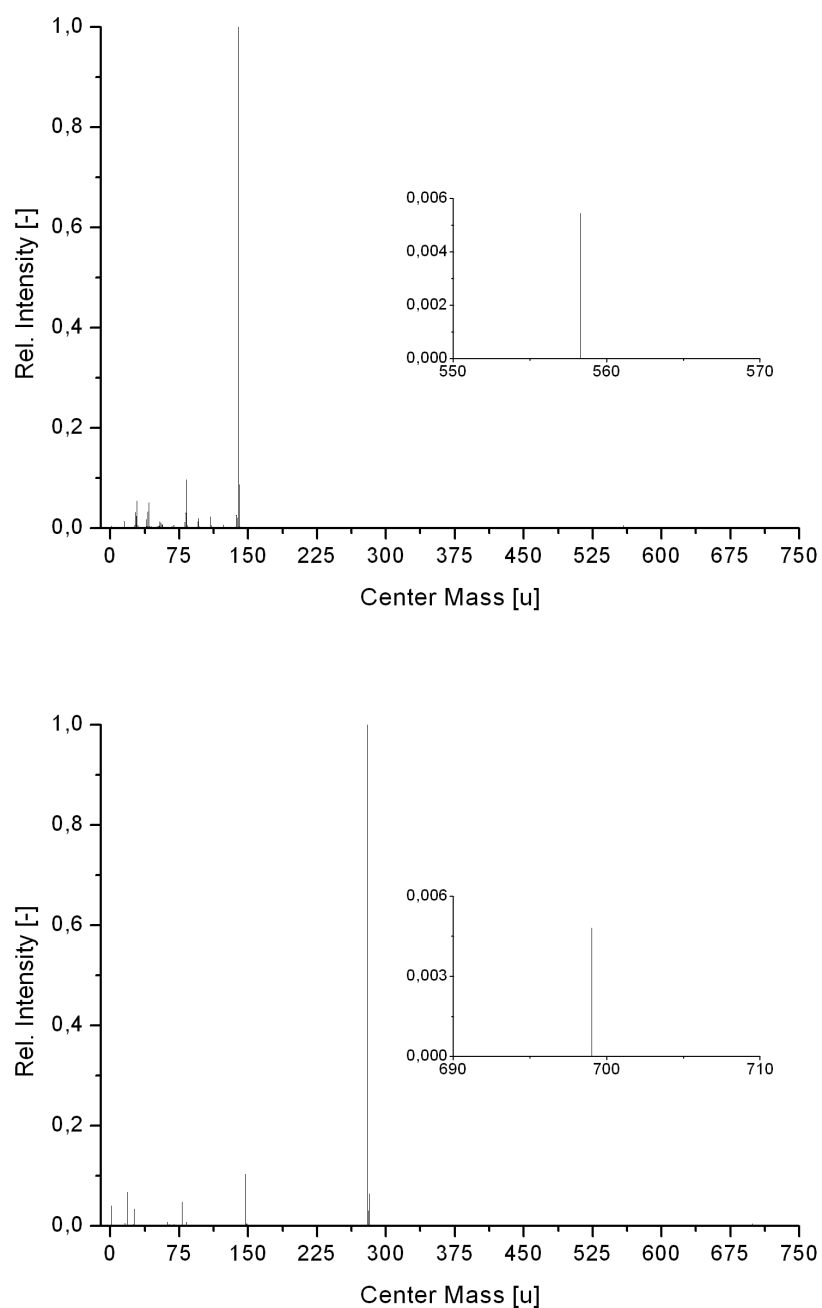| Cation	Anion	C^+	A^-
1-butyl-3-methylimidazolium	acetate	$C_4C_1im^+$	CH_3COO^-
1-butyl-3-methylimidazolium	iodide	$C_4C_1im^+$	I^-
1-butyl-3-methylimidazolium	nitrate	$C_4C_1im^+$	NO_3^-
1-butyl-3-methylimidazolium	methylsulfate	$C_4C_1im^+$	$CH_3SO_4^-$
1-butyl-3-methylimidazolium	trifluoromethansulfonate	$C_4C_1im^+$	$CF_3SO_3^-$
1-butyl-3-methylimidazolium	tetrafluoroborate	$C_4C_1im^+$	BF_4^-
1-butyl-3-methylimidazolium	bis(trifluoromethylsulfonyl)imide	$C_4C_1im^+$	NTf_2^-
1-butyl-3-methylimidazolium	hexafluorophosphate	$C_4C_1im^+$	PF_6^-
1-butyl-3-methylimidazolium	2(2-methoxyethoxy)ethylsulfate	$C_4C_1im^+$	$C_1OC_4SO_4^-$
butyltrimethylammonium	bis(trifluoromethylsulfonyl)imide	$N_{1,1,1,4}^+$	NTf_2^-
tributylmethylammonium	bis(trifluoromethylsulfonyl)imide	$N_{1,4,4,4}^+$	NTf_2^-
methyltrioctylammonium	bis(trifluoromethylsulfonyl)imide	$N_{1,8,8,8}^+$	NTf_2^-
triethylsulfonium	bis(trifluoromethylsulfonyl)imide	$S_{2,2,2}^+$	NTf_2^-
butylpyridinium	bis(trifluoromethylsulfonyl)imide	C_4py^+	NTf_2^-
1-butyl-1-methylpyrrolidinium	bis(trifluoromethylsulfonyl)imide	$C_4C_1pyrr^+$	NTf_2^-
3-octylthiazolium	bis(trifluoromethylsulfonyl)imide	C_8thiaz^+	NTf_2^-
trihexyltetradecylphosphonium	bis(trifluoromethylsulfonyl)imide	$P_{6,6,6,14}^+$	NTf_2^-
choline	bis(trifluoromethylsulfonyl)imide	$chol^+$	NTf_2^-
1-ethyl-3-methylimidazolium	bis(trifluoromethylsulfonyl)imide	$C_2C_1im^+$	NTf_2^-
1-hexyl-3-methylimidazolium	bis(trifluoromethylsulfonyl)imide	$C_6C_1im^+$	NTf_2^-
3-methyl-1-octylimidazolium	bis(trifluoromethylsulfonyl)imide	$C_8C_1im^+$	NTf_2^-
tributylmethylammonium	dibutylphosphate	$N_{1,4,4,4}^+$	dbp^-
choline	L-(+)-lactate	$chol^+$	lac^-

Figure 2.13: *1-Butyl-3-methylimidazolium bis(trifluoromethylsulfonyl)imide measured with Bi_7^+ in positive (top) and negative (bottom) ion mode.*

This fragmentation pattern is in principle representative for all 1-alkyl-3-methylimidazolium based ionic liquids. The main difference is the position of the quasimolecular peak and the unfragmented cation; the intervall between the unfragmented methylimidazolium cation (m/z = 83) and the unfragmented 1-alkyl-3-methylimidazolium cation is dominated by peaks resulting from a successive loss of C_xH_y from the alkyl side chain. The range below m/z = 83 remains comparable as it only consists of fragments from the imidazolium ring and the alkyl side chain.

The fragmentation of the ammonium based ionic liquids $[N_{1,1,1,4}][NTf_2]$, $[N_{1,4,4,4}][NTf_2]$ and $[N_{1,8,8,8}][NTf_2]$ is dominated by a loss of alkanes and alkenes originating either from a cleavage at the N-atom or from a cleavage of the side chains. Figure 2.14 shows the most likely fragmention pathway according to the masses occuring in the mass spectra. Other structural isomers would of course be possible, especially in SIMS, where the ionisation energy is very high. However, such isomers where a further fragmentation would not result in the measured masses and isomers that result directly in a smaller mass in the spectra by avoiding representative fragments, were excluded. The low mass range (below m/z = 60) is identical concerning daughter ions origination from the ammonium cations. This range also contains all alkyl fragments. The mass range from m/z = 60 up to the unfragmented cation shows mass fragments arising from loss of C_xH_y of the cation. The high mass range contains the trimolcular clusters $[(CA)C]^+$ in varying intensities (and ion yields). The fragmentation of $[chol][NTf_2]$ is similar to that of $[N_{1,1,1,4}][NTf_2]$. The difference is, that the side chain containing the functional group is removed first, leaving directly the daugther ion at m/z = 58. $[C_4C_1pyrr][NTf_2]$ in turn looses first parts of the side chain leaving the ring undestroyed before it joins the fragmentation pathway of the other ammonium based cations at m/z = 44 and m/z = 46.
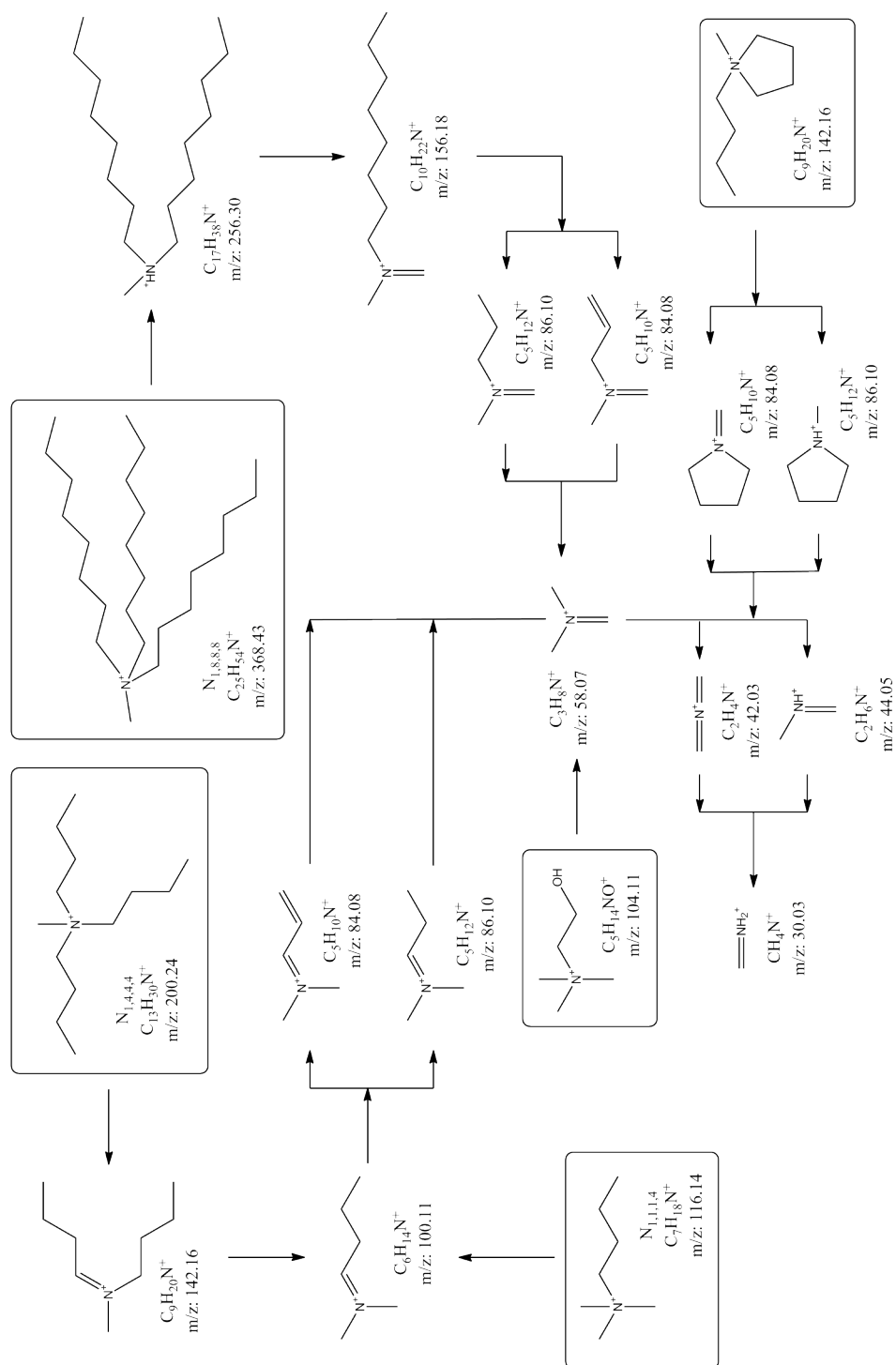
Figure 2.14: *Proposed fragmentation pathway of the cations of the ammonium based ionic liquids.*

[C_4py][NTf$_2$] and [C_8thiaz][NTf$_2$] have also certain features in common. From both cations the side chain is cleaved first by loss of C_xH_y appearing in the medium mass range. However, before the side chain is lost completely, a methanide group is preserved at the N-atom and the usually localised charge is delocalised over the heteroaromatic ring (see Figure 2.15 and 2.16). The unfragmented heteroaromatic ring is found in both mass spectra. The low mass range contains daugther ions belonging to the side chain and the fragmented heteroaromatic ring. The high mass range contains again the trimolcular cluster at m/z = 552 ([C_4py][NTf$_2$]) and m/z = 676 ([C_8thiaz][NTf$_2$]) respectively.
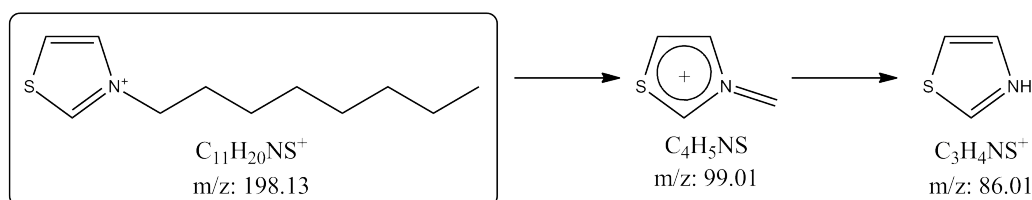

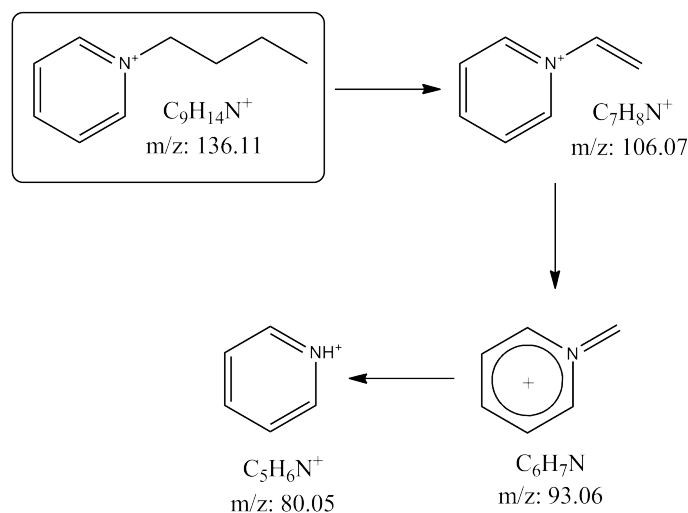Figure 2.15: *Proposed fragmentation pathway of the thiazolium cation .*

Figure 2.16: *Fragmentation pathway of the pyridinium cation .*

The sulfonium cation S$_{2,2,2}$$^+$ of the ionic liquid [S$_{2,2,2}$][NTf$_2$] looses successively its side chains (see Figure 2.17. Again the trimolecular cluster can be found at m/z = 518.

$C_6H_{15}S^+$
m/z: 119.09
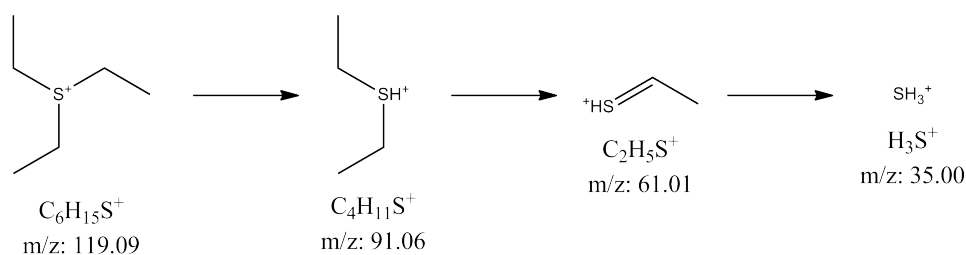
$C_4H_{11}S^+$
m/z: 91.06

$C_2H_5S^+$
m/z: 61.01

H_3S^+
m/z: 35.00

Figure 2.17: *Proposed fragmentation pathway of the sulfonium cation .*

Ionic liquids with sulfate or sulfonate anions like in $[C_4C_1im][CH_3SO_4]$, $[C_4C_1im][C_1OC_4SO_4]$ or $[C_4C_1im][CF_3SO_3]$ have also a few similarities in the fragmentation pattern (see 2.18).

$C_5H_{11}O_6S^-$
m/z: 199.03

$C_4H_7O_6S^-$
m/z: 183.00

$C_4H_7O_5S^-$
m/z: 167.00

SO_3^-
O_3S^-
m/z: 79.96

HO_4S^-
m/z: 96.96

$C_2H_3O_4S^-$
m/z: 122.98

$C_2H_3O_5S^-$
m/z: 138.97

$CF_3O_3S^-$
m/z: 148.95

$CH_3O_4S^-$
m/z: 110.98
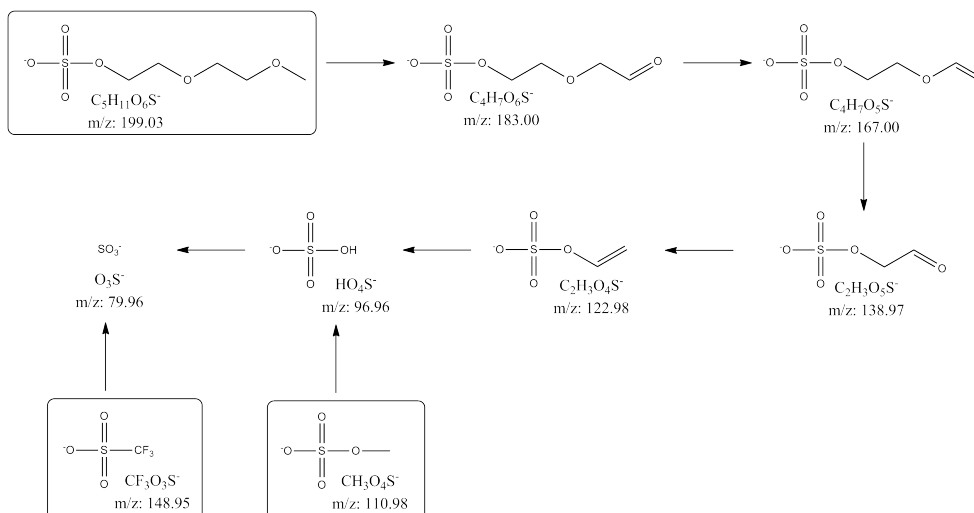
Figure 2.18: *Proposed fragmentation pathway of the sulfate and sulfonate anions.*

$CF_3SO_3^-$ looses its CF_3 group to leave SO_3^- at m/z = 80, whereas in $CH_3OSO_3^-$ the C-O bond is cleaved first resulting in an HSO_4^- daughter ion at m/z = 97, which is further fragmented to give SO_3^-. In anions with a longer side chain like in $C_1OC_4SO_4^-$ the side chain is consecutively shortened by loss of C_xH_y and O to give the intermediates at m/z = 183, m/z = 167, m/z = 139 and m/z = 123. It then joins the fragmentation pathway for the methylsulfate. Trimolecular clusters of the type $[(AC)A]^-$ were found at m/z = 537 ($[C_4C_1im][CF_3SO_3]$), m/z = 361 ($[C_4C_1im][CH_3SO_4]$) and m/z = 437

$([C_4C_1im][CF_3SO_3])$.

$C_3H_5O_3^-$
m/z: 89.02

$C_3H_3O_2^-$
m/z: 71.01

$C_2H_3O_2^-$
m/z: 59.01

CHO_2^-
m/z: 45.00

$C_3H_5O_2^-$
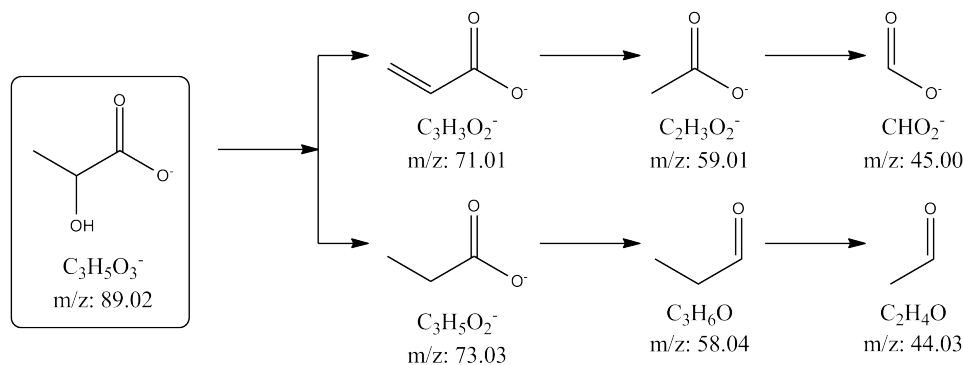m/z: 73.03

C_3H_6O
m/z: 58.04

C_2H_4O
m/z: 44.03

Figure 2.19: *Proposed fragmentation pathway of the lactate anion.*

The fragmentation of lactate is shown in Figure 2.19. In a first step the functional group OH is separated to give either a daughter ion with a terminal double bond at m/z = 71 or without the double bond (m/z = 73). The degaradation can then proceed as shown in Figure 2.19 and all presented fragment ions can be found in the corresponding mass spectrum. The daughter ion at m/z = 59 is conform to the acetate ion. This is also the starting point for the fragmentation of the acetate anion. In both ionic liquids, $[C_4C_1im][CH_3COO]$ and [chol][lac], the trimolecular cluster $[(AC)A]^-$ is found at m/z = 257 and m/z = 282 respectively. In $[C_4C_1im][CH_3COO]$ even a higher cluster of the general form $[(AC)_2A]^-$ can be found as well as a trimolecular cluster of the form $[(AH)A]^-$, where H is a proton. Both cluster occurences can be attributed to the high basicity of the acetate anion (compared to the other anions); the second cluster is most probably given by hydrogen bridge-bonding of the two anions.

The low mass range up to m/z = 300 of the negative spectra of $[C_4C_1im][NTf_2]$ consists of fragments resulting from a single-bond cleavage of the intact anion. The degradation pattern can be explained as seen in Figure 2.20. First CF_3SO_2 is separated to form the peak at m/z = 147 and after a loss of CF_3, the last daugther ion at m/z = 78 is formed leaving the NSO_2^- anion. In the high mass range the negative trimolecular cluster is found at m/z = 699.

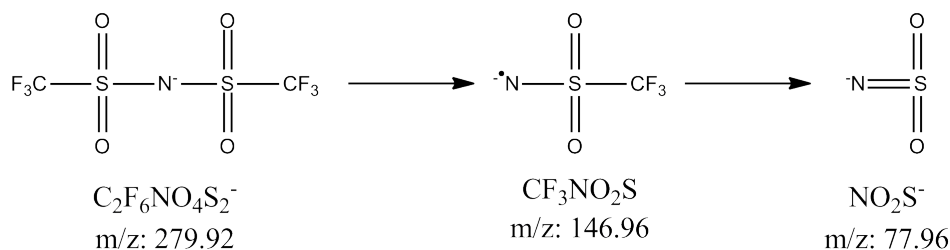The dibutylphosphate anion in $[N_{1,4,4,4}][dbp]$ looses successively its two

Figure 2.20: *Proposed fragmentation pathway of the bis(trifluoromethylsulfonyl)imide anion.*

butyl side chains by elimination of C_xH_y giving the low intensity daughter ions between m/z = 90 and m/z = 200. The resulting PO_3^- at m/z = 79 is then further decomposed to PO_2^- at m/z = 63. The negative trimolecular cluster is again found at m/z = 618.
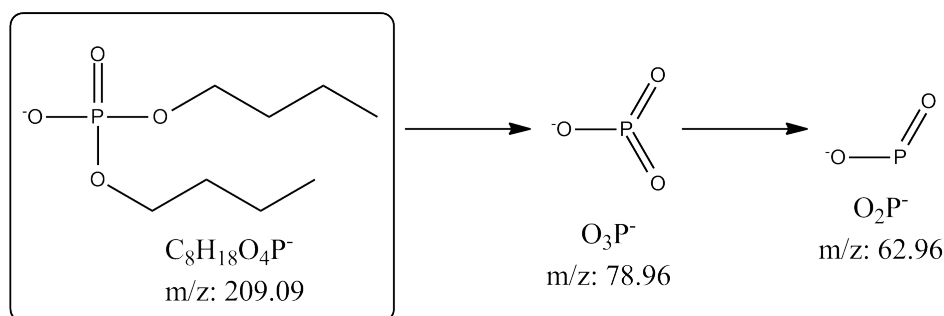
Figure 2.21: *Proposed fragmentation pathway of the dibutylphosphate anion.*

The inorganic anions BF_4^-, PF_6^-, NO_3^- and I^- have rather simple mass spectra. The negative trimolecular cluster is found for all of these anions with the corresponding cation $C_4C_1im^+$. Degradation product like $BF_3^{-\cdot}$ or $PF_5^{-\cdot}$ can be found, altough with negligible intensities and ion yields. The iodide anion shows signals for $I_2^{-\cdot}$ and I_3^- at m/z = 253.8 and m/z = 380.7.

2.3.3 Occurence of Cluster Ions

It can be seen, that trimolecular secondary cluster ions (and in some cases even larger cluster ions) occur in all investigated ionic liquids in positve and negative ion mode. This is mainly attributed to intermolecular interactions,

such as hydrogen bonding, electrostatic (coulomb) and Van der Vaals interactions. It is evident, that hydrogen bonding can occur in ionic liquids, especially in ionic liquids with proton donating functional groups or other with acidic protons like 1,3-dialkylimidazolium based ones. From studies on the molecular structure of ionic liquids in solid and liquid phase, it is proposed that "pure" imidazolium ionic liquids can be regarded as polymeric hydrogen-bonded supramolecules and should be, in some cases, considered as nanostructured materials with polar and non-polar regions rather than homogeneous solvents [130]. Such hydrogen bonding is demonstrated by an increase of chemical shift with increasing anion basicity (increasing H-bonding ability) in ^{1}H-NMR spectroscopy [131], by appearance of characteristic hydrogen bonding bands in IR spectroscopy [132, 133] and single crystal diffraction [133]. Also computational methods, such as semi-empirical [134], ab initio [134, 135, 136, 137] and density functional theory methods [135, 138], were also used to describe the structure of these substances in the gas phase as well as in the liquid phase. They state, that the anion in 1-butyl-3-methylimidazolium based ionic liquids is located in hydrogen bonding positions with the ring protons (particularly H-2) and to a certain extent to the alkyl protons of the side chains. For example, the cation can form a hydrogen bond with up to three halide ions [138]. Due to the ability of the ionic liquids to form hydrogen bonds they can organise as clusters through association of the imidazolium cation with the anion. It is not clear from theoretical approaches if the ionic liquid form trimeric ring clusters or long chains [135], since the ring trimer is calculated to be as stable as a nonamer chain. It is also argued that such a supramolecular structure is mantained in the gas phase by the appearance of large cluster ions of the type $[(C)_x(A)_{x-n}]^{n+}$ and $[(C)_{x-n}(A)_x]^{n-}$ (x, n = 1, 2, 3, ... and x n) during electrospray ionisation mass spectrometry [139]. However such large cluster ions also occur in the mass spectrometric analysis (FAB [140], SIMS [141] and ESI [142]) of purely inorganic salts (alkali salts), where no hydrogen bonding can occur. Therefore such a conclusion is daring considering the energy of hydrogen bonding (approx. 0.1 eV to 2.0 eV) compared to ionic interactions (approx. 6 eV up to several hundred eV). On this basis it is doubtful that hydrogen bonding plays a major role in the occurence of large cluster ions

in the mass spectrometric analysis of the ionic liquid gas phase. Hydrogen bonding can have a certain influence on the cation-anion interaction in tri-molecular clusters and is evidenced especially in mixed clusters [143], but they are too weak to solely explain the occurence of large cluster ions in ESI. Still the appearance of ionic liquid cluster ions in ESI [139, 143, 144], FAB [145] and SIMS [62, 15, 16] is not in contradiction to the previously calculated organisation of ionic liquids in the condensed phase, where hydrogen bonds certainly influence the physicochemical properties. The energy deposition on the surface in ToF-SIMS experiments is very high, and possible hydrogen-bonded long chain molecules are easily cleaved to smaller oligomers. It is therefore not possible to determine whether a trimeric ring or a long chain polymer is present. ToF-SIMS and FAB-MS results would suggest both, the presence of ring clusters as well as long chains, whereas ESI-results support the theory of supramolecular chains.

2.3.4   Mass Spectrometric Interaction Scale

The knowledge of cation-anion interaction strength in ionic liquids is funda-mental for understanding the properties of pure and dissolved ionic liquids. It may also provides information on the mechanism of chemical reactions carried out in ionic liquids. The interaction strenght is mainly attributed to coulomb interactions. Additionally, Van der Vaals interaction between alkyl chains, $\pi - \pi$ stacking and hydrogen bonds are also present in the condensed phase. For a mass spectrometric interaction scale, where with gas phase ions is dealt , only electrostatic interaction and hydrogen bonding have an effect in the trimolecular clusters. The interaction strength of ionic liquids has also been investigated by means of ESI-MS [139, 143, 144]. In these stud-ies a wide range of ionic liquids were investigated by mass selection of the isolated trimolecular cluster and subsequent collision induced dissociation. Mixed trimolecular clusters, i.e. a cluster with one cation (anion) and two different anions (cations), were also analysed to get a qualitative order of intrinsic strength by comparing the relative abundances of the mixed anions or cation. To build up a qualitative order of intrinsic cation-anion strength, the signal intensity ratio of the anion (cation) and the negative (positive) tri-

molecular cluster is investigated. This takes fluctuations of the primary ion gun and the measuring system into account and enhances the reproducibility of the SIMS results. During a typical SIMS experiment a certain energy is deposited on the surface by the primary ions. This leads to a decay of the higher structure in the liquid phase and the interaction strength can then be estimated qualitatively on the basis of the afore mentioned intensity ratio. The SIMS mass spectra of all investigated ionic liquids can be found in the appendix. The intensity ratios are summarised in Table 2.7 for the determination of the interaction strength of anions towards $C_4C_1im^+$ and in Table 2.8 for cations towards NTf_2^-. The increasing intensity ratio reflects the weaker

Table 2.7: *Intensity ratio of different anions and negative trimolecular cluster with fixed cation. The intensities at FWHM were used to calculate the ratio.*

Cation	Anion	$I_{[A]^-}/I_{[(AC)A]^-}$
$C_4C_1im^+$	CH_3COO^-	18.98
$C_4C_1im^+$	NO_3^-	22.41
$C_4C_1im^+$	I^-	52.37
$C_4C_1im^+$	BF_4^-	96.74
$C_4C_1im^+$	$CF_3SO_3^-$	107.34
$C_4C_1im^+$	PF_6^-	172.90
$C_4C_1im^+$	NTf_2^-	179.21
$C_4C_1im^+$	$CH_3SO_4^-$	360.23
$C_4C_1im^+$	$C_1OC_4SO_4^-$	381.76
$N_{1,4,4,4}^+$	dbp^-	31.04
$N_{1,4,4,4}^+$	NTf_2^-	227.13

cation-anion interaction. Weaker bound anions are therefore easier removed from the higher structure of the ionic liquid (the surface or the trimolecular cluster ion) which can be seen by an increase of the anion intensity (or anion yield) and a simultaneously decrease of the trimolecular cluster intensity (or cluster ion yield). The intrinsic strength in the series of anions coordinated towards $C_4C_1im^+$ decreases therefor in the order $CH_3COO^- > NO_3^- > I^- >$

BF_4^- > $CF_3SO_3^-$ > PF_6^- > NTf_2^- > $CH_3SO_4^-$ > $C_1OC_4SO_4^-$. This is in good agreement with the results from ESI experiments [139, 143, 144]. The only exception is $CH_3SO_4^-$ which is in an unusual position compared to the ESI results. This might be due to a possible demethylation of the anion. The higher intensity of the HSO_4^- ion is an indication, since the anion is usually the most intensiv ion in SIMS analysis of ionic liquids. In the series of cations coordinated towards NTf_2^- the influence of different alkyl side chain length can be seen. The stronger inductive effect of a longer alkyl chain decreases the positive charge by its electron donating effect. This should then result in a weaker intrisic strength of the cation towards the anion. This is reflected

Table 2.8: *Intensity ratio of different cations and positive trimolecular cluster with fixed anion. The intensities at FWHM were used to calculate the ratio.*

Cation	Anion	$I_{[C]^+}/I_{[(CA)C]^+}$
$S_{2,2,2}^+$	NTf_2^-	120.75
C_4py^+	NTf_2^-	214.05
$chol^+$	NTf_2^-	243.56
$C_4C_1pyrr^+$	NTf_2^-	260.01
C_8thiaz^+	NTf_2^-	262.58
$P_{6,6,6,14}^+$	NTf_2^-	2597.80 [a]
$C_2C_1im^+$	NTf_2^-	101.96
$C_4C_1im^+$	NTf_2^-	154.30
$C_6C_1im^+$	NTf_2^-	194.59
$C_8C_1im^+$	NTf_2^-	321.82
$N_{1,1,1,4}^+$	NTf_2^-	178.48
$N_{1,4,4,4}^+$	NTf_2^-	482.66
$N_{1,8,8,8}^+$	NTf_2^-	1581.16 [a]

[a] The full peak area of the trimolecular cluster was taken for the calculation of the ratio due to the low intensity.

by an increase of the intensity ratio as seen in Table 2.8 for the imidazolium and the ammonium series. The weaker cation-anion interaction increases the intensity (or the ion yield) of the anion and decreases the intensity (or the

ion yield) of the corresponding trimolecular cluster. This is also true for the other cations in the NTf_2^- based ionic liquids. The following overall order of interaction strength of cations towards NTf_2^- can be found: $C_2C_1im^+$ > $S_{2,2,2}^+$ > $C_4C_1im^+$ > $N_{1,1,1,4}^+$ > $C_6C_1im^+$ > C_4py^+ > $chol^+$ > $C_4C_1pyrr^+$ > C_8thiaz^+ > $N_{1,4,4,4}^+$ > $N_{1,8,8,8}^+$ > $P_{6,6,6,14}^+$. This is also in good agreement with the results from ESI experiments [143, 144].

2.3.5   Correlation with Solvent Parameters

It is shown, that SIMS data can in principle be correlated with solvent parameters [16]. Several different "polarity" scales (Kamlet-Taft, E_T30) are established for common solvents and ionic liquids on the basis of a solvatochromic indicator. These polarity scales have the major drawback, as they do not consider the competition of the cation or anion for the probe dye solute. A moderating effect has already been proposed by Tom Welton in 2003 [123] but was never included in the well-established polarity scales. It is shown, that SIMS data can in principle be correlated with solvent parameters [16]. Several different "polarity" scales (Kamlet-Taft, E_T30) are established for common solvents and ionic liquids on the basis of a solvatochromic indicator. They have tha major drawback, as they do not consider the competition of the cation or anion and the probe dye solute. A moderating effect has already been proposed by Tom Welton in 2003 [123] but was never included in the well-established polarity scales. Therefore the also well known donor-acceptor approach for common solvents [91] and ions in solution [102, 103], extended to ionic liquids (cations solvated by anions and *vice versa*, taking the moderationg effect into account) (paper in preparation, see section XX), was used. The first results with five different 1-butyl-3-methylimidazolium based room temperature ionic liquids (acetate, nitrate, iodide, hexafluorophosphate and bis(trifluoromethylsulfonyl)imide) have shown, that the secondary anion yield or the secondary anion yield enhancement can be related to solvent parameters [16]. This can also be seen on the left hand side of Figure 2.22. The anions are regarded as bases and were desorbed from the $C_4C_1im^+$ matrix, and the donor number should correlate to the anion yield, whereas the cations are regarded as acids and were desorbed from the NTf_2^- matrix, and
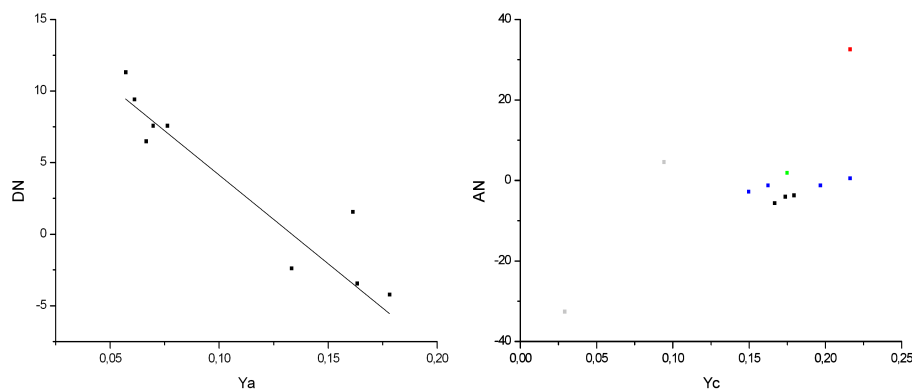
Figure 2.22: *Correlation of DN with the anion yield Y_a (left) and AN with the cation yield Y_c (right).*

should therefore be correlated to the acceptor number. Figure 2.22 shows the correlation of DN with the anion yield Y_a and AN with the cation yield Y_c. It can be seen, that the DN corresponds well to Y_a. However, the correlation is less pronounced with the cations forming a distinctive cluster at around AN = 0. It seems that the AN and DN are dependent on the size of the ions and on functional groups present in the ions. The choline cation (red square) should be a rather small ion, similar to $N_{1,1,1,4}^+$, but exhibits, in comparison, a rather high AN. $P_{6,6,6,14}^+$ is a rather large cation and shows a low AN (gray square, bottom left). All other cations seem to be similar in ion size and exhibit therefore similar acceptor numbers. To investigate this in more detail, measurements of the actual ionic radii or even the actual Stokes radii would be necessary. To obtain such values electric conductivity measurements with following Fuoss-Kraus analysis [146, 147, 148] might be reasonable. Unfortunately, this is far beyond the frame of the present investigation and would itself need experiments in an extensive amount.

2.3.6 Conclusion

A systematic study on ionic liquids was carried out by means of ToF-SIMS. The substances were examined by their mass spectra. All ionic liquids show simple and unique fragmentation pattern under Bi-cluster ion bombardment.

High secondary ion cluster of the general formula $[(CA)C]^+$ and $[(AC)A]^-$ were found in positive and negative ion mode. This can be attributed mainly to Coulomb interactions and/or hydrogen bonding. It is furthermore shown, that the interaction strength can be estimated from the intensity ratio of the unfragmented ion (cation or anion) and the trimolecular cluster ion ($[(CA)C]^+$ or $[(AC)A]^-$). The donor and acceptor number correlate well with the yield of the cation or anion. There is an evidence, that these numbers correlates also with the ionic radii or the Stokes radii. There is a further evidence, that AN and DN is not only dependent on the size of the ions but also on functional groups present ions.

Chapter 3

Conclusion

The SIMS technique, usually implemented to solid analytes, was applied to a liquid, vacuum stable organic-inorganic hybrid material (i.e. ionic liquids). This not only widens the understanding of the sputter process, but could also be used to estimate interionic interactions in ionic liquids.

The present study demonstrates the principle application of mono-atomic and poly-atomic Bi primary ions (Bi_{1-7}^{+} and $Bi_{1,3,5,7}^{++}$) for the analysis of ionic liquids with SIMS. Especially the interaction with a liquid surface as well as the mechanisms of the emission of secondary ions was investigated for mono-atomic and cluster ion bombardment. The results of the interaction of the primary ions with a liquid surface gives new insight about the underlying sputter process. The results show that the damage cross section, the ion formation efficiency and the fragmentation significantly deviate from the published results of solid organic samples. Apparently, the size of the primary cluster ion (Bi_{2-7}^{+} and $Bi_{3,5,7}^{++}$) has no significant impact on most of the discussed parameters. Only the change from mono-atomic to multi-atomic primary particles and the charge thereof has an influence. Only the yield and yield enhancement follows the usual observations.

Furthermore, the well known donor acceptor approach from Viktor Gutmann was extended to ionic liquids for the first time. The basic idea of this approach was, that cations are solvated by anions and anions solvated by cations. Therefore, there is a mutual interaction between the ions, which was not taken into account by the usual polarity scales, like the Kamlet-

Abboud-Taft or the Dimroth-Reichardt scale. It could be shown, that ionic liquids cannot be considered like conventional solvents in terms of their donor and acceptor properties. The proposed donor-acceptor approach to ionic liquids might give some new insights for a better understanding of ionic liquids and chemistry carried out in ionic liquids.

The strength of the interactions in the ionic liquid could be estimated by a mass spectrometric approach. Therefore, the intensity ratios of the intact secondary cations (or anions) to the trimolecular secondary ion cluster (in positive or negative ion mode) were calculated to give a qualitative order of the anions and cations, respectively. The comparison of the donor and acceptor numbers with the secondary ion yield for the cations and anions leads to the assumption, that the donor and acceptor numbers of neat ionic liquids correlate with the ionic radii or Stokes radii. It is further evidenced, that these numbers are also dependent on functional groups present in the cation or anion. the decomposition of the intact ions in the ionic liquid is investigated. Despite the quite high induced primary energy into the samples, the ionic liquids show a quite clear fragmentation pattern compared to organic solids. Fragmentation pathways for a wide range of ions are proposed.

Chapter 4

Experimental

4.1 Sample Preparation

The ionic liquids used in the study were either purchased from Sigma-Aldrich (Steinheim, Germany) or TCI (Tokyo, Japan) or were a donation from AC^{2}T (Wiener Neustadt, Austria) or the Institute of Applied Synthetic Chemistry (Vienna University of Technology, Austria) and were used without further purification except as noted below.

4.1.1 Preparation for SIMS

Ionic liquids can absorb considerable amounts of water from air. As a consequence the vacuum in the main chamber of the SIMS is negatively affected. To circumvent this the ionic liquids were dried at $40\,^\circ$C at reduced pressure for at least two days. The dried ionic liquids were stored at room temperature in a desiccator to the exclusion of light. In the first attempts to prepare the ionic liquids for the SIMS measurements they were coated on a clean Si-wafer. However due to the wetting behaviour on silicon the substances form a drop. This results in a curved surface that hinder a correct adjustment of the extractor distance. Furthermore, this thereby induced topography reduces the mass resolution by peak broadening. In a private notice Frank Rutten suggested a preparation used for the measurement in XPS and SIMS [62]. This includes a custom-made molybdenum grid (4 square holes with a width of approx. 2 mm) that is sometimes used for particularly badly charg-

ing samples in SIMS. The surface of the ionic liquids is thereby flattened and good spectra and images can be obtained. This improves the the SIMS results but gives problems in sealing the grid, usually carried out with commercial aluminium foil. To eliminate this drawback a new Mo sample holder is designed by drilling a small cavity (approx. 2 mm in diameter) into a small Mo-plate. This cavity is filled with the carefully dried ionic liquid and a flat surface can be obtained. By the use of that sample preparation deviating secondary ion intensities caused by different sample preparation conditions and matrix effects using different wafers (e.g. Si, Al) for monolayer production of organic samples [13] are excludes. The spectra can be obtained from neat ionic liquids in this customised molybdenum sample holder to ensure a flat surface for an optimised adjustment of the extraction distance and to obtain good spectra (i.e. high mass resolution and small FWHM).

4.1.2 Preparation for UV/VIS

A small amount of the indicator ($[Cu(acac)(tmen)][ClO_4]$ or $[Fe(phen)_2(CN)_2]$) dissolved in dichloroethane (DCE) is added to 400 μl ionic liquid dissolved in DCE. This ensures a homogeneous distribution of the indicators. The solvent is then removed at reduced pressure (approx. 10^{-3} mbar). The so prepared samples are transferred into a cuvette (108.002-QS, Hellma GmbH, Müllheim, Germany) and are measured against the pure, dried ionic liquid.

4.2 Measuring Conditions

4.2.1 SIMS Measurements

All ToF-SIMS spectra were recorded on a Tof-SIMS[5] instrument (ION-TOF GmbH, Münster, Germany) equipped with a dual stage reflectron ToF-analyser and a bismuth liquid metal ion gun (LMIG) as primary ion source mounted at 45° with respect to the sample surface. Primary ion species with the general cluster composition of Bi_n^+) (n = 1-7) and Bi_n^{++}) (n = 1, 3, 5, 7) were selected by appropriate mass filter settings. For an enhanced target

current of large cluster ions the emission current was reduced to 0.5 A. The primary ion current was directly measured using a Faraday cup detector located on a grounded sample holder (for Bi_1^+, Bi_2^+, Bi_3^+, Bi_1^{++}, Bi_3^{++}) or was determined indirectly via extrapolation of target current measurements with adequate variation of the pulse width at a given cycle time, usually 20 μs (for Bi_4^+, Bi_5^+, Bi_6^+, Bi_7^+, Bi_5^{++}, Bi_7^{++})[149, 15, 16]. The difference between the measured ion currents was at maximum $\pm$ 5 % which is in good agreement to previously published data [149, 14]. Typical operation conditions are summarised in Table 4.1 at a primary ion energy of 25 keV for singly charged ion clusters and 50 keV for doubly charged ion clusters. For

Table 4.1: *Operation conditions for a Bi-LMIG. The values in parenthesis are for a reduced target current at a reduced pulse width to prevent detector saturation for unfragmented cations and anions of ionic liquids.*

Ion species	Emission current	Pulse width	Target current
	A	ns	pA
Bi_1^+	0.50	19.9 (6.6)	0.4200 (0.251)
Bi_2^+	0.50	25.0 (14.5)	0.5680 (0.263)
Bi_3^+	0.50	25.0 (14.5)	0.4640 (0.234)
Bi_4^+	0.50	25.0	0.1125
Bi_5^+	0.50	40.2	0.0545
Bi_6^+	0.35	40.2	0.0058
Bi_7^+	0.35	40.2	0.0059
Bi_1^{++}	4.00	19.9	0.0077
Bi_3^{++}	0.50	25.0 (19.9)	0.3080 (0.294)
Bi_5^{++}	0.50	30.1	0.0850
Bi_7^{++}	0.35	30.1	0.0017

each measurement the primary ion dose density was set to $1x10^{10}$ ions cm^{-2} ensuring static conditions [2]. The primary ion beam was scanned randomly over an area of 150x150 μm at a resolution of 64x64 pixels for all samples studied. Due to the conductivity of the samples, no charge compensation was necessary. ToF-SIMS spectra were acquired in positive and negative ion

mode for 3 independently prepared sets of samples with one spot per sample analysed. The vacuum in the analysis chamber was kept in the range of 10^{-8} mbar and 10^{-9} mbar during all measurements. The mass scale was calibrated using a number of well defined and easily assignable secondary ions [15, 16]; for positive spectra, H^+, C^+, CH^+, CH_2^+, CH_3^+, $C_2H_2^+$, $C_2H_5^+$, $C_3H_2^+$, $C_3H_7^+$, $C_4H_2^+$ and $C_4H_9^+$, for negative spectra, H^-, C^-, CH^-, C_2^-, C_2H^-, C_3^-, C_3H^-, C_4^- and C_4H^- were used. This allowed mass assignments of the main fragments as well as sputtered ion clusters of the ionic liquids based on their absolute mass.

Measuring Low Ion Currents

Low target currents (e.g. Bi_7^+) can be determined in a Faraday cup indirectly by calculating the current from the emission of the LMIG. The emission of a certain primary ion is constant and can be determined by regression analysis of the target current by variation of the pulse width for a particular primary ion. To improve the target current measurement in the Faraday cup the cycle time is reduced to 20 μs and higher count rates are obtained due to a shorter time between two subsequent primary ion pulses per second. However, he pulse width cannot be increased infinitely since the next ion pulse is not blanked out anymore at a certain width. This can be seen in the mass spectra by the occurence of a second H-signal at sligthly higher m/z (approx. 1.5). From equation 4.1

$$t_c \;=\; t_c(ex) \;*\; (20 \;/\; c_t) \tag{4.1}$$

the target current t_c can be obtained by extrapolating the target current $t_c(ex)$ at the desired pulse width p_w, determined either graphically or from a regression analysis of the measured target current at different pulse width. Table 4.2 and Figure 4.1 show such a target current determination for Bi_7^+.

4.2.2 UV/VIS Measurements

UV-Vis spectra were obtained on a Perkin-Elmer Lambda 900 spectrophotometer (Shelton, CT, USA) in transmission mode at room temperature.

Table 4.2: *Determination of the target current by variation of the pulse width.*

Cycle time	Pulse width	Target Current
μs	ns	pA
20	30.1	0.015
20	40.2	0.028
20	50.0	0.039
20	60.2	0.050
20	70.3	0.063
100	40.2	0.0055 [a]

[a] value calculated from Equation 4.1

The spectral range was 300 nm to 1000 nm.

4.3 Mass filter adjustment for the Bi-cluster LMIG

In cluster SIMS analysis the adjustments for the mass filter are crucial to obtain a clean signal for just one cluster species. The following procedure describes in detail the adjustment of the mass filter for the bismuth cluster LMIG and is the same for all operation modes (high current bunched, burst alignment, collimated mode) of the LMIG. However, the exact timing values are depending on the energy of the primary ions as well as on the operation mode. Therefore the adjustment has to be done for every ion energy and operation mode individually. Also the extractor voltage has a slight impact on the timing and should therefore be kept constant.[*]

---

[*]A simulation upon a changing of the extractor voltage from 8000 V to 10000 V shows a shift in timing of 10 ns for Bi_1^+ for Bi_3^+ the shift is already 17 ns. Since the timing of all clusters with an n/z below 3 is increased by 30 ns it is not necessary to readjust the mass filter. For all cluster species with an m/z equal or greater then 3 the timing of the mass filter has to be readjusted following the described procedure.
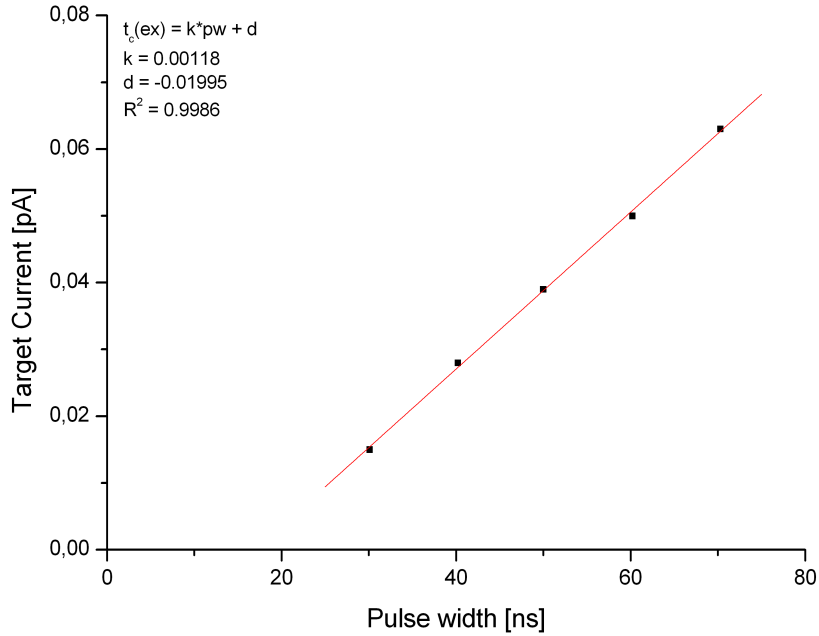
Figure 4.1: *Target current by variation of the pulse width measured at 20 μs cycle time.*

4.3.1 Principle of the mass filter

The DC ion beam contains many different single charged (Bi_{1-7}^+) and double charged ($Bi_{1,3,5,7}^{++}$) cluster ion species. Newer LMIG emitters (G-TIP) also contain Mn^+ and Bi_nMn^+ cluster ions. To separate these different ions the LMIG column is equipped with an electro-dynamic mass filter consisting of two pulsing systems. The first one is the so-called pre-chopper the second one the chopper. During operation the pre-chopper is cutting a short ion package, containing all different ions, out of the DC ion beam. All ions have the same energy, but due to their difference in mass the ions become separated while they are travelling down the column. The second pulsing system (chopper) ensures that only one of the ion packages is transmitted. All other packages are blocked.

4.3.2 Adjusting the mass filter

Before adjusting the mass filter the emitter should be run in the unbunched high current mode. Therefore the buncher voltage must be reduced to 0 V. The analyser has to be set up for ion detection, usually at a detector voltage of 8500 V, and the raster during the spectrum acquisition should be decreased.

4.3.3 Adjusting the pre-chopper offset

For cluster species with a n/z larger than 4 (n stands for the number of Bi atoms in the primary ion cluster) it is more convenient to change into negative polarity for the following adjustment, due to weak H-peak intensities. The following procedure should be maintained:

- Set the chopper offset to 1000 ns.
- Set the pulse width to the listed value in Table 4.3.
- Set the pre-chopper lead to the listed value in Table 4.3.
- Set the pre-chopper to a value of ca. 30 ns (Bi_1^+) to 100 ns (Bi_7^+).
- Acquire a spectrum on an unstructured Si wafer and read out the H-width (time of flight scale on the abscissa)
- Change the pre-chopper offset and acquire a new spectrum until the H-width corresponds to the chosen value for the pulse width.

The value for the pre-chopper offset should be noted for the adjustment of the pre-chopper lead.

4.3.4 Adjusting the chopper offset

The following procedure should be maintained:

- Set the pre-chopper offset to 200 ns.
- Set the pulse width to the listed value in Table 4.3.
- Set the pre-chopper lead to the listed value in Table 4.3.
- Set the chopper to a value of ca. 30 ns (Bi_1^+) to 100 ns (Bi_7^+).
- Acquire a spectrum on an unstructured Si wafer and read out the H-width (time of flight scale on the abscissa).

Table 4.3: *Starting values for the pulse width and the pre-chopper lead at an ion energy of 25 keV.*

Ion species	Pulse width	Pre-chopper lead
	ns	ns
Bi_1^+	20	1260
Bi_2^+	25	1790
Bi_3^+	25	2160
Bi_4^+	25	2510
Bi_5^+	40	2810
Bi_6^+	40	3080
Bi_7^+	40	3330
Bi_1^{++}	20	890
Bi_3^{++}	25	1560
Bi_5^{++}	30	1990
Bi_7^{++}	30	2400

- Change the chopper offset and acquire a new spectrum[†] until the H-width corresponds to the chosen value for the pulse width.

The value for the chopper offset should be noted for the adjustment of the pre-chopper lead.

4.3.5 Adjusting the pre-chopper lead

For convenience the cycle time (to 35 μs) and/or the pixel resolution (to 64 x 64) should be reduced. Then the following procedure should be maintained:

- Set the pulse width to 10 ns.
- Set the pre-chopper and the chopper offset to the previously determined value.
- Set the pre-chopper lead to the listed value in Table 4.3.
- Start the spectrum aquisition in the navigator and vary the pre-chopper lead until the count rate in the F-panel has reached a maximum.

[†]For reproducibility (constant hydrogen coverage) the new spectrum should be recorded on another position on the Si wafer.

4.3.6 Additional step for the bunched mode

For all cluster species below an n/z of 3 there are no interferences with other emitted species. Therefore the timing for the pre-chopper offset can be increased by 30 ns and the pre-chopper lead by 15 ns before the adjustment of the buncher.

4.3.7 Adjusting the buncher voltage and the buncher delay (in bunched mode only)

The buncher compresses the ion packages from 20-50 ns to sub-nanosecond pulses. The buncher delay specifies the time upon which the buncher is triggered. The trigger should occur, when the ion package is located exactly in the centre of the two buncher electrodes. For a quick adjustment of the buncher voltage the buncher delay should be set to the values listed in Table 4.4. Start the spectrum acquisition with a disabled raster and change to the differential mode. Change the buncher voltage until the H-peak height reaches a maximum (the H-width is minimised). For fine tuning the buncher delay should be changed until a Gaussian peak shape is reached. If the H-peak shows fronting (tailing to the left side) the delay needs to be reduced, if the H-peak shows tailing (tailing to the right side) the delay needs to be increased. Good values for the buncher can be obtained if this procedure is repeated a second time.

For a finer adjustment of the buncher voltage a systematic and more time consuming procedure was developed. In principle (starting either from a good value for the delay or after the quick adjustment described above) a wide range of the buncher voltage is scanned in small intervals (20 V) and the H-peak height (in SurfaceLab 6 refer to the mass resolution) and the H-peak width is plotted against the buncher voltage. The spectrum acquisition is started with a small field of view (10 x 10 μm with a 4 x 4 pixel resolution) and a spectrum is acquired (usually at a cycle time of 100 μs) for a fixed time. Afterwards the buncher voltage is increased (20 V) and a new spectrum is recorded for the same time as before. This is repeated until a buncher voltage range of $\pm$200 V of the values given in Table 4.4 for each ion species is scanned. Figure 4.2 shows the trend of the height and width

Table 4.4: *Starting values for the buncher delay and the buncher voltage at an ion energy of 25 keV.*

Ion species	Buncher delay ns	Buncher voltage V
Bi_1^+	178.5	2183
Bi_2^+	232.4	2195
Bi_3^+	285.5	1980
Bi_4^+	321.5	2010
Bi_5^+	349.2	2260
Bi_6^+	393.0	2164
Bi_7^+	427.3	2097
Bi_1^{++}	130.9	2424
Bi_3^{++}	210.9	2120
Bi_5^{++}	254.3	2167
Bi_7^{++}	290.2	2360

for Bi_1^+. The optimised buncher voltage is then estimated from the local extrema.
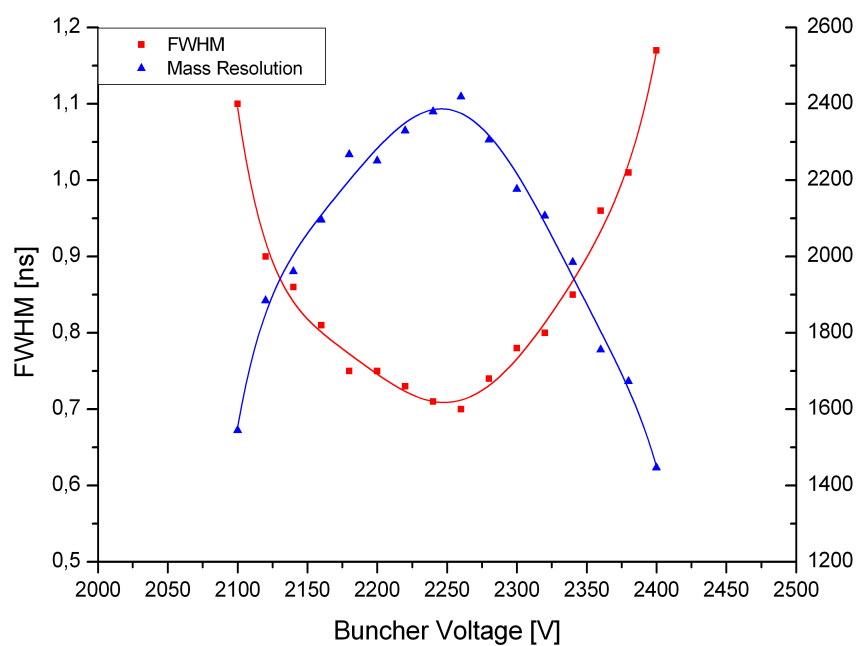
Figure 4.2: *Dependence of the H-peak width at FWHM and the mass resolution of the H-peak on the buncher voltage. The local extrema are at approx. 2263 V.*

Mass Spectra

This section provides the mass spectra for the ionic liquids discussed in Chapter 2.3.
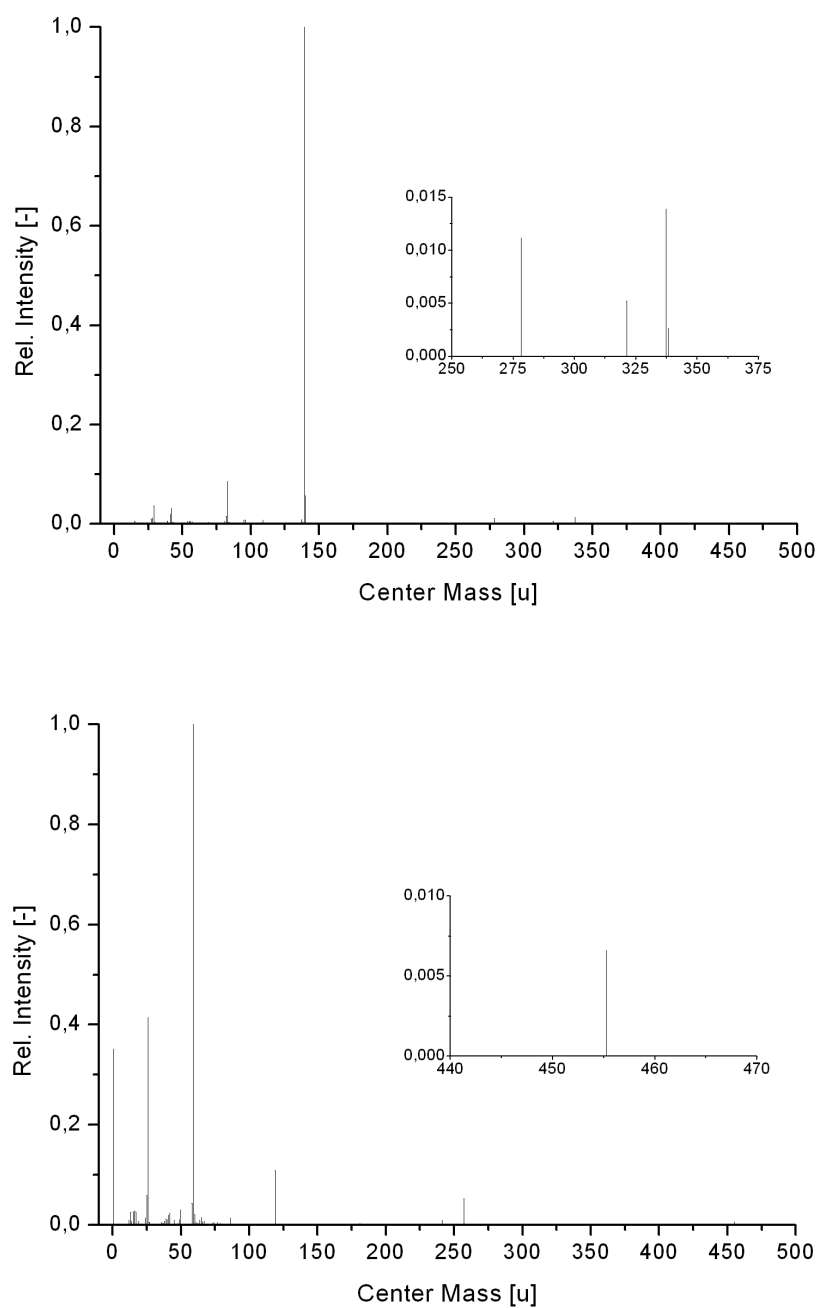
Figure 4.3: *1-Butyl-3-methylimidazolium acetate measured with Bi_7^+ in positive (top) and negative (bottom) ion mode.*
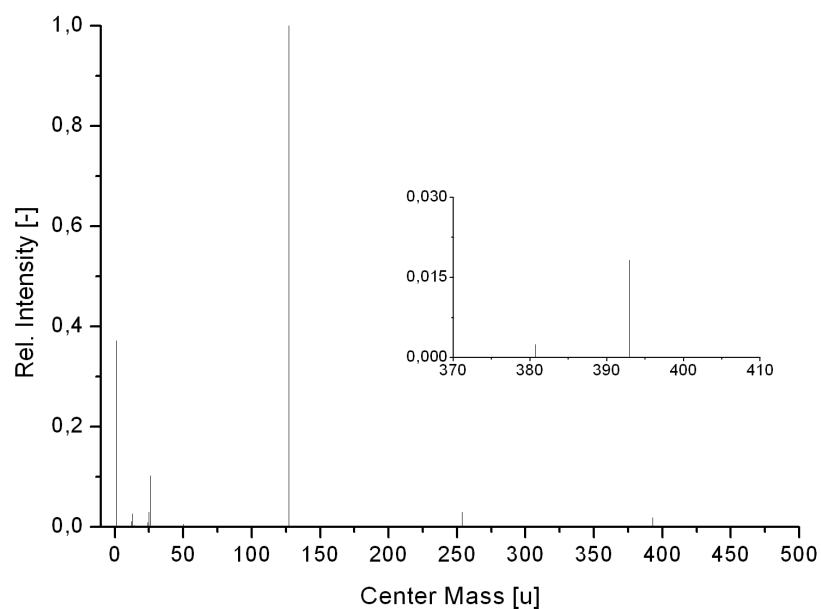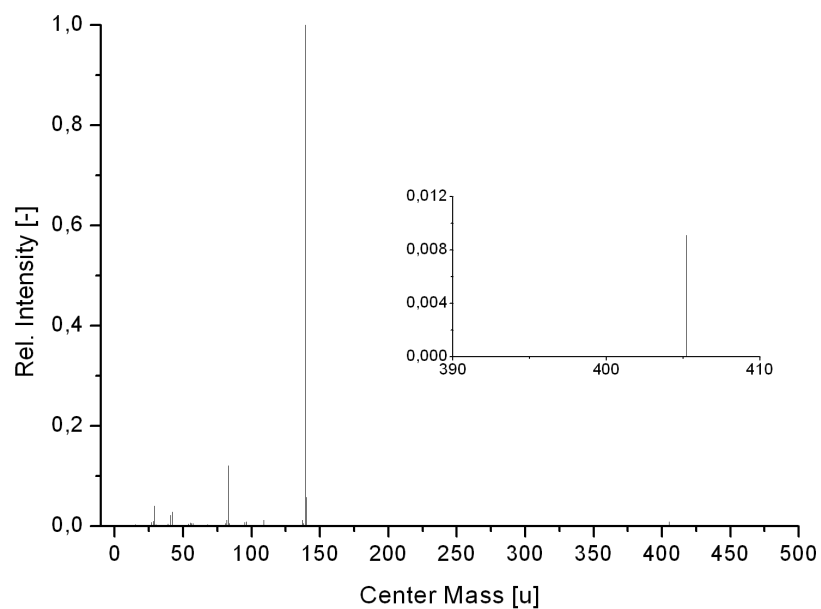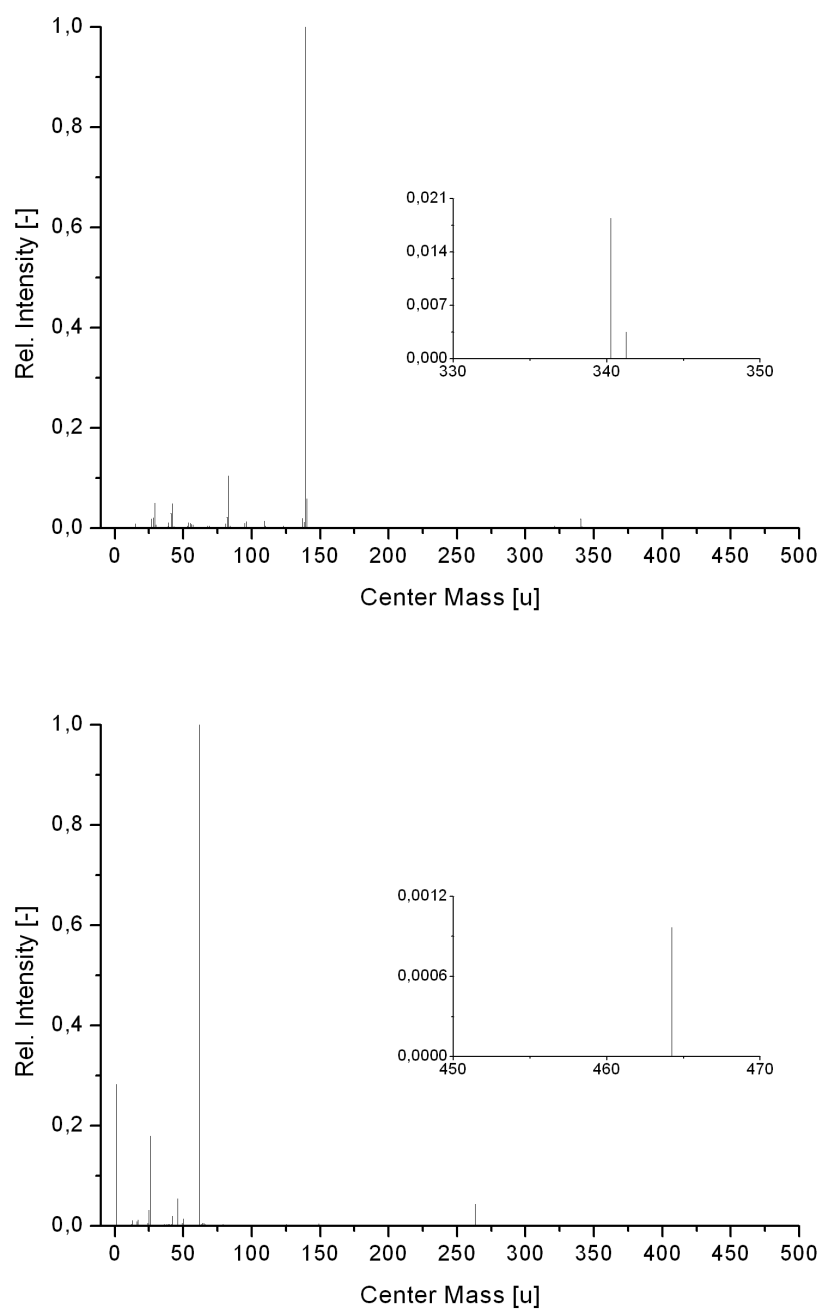
Figure 4.4: *1-Butyl-3-methylimidazolium iodide measured with Bi_7^+ in positive (top) and negative (bottom) ion mode.*

Figure 4.5: *1-Butyl-3-methylimidazolium nitrate measured with $Bi_7{}^+$ in positive (top) and negative (bottom) ion mode.*
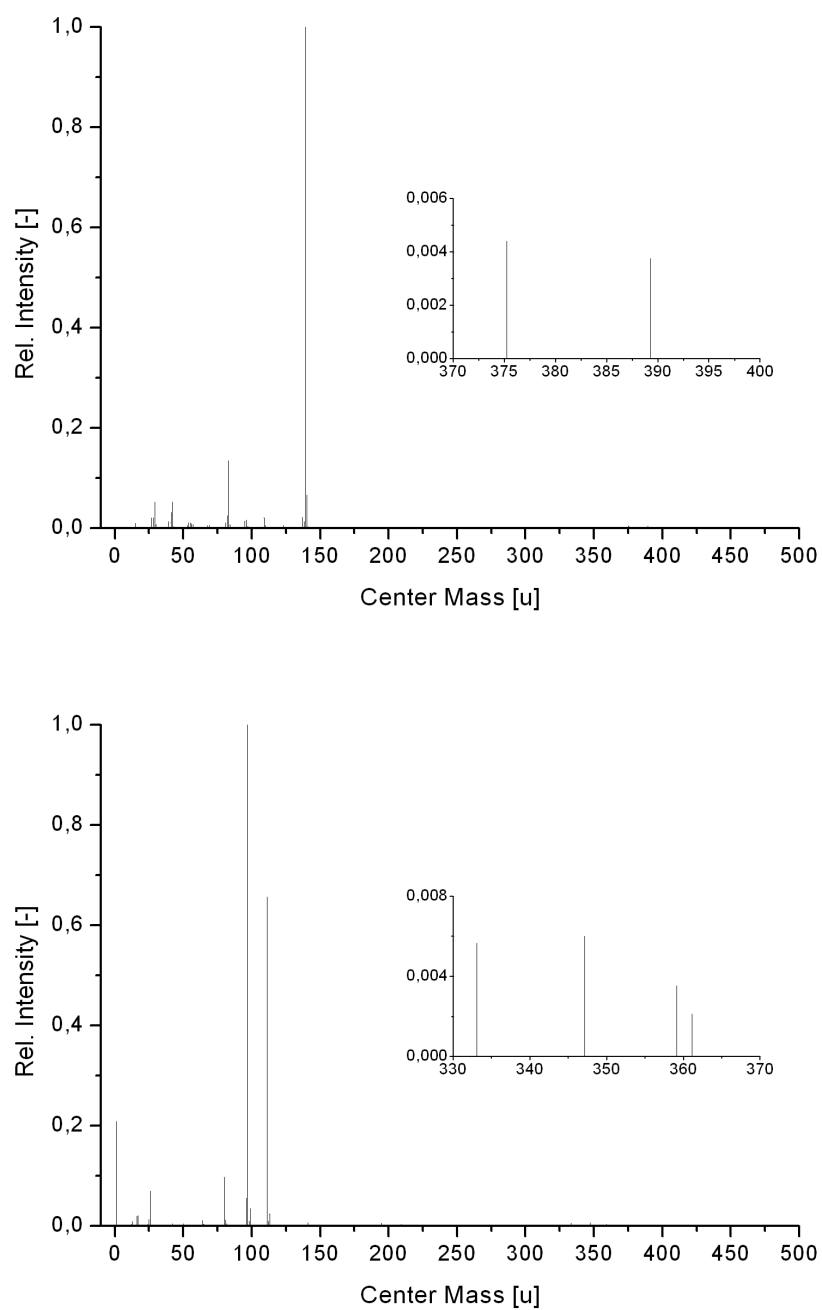
Figure 4.6: *1-Butyl-3-methylimidazolium methylsulfate measured with* Bi_7^+ *in positive (top) and negative (bottom) ion mode.*
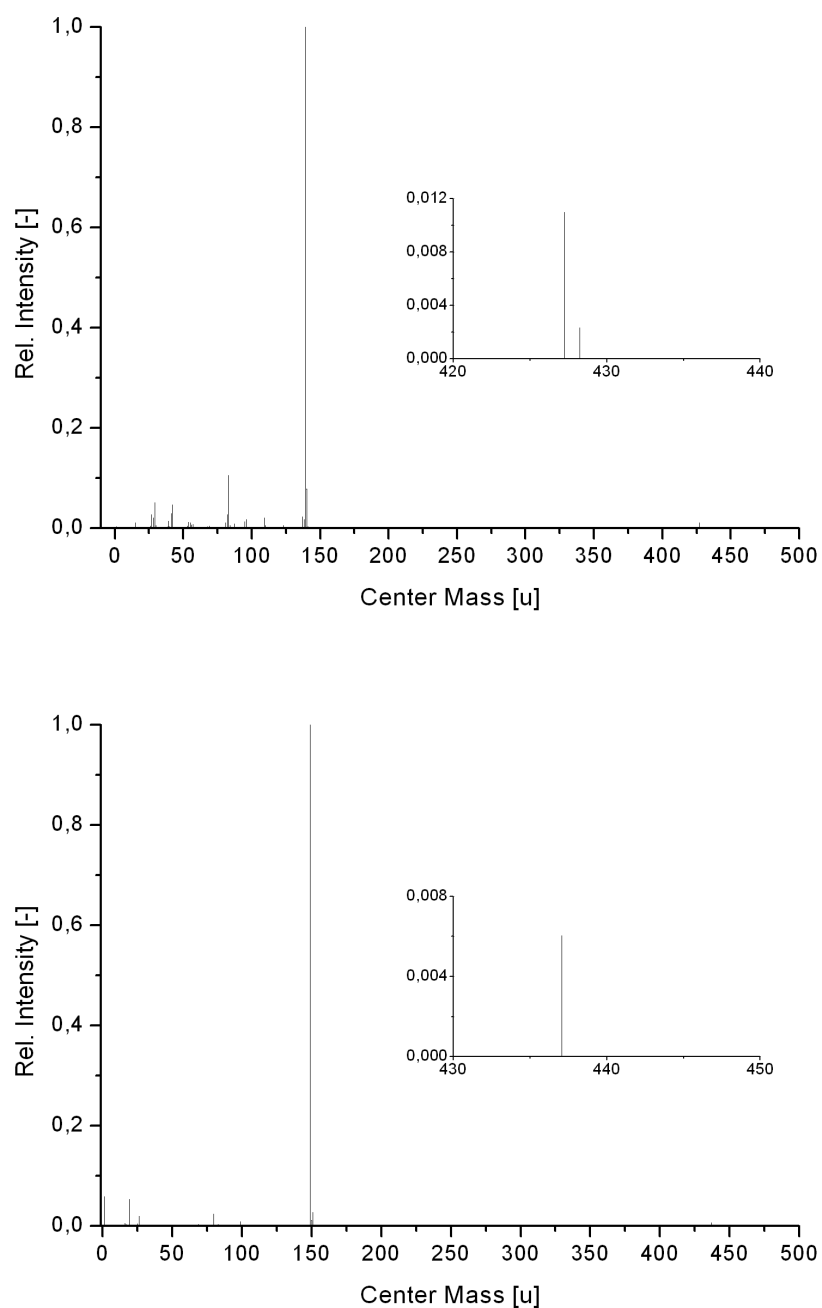
Figure 4.7: *1-Butyl-3-methylimidazolium trifluoromethansulfonate measured with Bi_7^+ in positive (top) and negative (bottom) ion mode.*
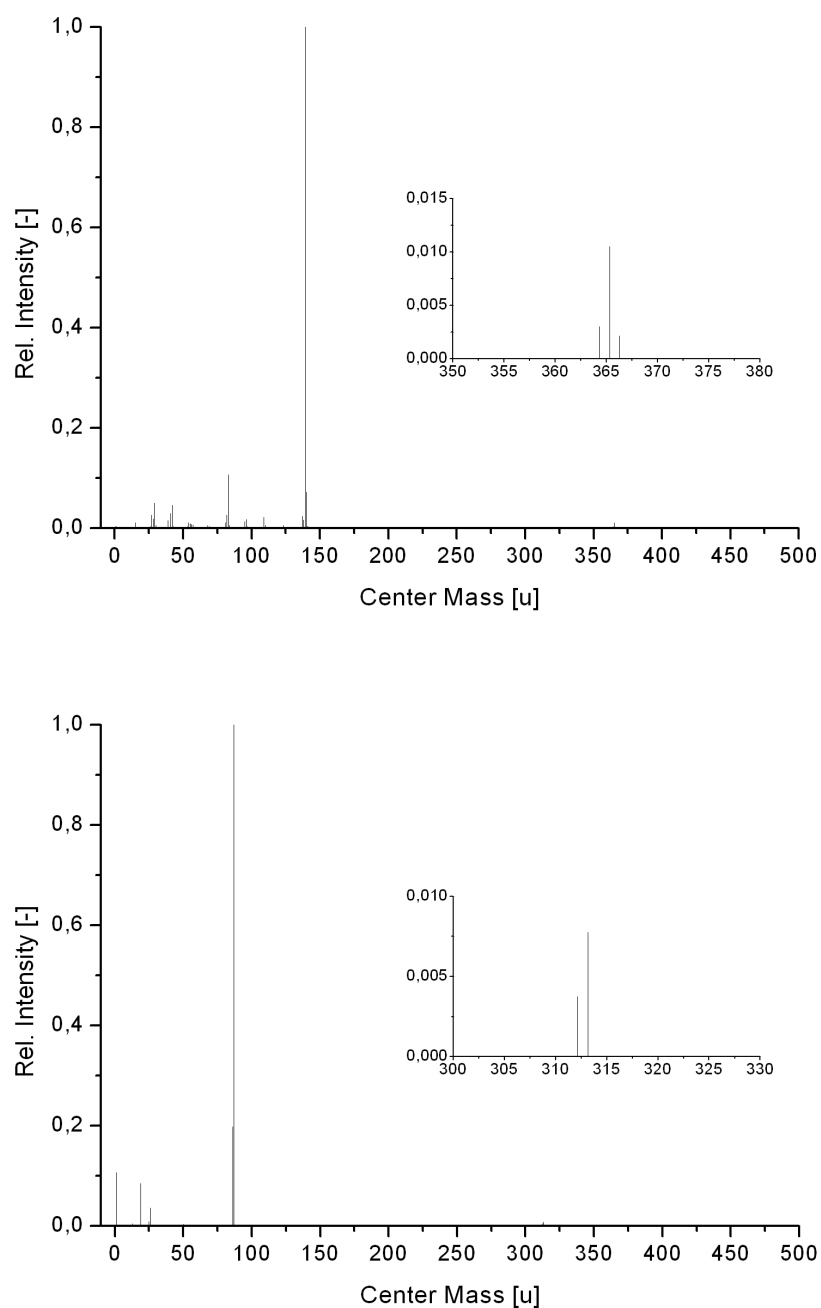
Figure 4.8: *1-Butyl-3-methylimidazolium tetrafluoroborate measured with* Bi_7^+ *in positive (top) and negative (bottom) ion mode.*
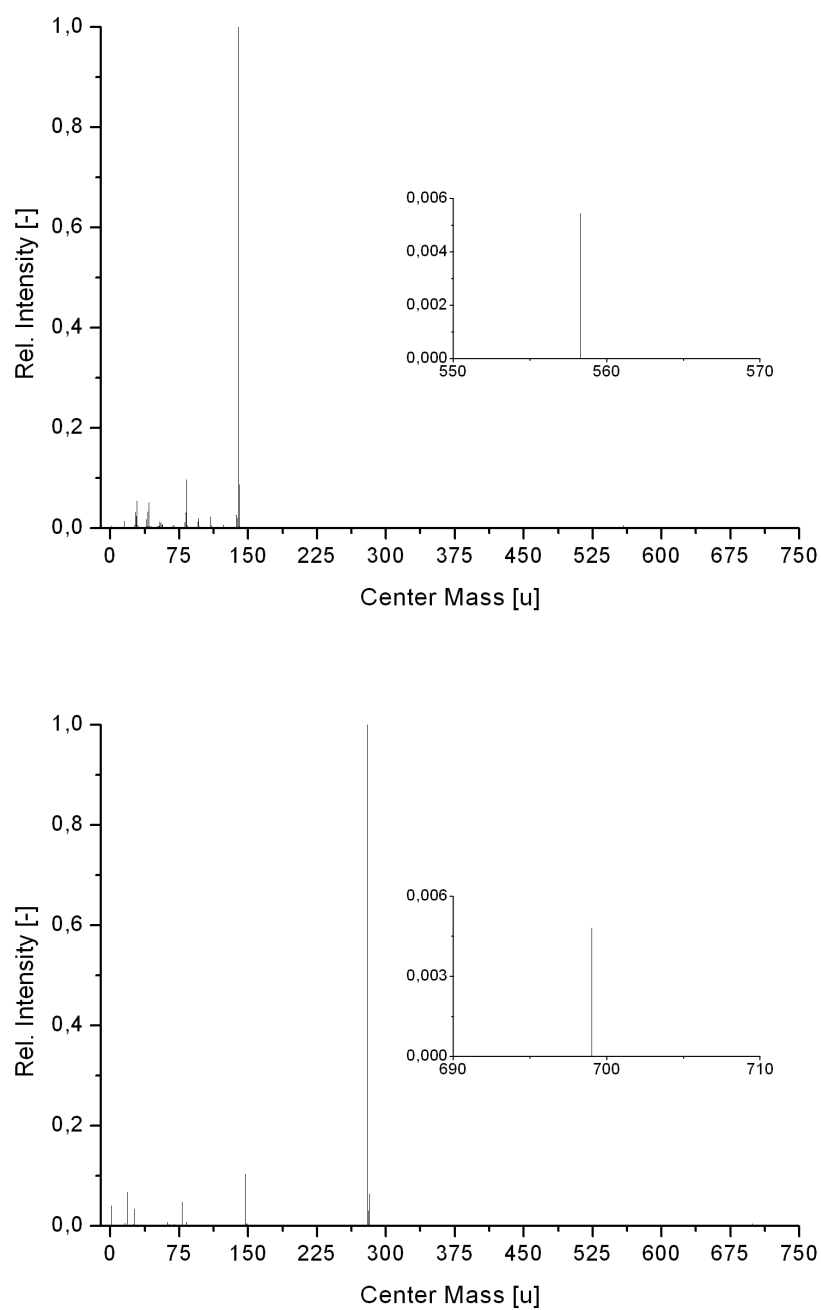
Figure 4.9: *1-Butyl-3-methylimidazolium bis(trifluoromethylsulfonyl)imide measured with Bi$_7^+$ in positive (top) and negative (bottom) ion mode.*
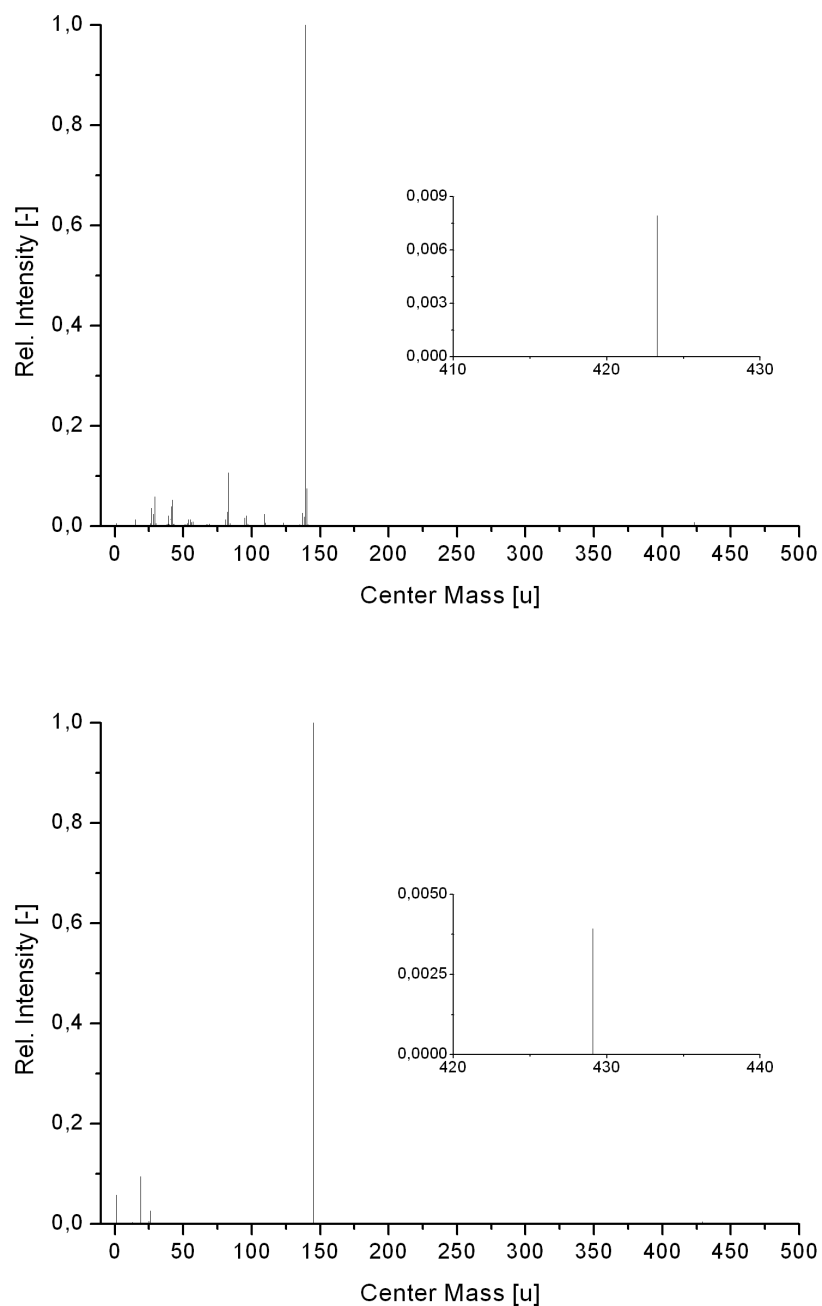
Figure 4.10: *1-Butyl-3-methylimidazolium hexafluorophosphate measured with Bi_7^+ in positive (top) and negative (bottom) ion mode.*
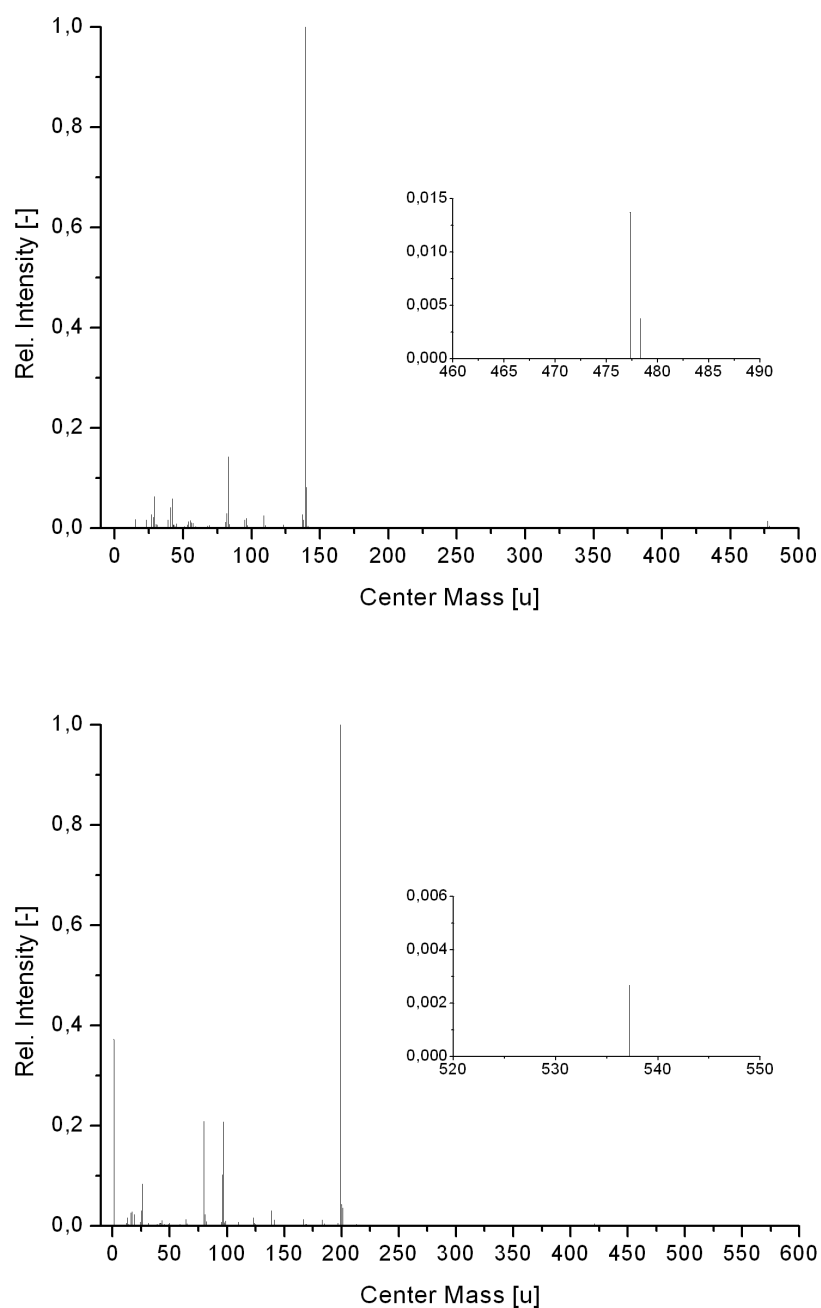
Figure 4.11: *1-Butyl-3-methylimidazolium 2(2-methoxyethoxy)ethylsulfate measured with Bi_7^+ in positive (top) and negative (bottom) ion mode.*

Figure 4.12: *Butyltrimethylammonium bis(trifluoromethylsulfonyl)imide measured with Bi_7^+ in positive (top) and negative (bottom) ion mode.*

Figure 4.13: *Tributylmethylammonium bis(trifluoromethylsulfonyl)imide measured with Bi_7^+ in positive (top) and negative (bottom) ion mode.*

Figure 4.14: *Methyltrioctylammonium bis(trifluoromethylsulfonyl)imide measured with Bi_7^+ in positive (top) and negative (bottom) ion mode.*

Figure 4.15: *Triethylsulfonium bis(trifluoromethylsulfonyl)imide measured with $Bi_7{}^+$ in positive (top) and negative (bottom) ion mode.*
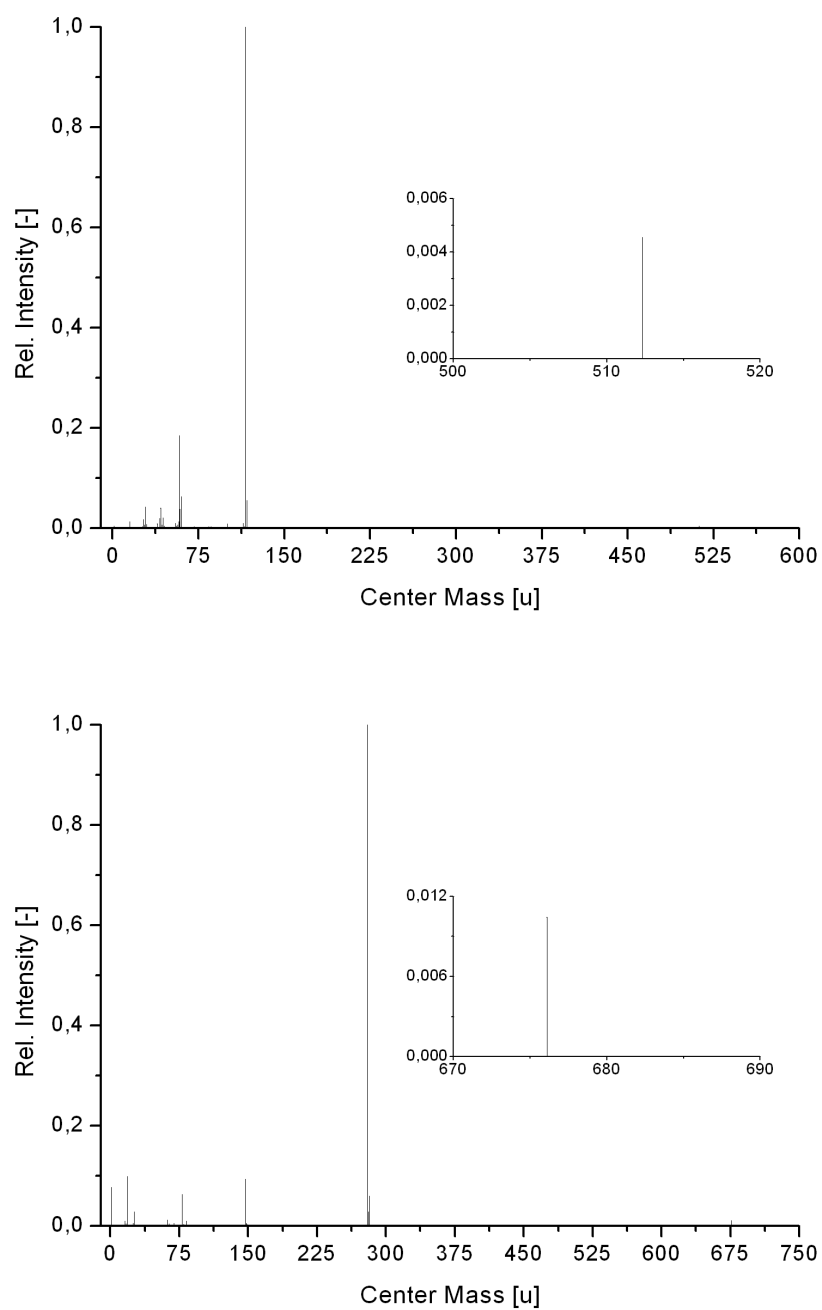
Figure 4.16: *Butylpyridinium bis(trifluoromethylsulfonyl)imide measured with Bi_7^+ in positive (top) and negative (bottom) ion mode.*

Figure 4.17: *1-Butyl-1-methylpyrrolidinium bis(trifluoromethylsulfonyl)imide measured with Bi_7^+ in positive (top) and negative (bottom) ion mode.*

Figure 4.18: *3-Octylthiazolium bis(trifluoromethylsulfonyl)imide measured with Bi_7^+ in positive (top) and negative (bottom) ion mode.*
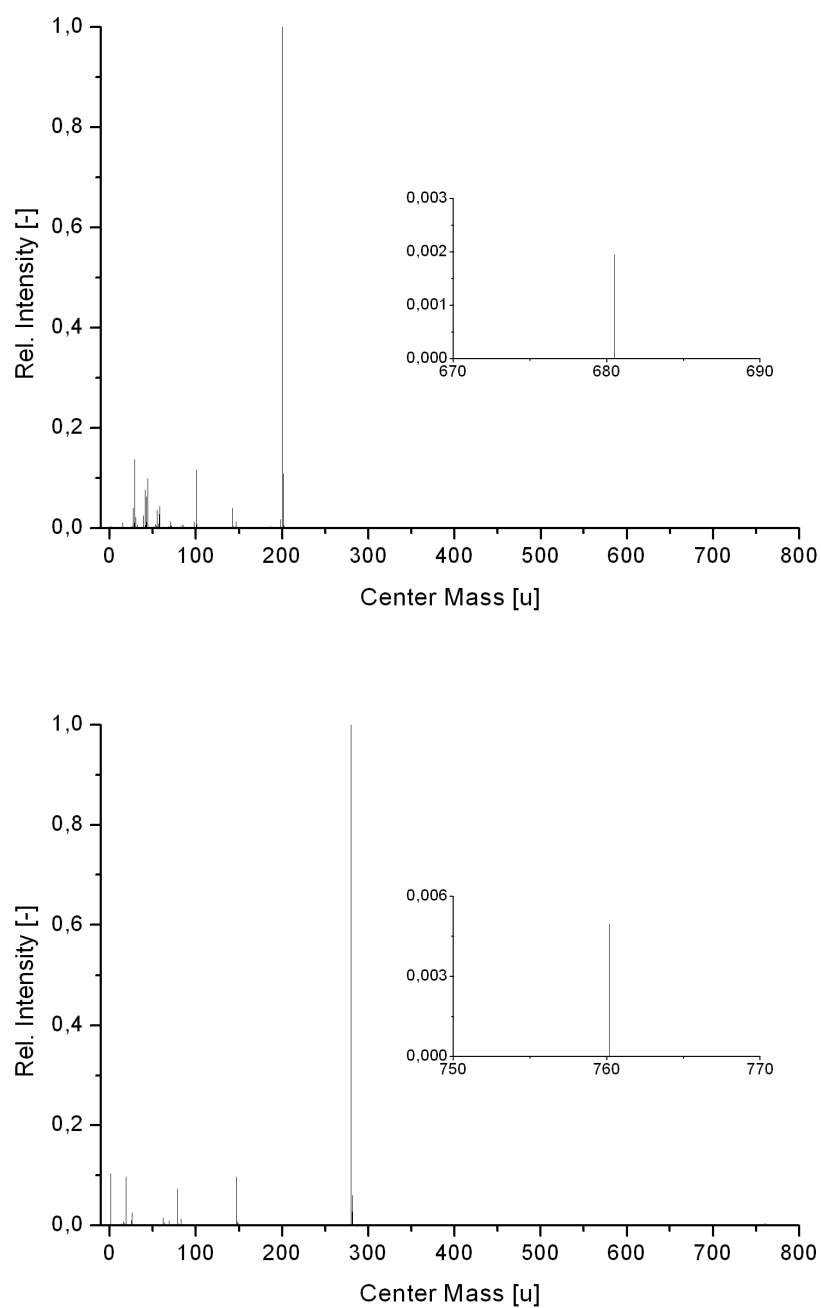
Figure   4.19:   *Trihexyltetradecylphosphonium bis(trifluoromethylsulfonyl)imide measured with Bi_7^+ in positive (top) and negative (bottom) ion mode.*

Figure 4.20: *Choline bis(trifluoromethylsulfonyl)imide measured with Bi$_7$$^+$ in positive (top) and negative (bottom) ion mode.*
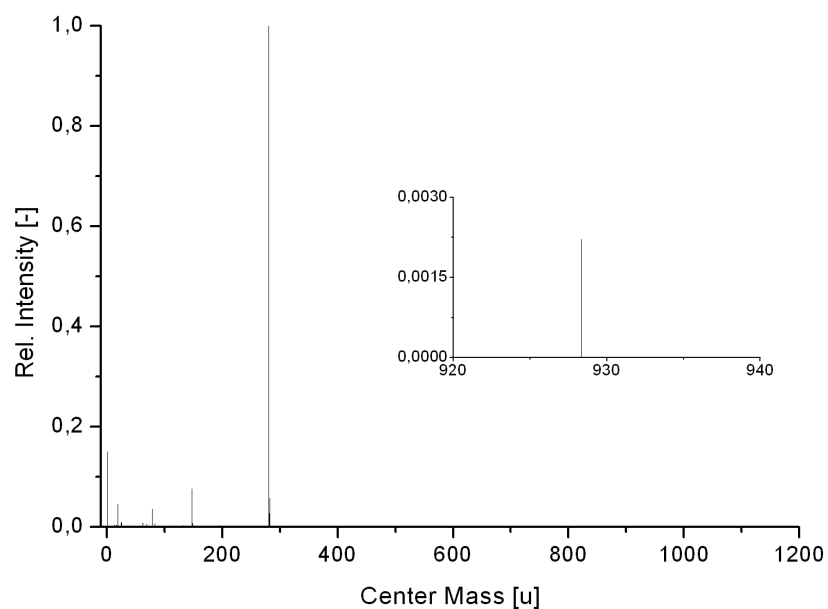
Figure 4.21: *1-Ethyl-3-methylimidazolium bis(trifluoromethylsulfonyl)imide measured with Bi_7^+ in positive (top) and negative (bottom) ion mode.*
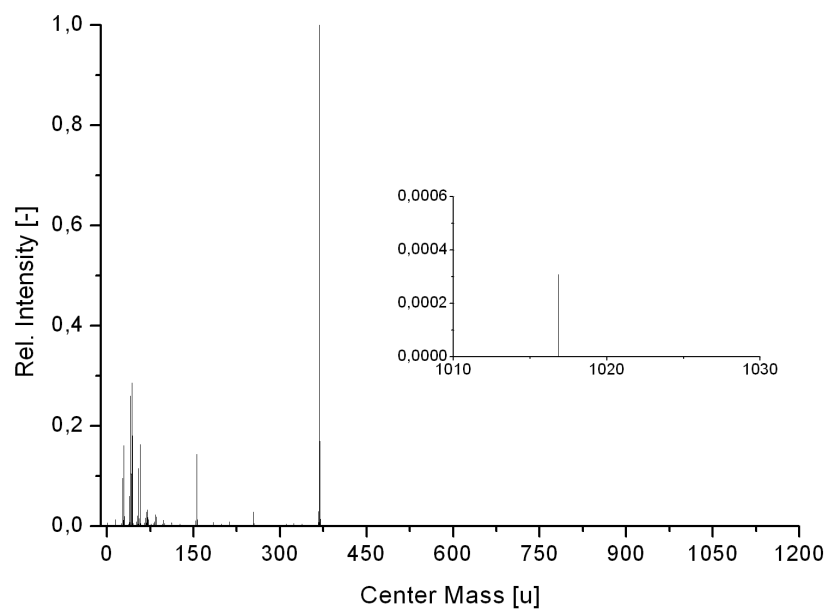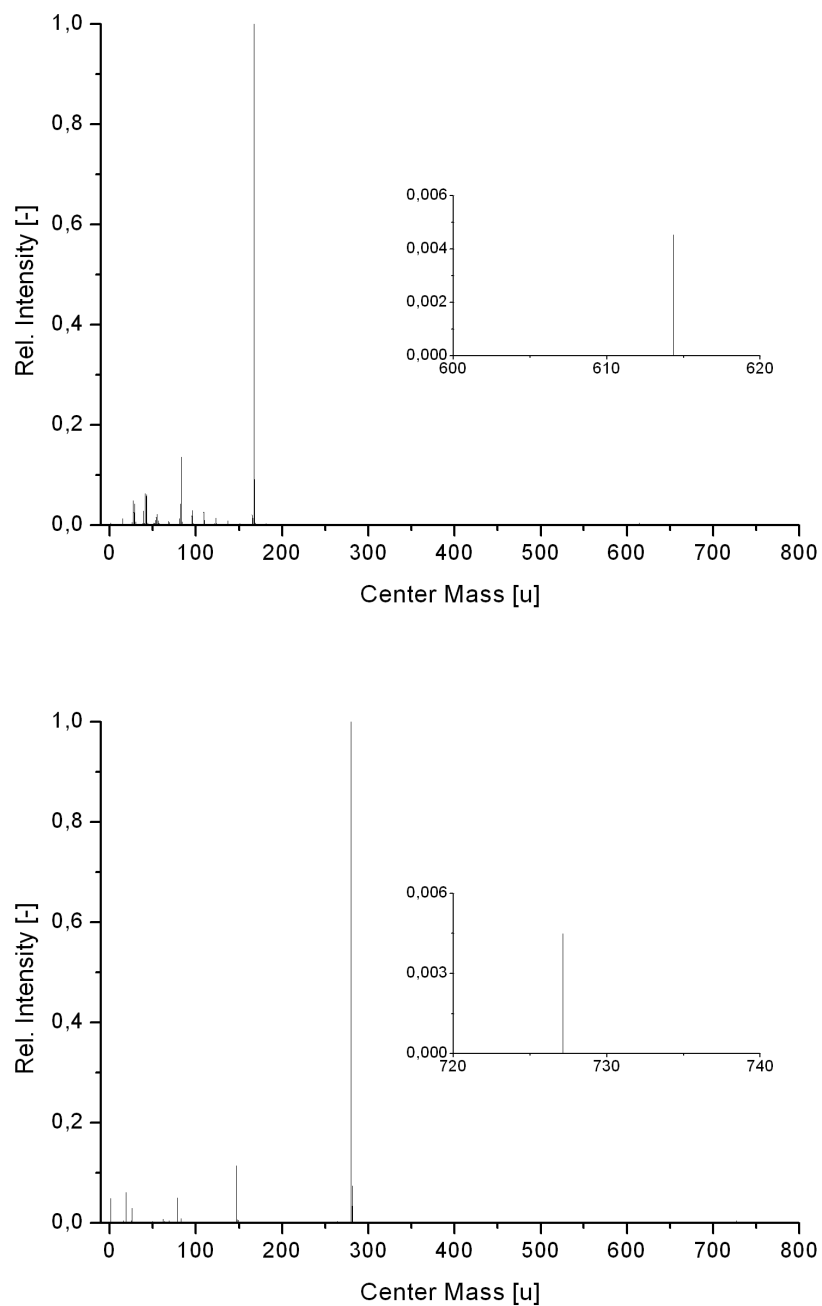
Figure 4.22: *1-Hexyl-3-methyl mimidazolium bis(trifluoromethylsulfonyl)imide measured with Bi_7^+ in positive (top) and negative (bottom) ion mode.*
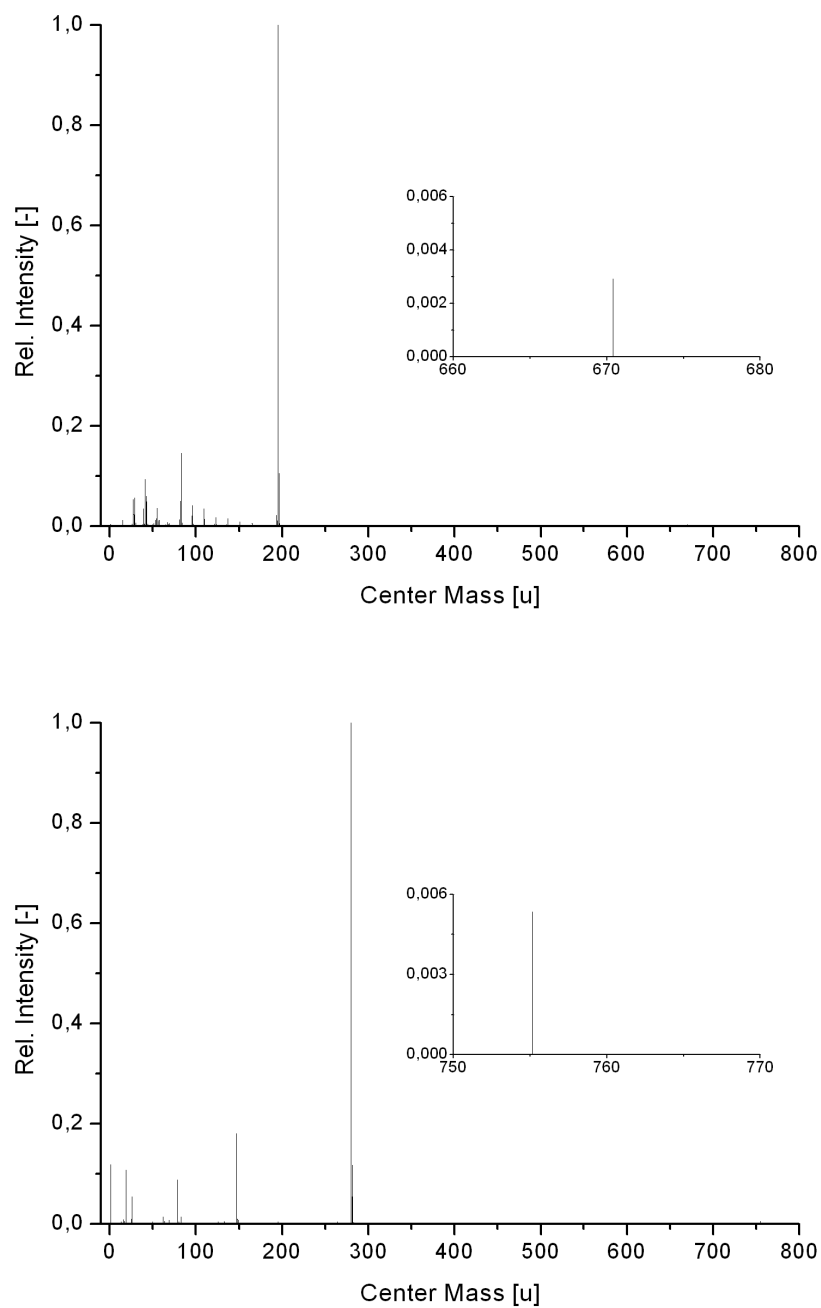
Figure 4.23: *3-Methyl-1-octylimidazolium bis(trifluoromethylsulfonyl)imide measured with Bi$_7^+$ in positive (top) and negative (bottom) ion mode.*
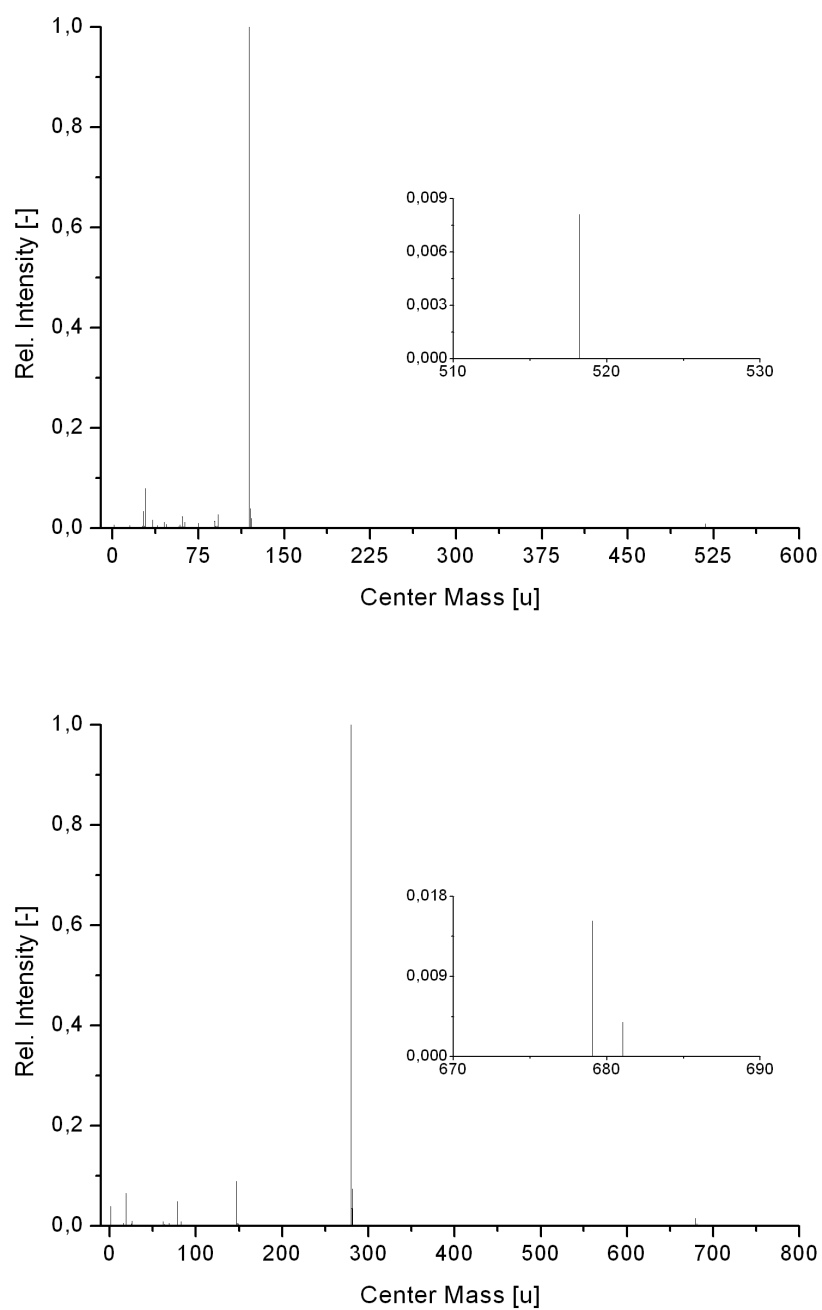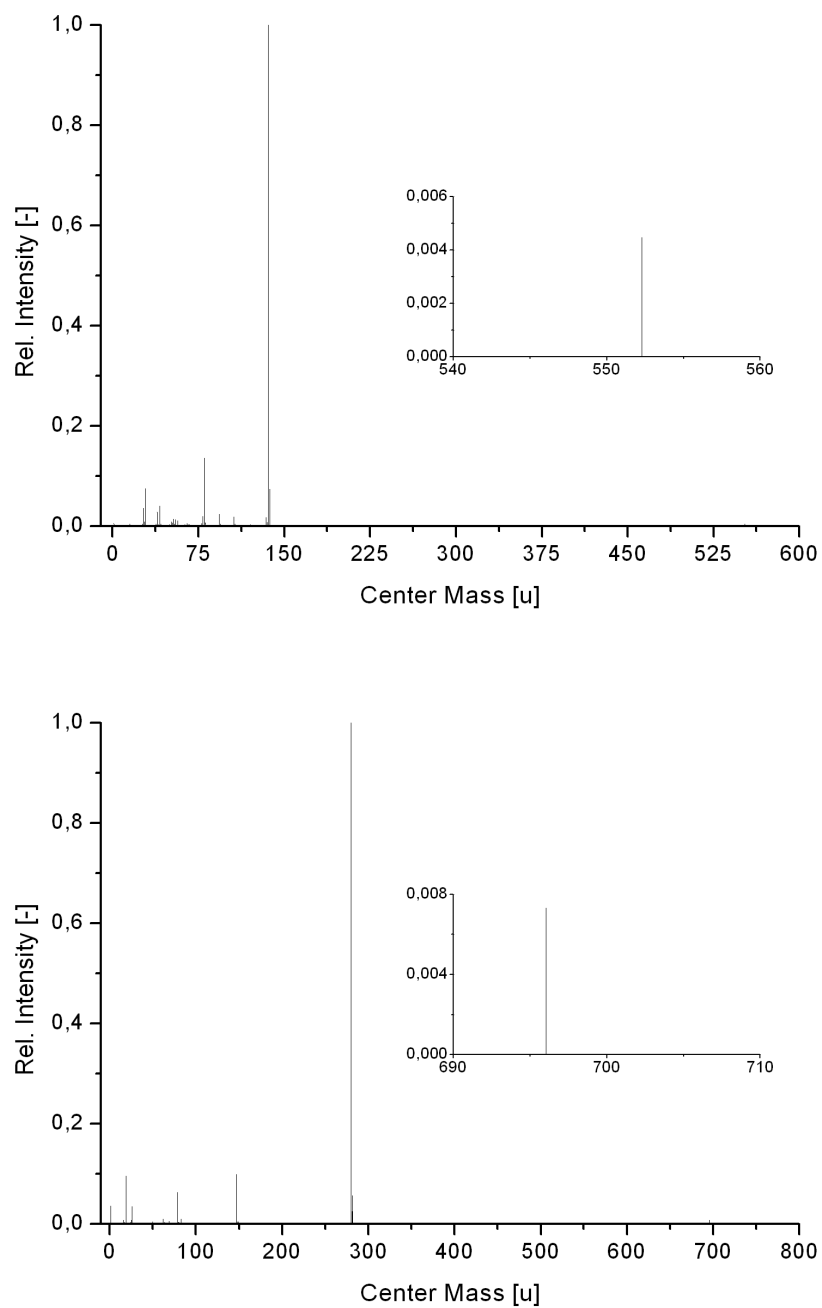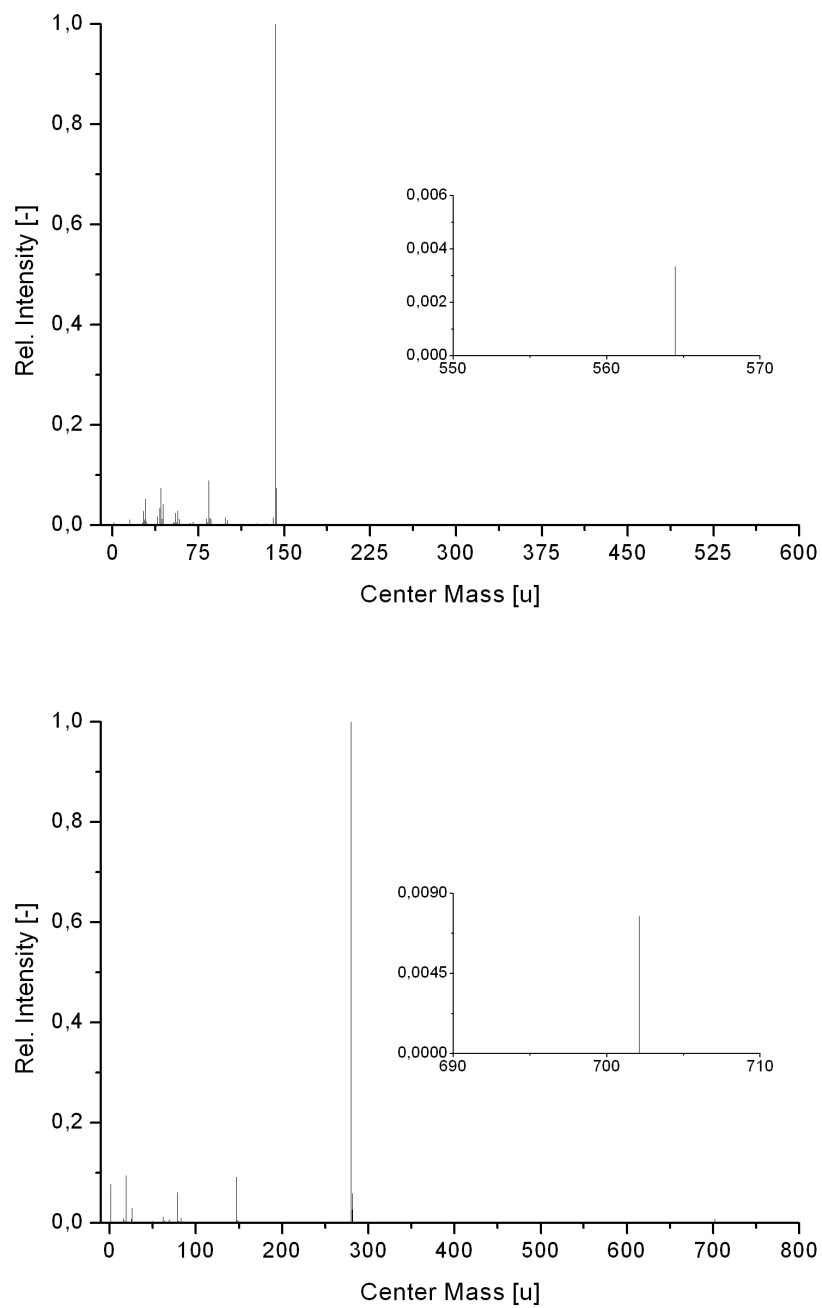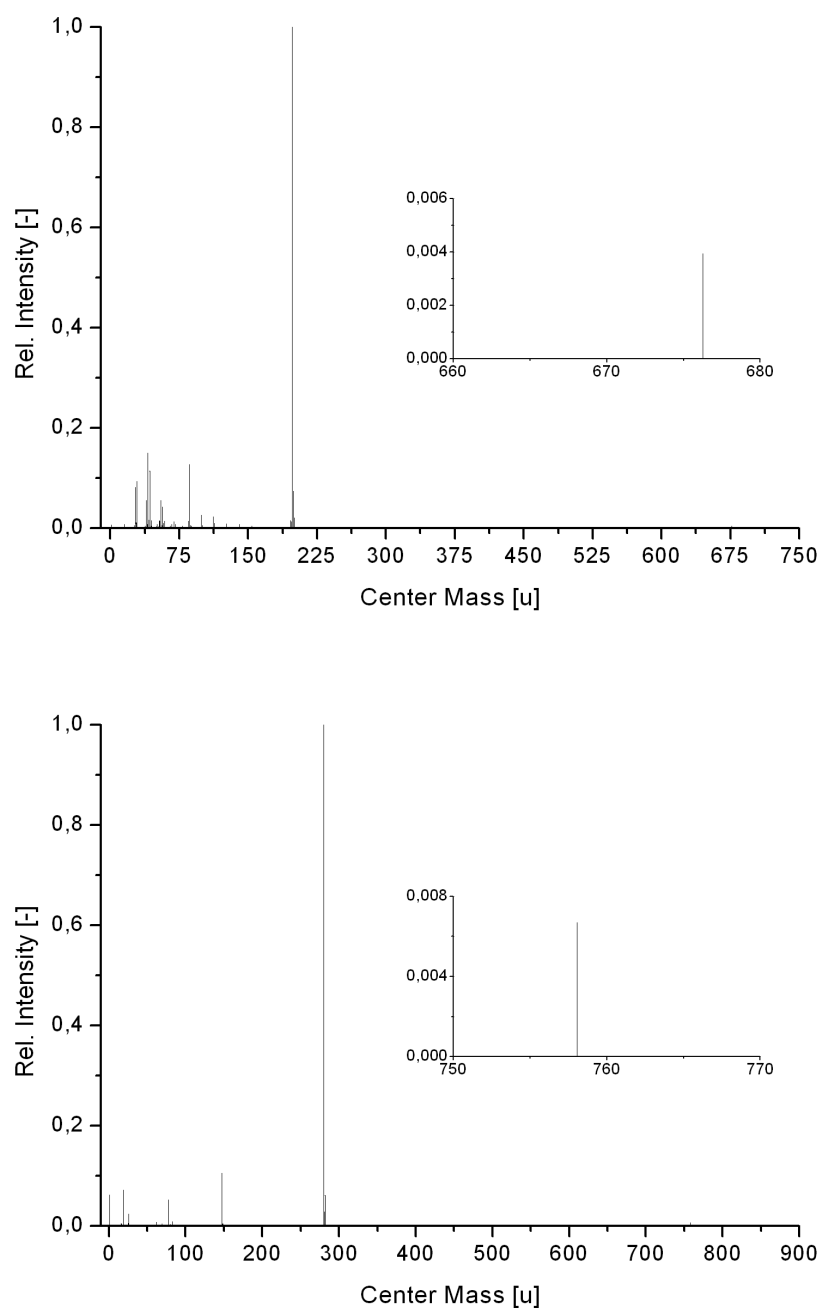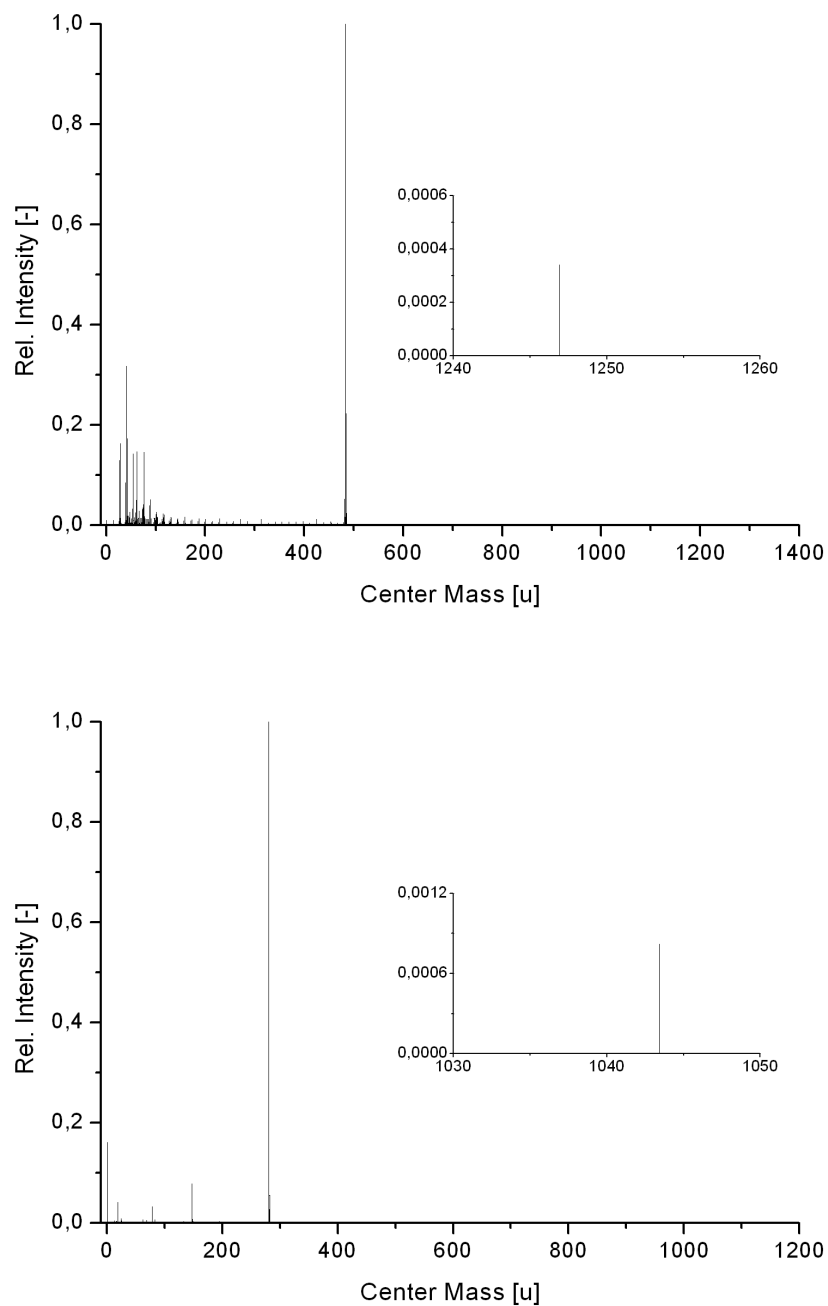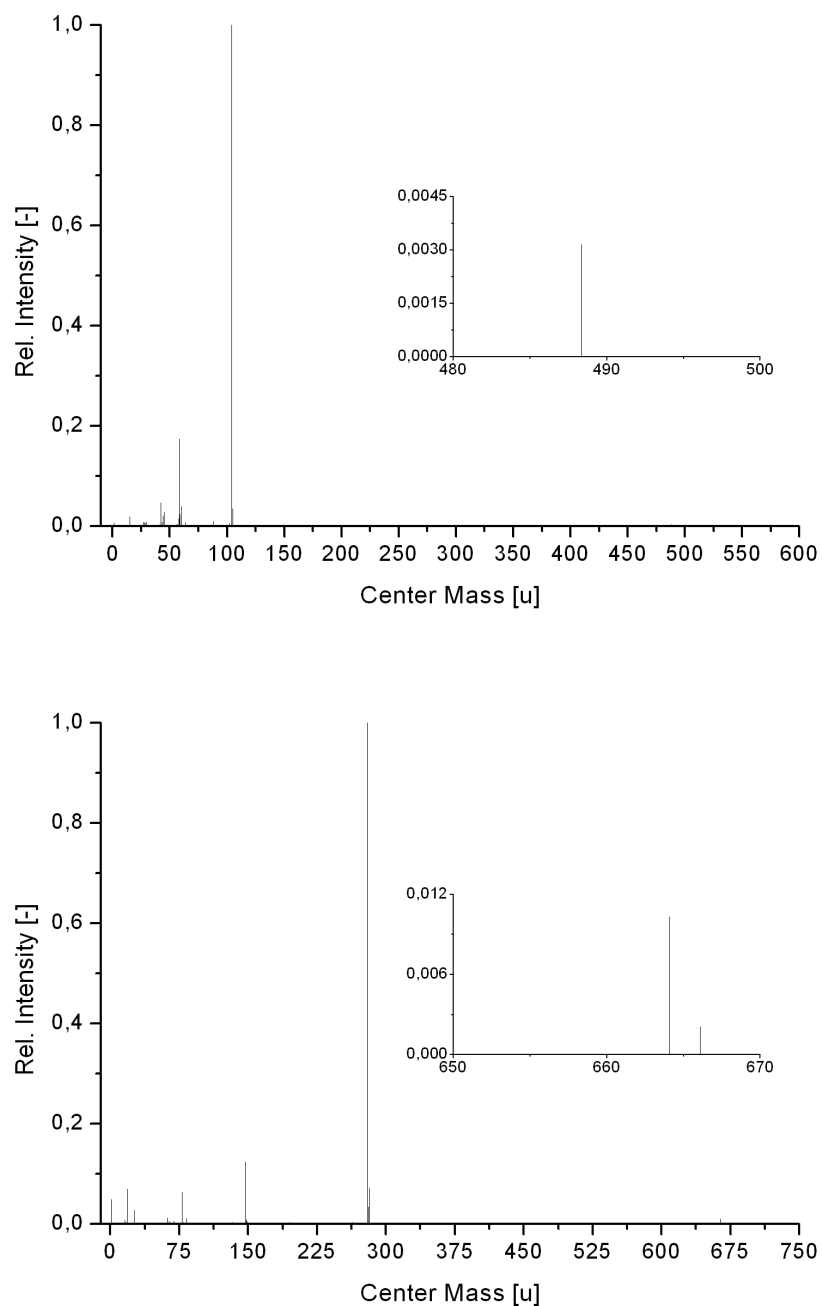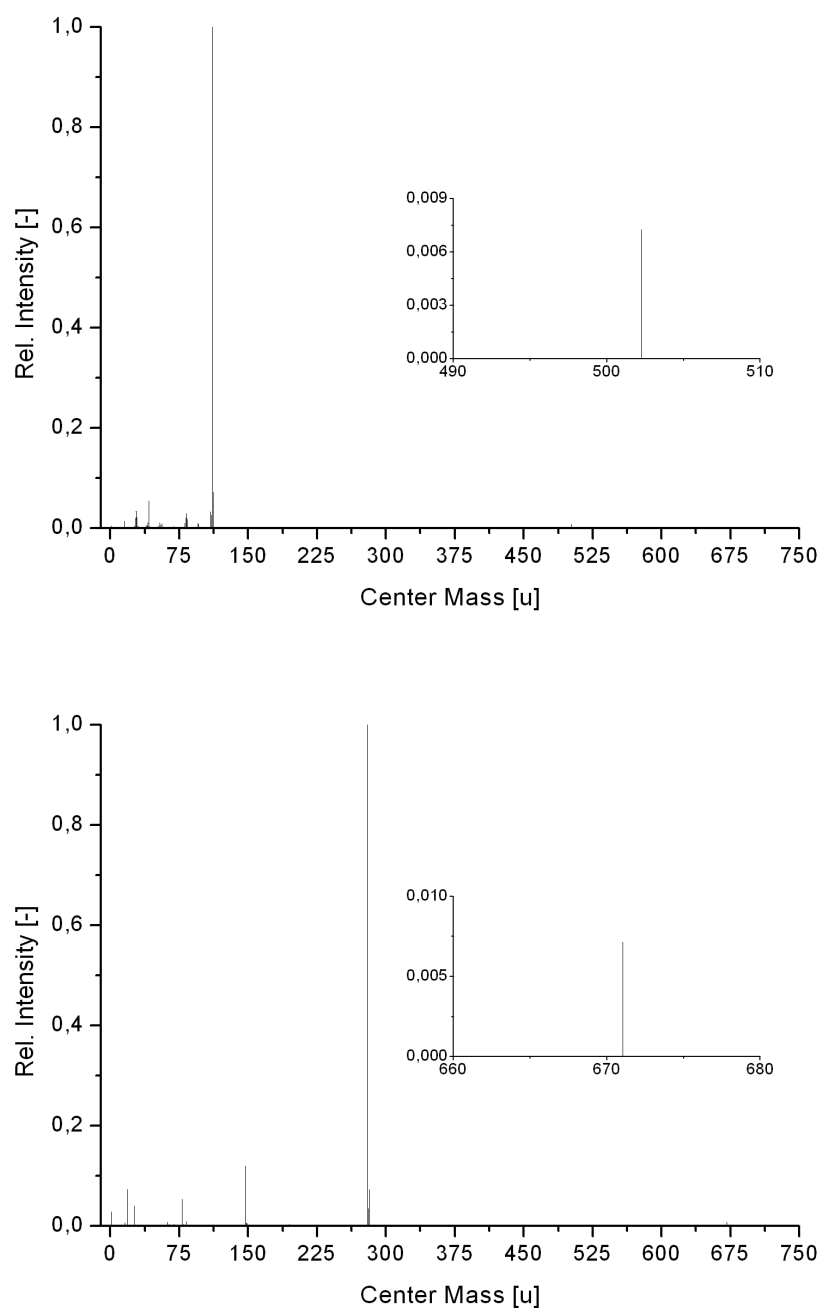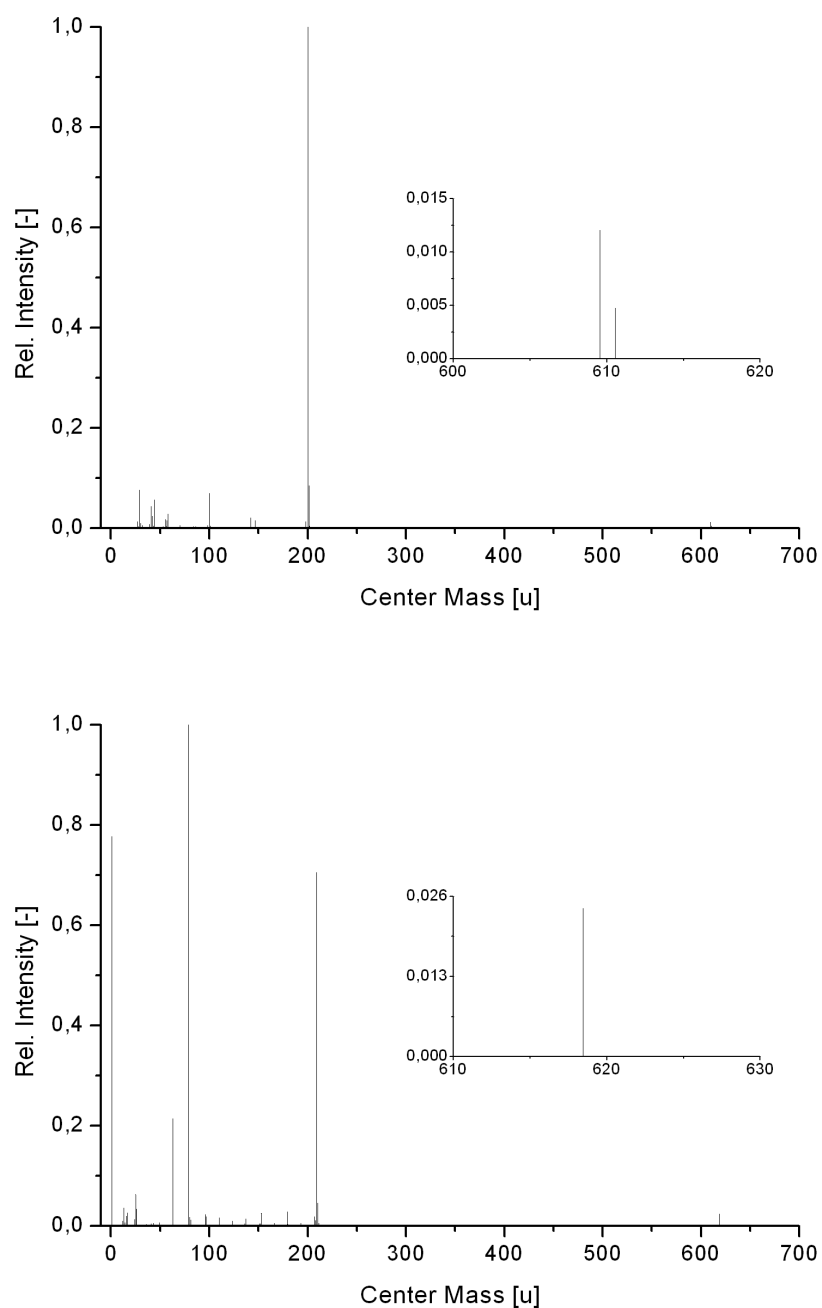
Figure 4.24:   *Tributylmethylammonium dibutylphosphate measured with* Bi_7^+ *in positive (top) and negative (bottom) ion mode.*
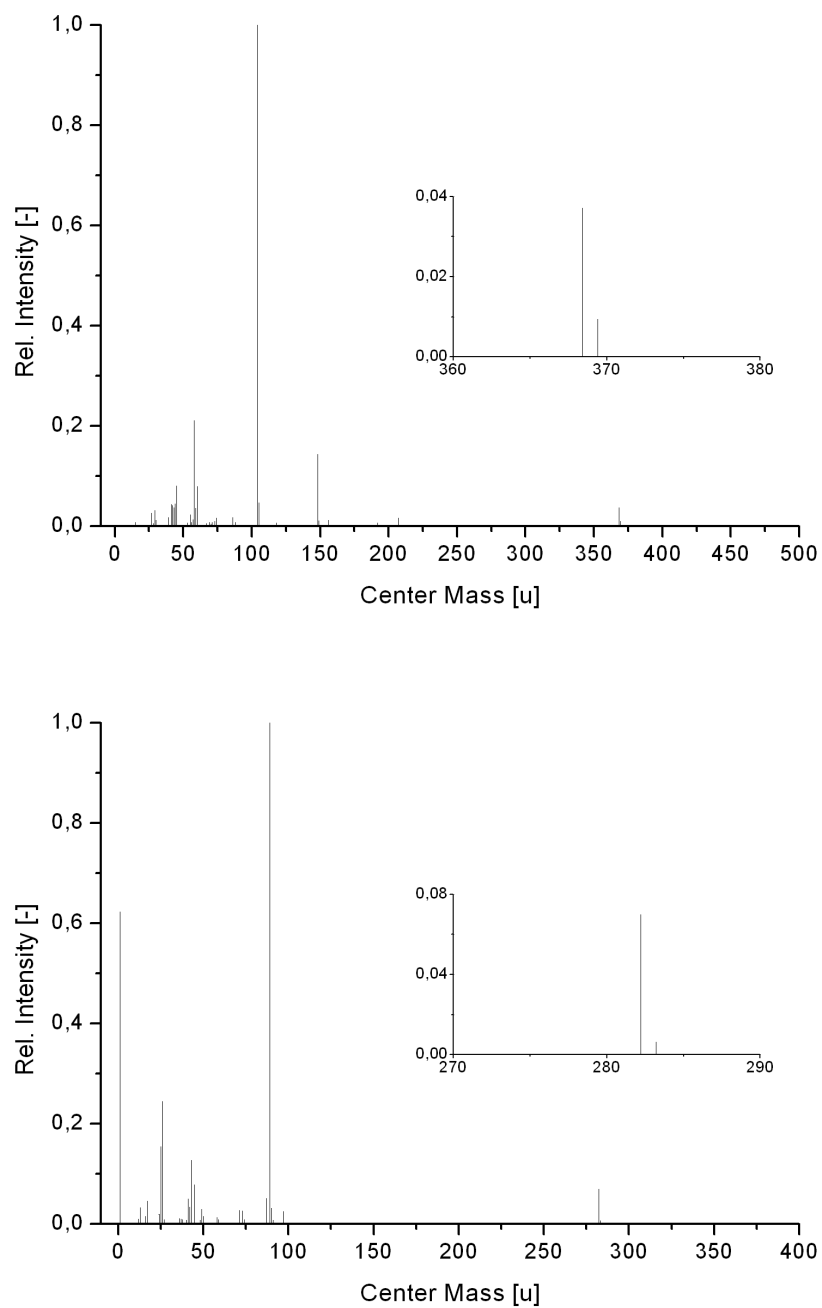
Figure 4.25: *Choline L-(+)-lactate measured with Bi_7^+ in positive (top) and negative (bottom) ion mode.*

Bibliography

[1] A. Benninghoven, F. G. Rudenauer, H. W. Werner, *Secondary Ion Mass Spectrometry: Basic Concepts, Instrumental Aspects, Applications and Trends*, John Wiley & Sons **1987**.

[2] J. C. Vickerman, D. Briggs, *TOF-SIMS: Surface Analysis by Mass Spectrometry.*, IM Publications & SurfaceSpectra Limited **2001**.

[3] J. C. Vickerman, A. Brown, N. M. Reed, eds., *Secondary Ion Mass Spectrometry: Principles and Applications (International Series of Monographs on Chemistry)*, Oxford University Press, USA **1990**.

[4] G. Gillen, S. Roberson, *Rapid Communications in Mass Spectrometry* **1998**, *12*, 1303.

[5] F. Koetter, A. Benninghoven, *Applied Surface Science* **1998**, *133*, 47 .

[6] N. Davies, D. E. Weibel, P. Blenkinsopp, N. Lockyer, R. Hill, J. C. Vickerman, *Applied Surface Science* **2003**, *203-204*, 223 .

[7] F. Kollmer, *Appl. Surf. Sci.* **2004**, *231-232*, 153.

[8] F. Kollmer, P. Hoerster, Mass spectrometers and liquid-metal ion source for the mass spectrometers. **2005**.

[9] A. Delcorte, P. Bertrand, B. J. Garrison, K. Hamraoui, T. Mouhib, O. A. Restrepo, C. N. Santos, S. Yunus, *Surface and Interface Analysis* **2010**, *42*, 1380.

[10] S. C. C. Wong, R. Hill, P. Blenkinsopp, N. P. Lockyer, D. E. Weibel, J. C. Vickerman, *Applied Surface Science* **2003**, *203-204*, 219 .

[11] K. Mochiji, *Hyomen Kagaku* **2010**, *31*, 599.

[12] S. Ninomiya, K. Ichiki, H. Yamada, Y. Nakata, T. Seki, T. Aoki, J. Matsuo, *Surface and Interface Analysis* **2011**, *43*, 95.

[13] G. Nagy, P. Lu, A. V. Walker, *J. Am. Soc. Mass Spectrom.* **2008**, *19*, 33.

[14] G. Nagy, A. V. Walker, *Int. J. Mass Spectrom.* **2007**, *262*, 144.

[15] M. Holzweber, H. Hutter, *Surf. Interface Anal.* **2010**, *42*, 1025.

[16] M. Holzweber, E. Pittenauer, H. Hutter, *J. Mass Spectrom.* **2010**, *45*, 1104.

[17] J. C. Riviere, S. Myhra, eds., *Handbook of Surface and Interface Analysis: Methods for Problem-Solving, Second Edition (Surfactant Science)*, CRC Press, 2nd ed. **2009**.

[18] V. E. Krohn, G. R. Ringo, *Applied Physics Letters* **1975**, *27*, 479.

[19] M. Benguerba, A. Brunelle, S. Della-Negra, J. Depauw, H. Joret, Y. L. Beyec, M. G. Blain, E. A. Schweikert, G. B. Assayag, P. Sudraud, *Nuclear Instruments and Methods in Physics Research Section B: Beam Interactions with Materials and Atoms* **1991**, *62*, 8 .

[20] B. Hagenhoff, R. Kersting, D. Rading, S. Kayser, E. Niehuis, *Second. Ion Mass Spectrom., SIMS XII, Proc. Int. Conf., 12th*, 833–836.

[21] R. Kersting, A. P. Pijpers, B. Hagenhoff, R. Verlaek, D. Stapel, A. Benninghoven, B. C. Schwede, *Second. Ion Mass Spectrom., SIMS XII, Proc. Int. Conf., 12th*, 825–828.

[22] R. N. S. Sodhi, *Analyst (Cambridge, U. K.)* **2004**, *129*, 483.

[23] M. W. Thompson, *Phil. Mag.* **1968**, *18*, 377.

[24] P. Sigmund, *Phys. Rev.* **1969**, *184*, 383.

[25] P. Sigmund, *Berichte der Bunsengesellschaft für physikalische Chemie* **1982**, *86*, 340.

[26] G. M. McCracken, *Rep. Prog. Phys.* **1975**, *38*, 241.

[27] G. Falcone, *Phys. Rev. B* **1986**, *33*, 5054.

[28] S. J. Pachuta, R. G. Cooks, *Chem. Rev.* **1987**, *87*, 647.

[29] L. Van Vaeck, A. Adriaens, R. Gijbels, *Mass Spectrom. Rev.* **1999**, *18*, 1.

[30] W. Gerhard, C. Plog, *Condensed Matter* **1983**, *54*, 59.

[31] C. Plog, L. Wiedmann, A. Benninghoven, *Surface Science* **1977**, *67*, 565 .

[32] M. Riedel, H. Düsterhöft, J.-P. Kuska, *Rapid Communications in Mass Spectrometry* **1997**, *11*, 667.

[33] A. Benninghoven, *Springer Ser. Chem. Phys.* **1982**, *19*, 438.

[34] A. Benninghoven, *Int. J. Mass Spectrom. Ion Phys.* **1983**, *53*, 85.

[35] W. Lange, M. Jirikowsky, A. Benninghoven, *Surf. Sci.* **1984**, *136*, 419.

[36] G. Leggett, *The static SIMS library*, SurfaceSpectra **1999**.

[37] R. Cooks, K. Busch, *International Journal of Mass Spectrometry and Ion Physics* **1983**, *53*, 111 .

[38] J. L. Wiza, *Nuclear Instruments and Methods* **1979**, *162*, 587 .

[39] M. Allaby, *Dictionary of Earth Sciences*, Oxford University Press, USA, 3rd ed. **2008**.

[40] R. Kersting, B. Hagenhoff, F. Kollmer, R. Moellers, E. Niehuis, *Appl. Surf. Sci.* **2004**, *231-232*, 261.

[41] P. Walden, *Bull. Acad. Imp. Sci. St.-Petersbourg* **1914**, 405.

[42] F. H. Hurley, J. Thomas P. WIer, *Journal of The Electrochemical Society* **1951**, *98*, 207.

[43] N. V. Plechkova, K. R. Seddon, *Chem. Soc. Rev.* **2008**, *37*, 123.

[44] P. Wasserscheid, T. Welton, eds., *Ionic Liquids in Synthesis (Green Chemistry (Wiley)(2 vol. set)*, Wiley-VCH, 2nd ed. **2007**.

[45] K. Bica, P. Gaertner, *Eur. J. Org. Chem.* **2008**, 3453.

[46] P. Majewski, A. Pernak, M. Grzymislawski, K. Iwanik, J. Pernak, *Acta Histochem.* **2003**, *105*, 135.

[47] M. Gamero-Castano, V. Hruby, *J. Propul. Power* **2001**, *17*, 977.

[48] A. S. Pensado, M. J. P. Comunas, J. Fernandez, *Tribol. Lett.* **2008**, *31*, 107.

[49] K. Binnemans, *Chem. Rev. (Washington, DC, U. S.)* **2005**, *105*, 4148.

[50] M. Koel, *Crit. Rev. Anal. Chem.* **2005**, *35*, 177.

[51] R. Liu, J.-f. Liu, Y.-g. Yin, X.-l. Hu, G.-b. Jiang, *Anal. Bioanal. Chem.* **2009**, *393*, 871.

[52] J. D. Stenger-Smith, J. A. Irvin, *Mater. Matters (Milwaukee, WI, U. S.)* **2009**, *4*, 103.

[53] L. Brown, *Trans. Inst. Met. Finish.* **2010**, *88*, 122.

[54] Y. Fujiwara, H. Nonaka, N. Saito, Formation method of ion beam for secondary ion mass spectrometry and ionic liquid thereof. **2009**.

[55] D. Chaturvedi, *Curr. Org. Chem.* **2011**, *15*, 1236.

[56] K. E. Johnson, *Electrochem. Soc. Interface* **2007**, *16*, 38.

[57] P. J. Scammells, J. L. Scott, R. D. Singer, *Aust. J. Chem.* **2005**, *58*, 155.

[58] C. Chiappe, D. Pieraccini, *Journal of Physical Organic Chemistry* **2005**, *18*, 275.

[59] D. R. MacFarlane, K. R. Seddon, *Aust. J. Chem.* **2007**, *60*, 3.

[60] H. Weingaertner, *Angew. Chem., Int. Ed.* **2008**, *47*, 654.

[61] K. R. J. Lovelock, I. J. Villar-Garcia, F. Maier, H.-P. Steinrück, P. Licence, *Chemical Reviews* **2010**, *110*, 5158.

[62] E. F. Smith, F. J. M. Rutten, I. J. Villar-Garcia, D. Briggs, P. Licence, *Langmuir* **2006**, *22*, 9386.

[63] F. J. M. Rutten, H. Tadesse, P. Licence, *Angew. Chem., Int. Ed.* **2007**, *46*, 4163.

[64] T. Hammer, M. Reichelt, H. Morgner, *Phys. Chem. Chem. Phys.* **2010**, *12*, 11070.

[65] S. Caporali, U. Bardi, A. Lavacchi, *Journal of Electron Spectroscopy and Related Phenomena* **2006**, *151*, 4 .

[66] M. J. Earle, J. M. S. S. Esperanca, M. A. Gilea, J. N. Canongia Lopes, L. P. N. Rebelo, J. W. Magee, K. R. Seddon, J. A. Widegren, *Nature (London, U. K.)* **2006**, *439*, 831.

[67] J. A. Widegren, Y.-M. Wang, W. A. Henderson, J. W. Magee, *J. Phys. Chem. B* **2007**, *111*, 8959.

[68] D. Strasser, F. Goulay, M. S. Kelkar, E. J. Maginn, S. R. Leone, *The Journal of Physical Chemistry A* **2007**, *111*, 3191.

[69] J. P. Leal, J. M. S. S. Esperança, M. E. Minas da Piedade, J. N. Canongia Lopes, L. P. N. Rebelo, K. R. Seddon, *The Journal of Physical Chemistry A* **2007**, *111*, 6176.

[70] J. P. Armstrong, C. Hurst, R. G. Jones, P. Licence, K. R. J. Lovelock, C. J. Satterley, I. J. Villar-Garcia, *Phys. Chem. Chem. Phys.* **2007**, *9*, 982.

[71] H. Tokuda, K. Hayamizu, K. Ishii, M. A. B. H. Susan, M. Watanabe, *The Journal of Physical Chemistry B* **2004**, *108*, 16593.

[72] H. Tokuda, K. Ishii, M. A. B. H. Susan, S. Tsuzuki, K. Hayamizu, M. Watanabe, *The Journal of Physical Chemistry B* **2006**, *110*, 2833.

[73] J. E. Gordon, G. N. S. Rao, *Journal of the American Chemical Society* **1978**, *100*, 7445.

[74] H. Tokuda, K. Hayamizu, K. Ishii, M. A. B. H. Susan, M. Watanabe, *The Journal of Physical Chemistry B* **2005**, *109*, 6103.

[75] T. G. Coker, B. Wunderlich, G. J. Janz, *Trans. Faraday Soc.* **1969**, *65*, 3361.

[76] J. G. Huddleston, A. E. Visser, W. M. Reichert, H. D. Willauer, G. A. Broker, R. D. Rogers, *Green Chem.* **2001**, *3*, 156.

[77] A. S. Larsen, J. D. Holbrey, F. S. Tham, C. A. Reed, *Journal of the American Chemical Society* **2000**, *122*, 7264.

[78] J. Dupont, P. A. Z. Suarez, R. F. De Souza, R. A. Burrow, J.-P. Kintzinger, *Chemistry – A European Journal* **2000**, *6*, 2377.

[79] A. Elaiwi, P. B. Hitchcock, K. R. Seddon, N. Srinivasan, Y.-M. Tan, T. Welton, J. A. Zora, *J. Chem. Soc., Dalton Trans.* **1995**, 3467.

[80] P. M. Dean, J. M. Pringle, D. R. MacFarlane, *Phys. Chem. Chem. Phys.* **2010**, *12*, 9144.

[81] W. A. Henderson, J. Young, Victor G., D. M. Fox, H. C. De Long, P. C. Trulove, *Chem. Commun. (Cambridge, U. K.)* **2006**, 3708.

[82] C. Hardacre, J. D. Holbrey, C. L. Mullan, M. Nieuwenhuyzen, W. M. Reichert, K. R. Seddon, S. J. Teat, *New J. Chem.* **2008**, *32*, 1953.

[83] M.-E. Moret, A. B. Chaplin, A. K. Lawrence, R. Scopelliti, P. J. Dyson, *Organometallics* **2005**, *24*, 4039.

[84] P. Mueller, *Pure Appl. Chem.* **1994**, *66*, 1077.

[85] M. J. Kamlet, J. L. M. Abboud, R. W. Taft, *Prog. Phys. Org. Chem.* **1981**, *13*, 485.

[86] C. Reichardt, K. Dimroth, *Fortschr. Chem. Forsch.* **1968**, *11*, 1.

[87] V. Gutmann, *The Donor-Acceptor Approach to Molecular Interactions*, Springer, 1st ed. **1978**.

[88] C. Reichardt, *Solvents and Solvent Effects in Organic Chemistry*, Wiley-VCH, 3rd ed. **2003**.

[89] J.-L. M. Abboud, R. Notario, *Pure Appl. Chem.* **1999**, *71*, 645.

[90] R. Schmid, V. N. Sapunov, *Non-Formal Kinetics: In Search for Chemical Reaction Pathways (Monographs in Modern Chemistry, V. 14)*, Vch Pub **1982**.

[91] V. Gutmann, *Electrochim. Acta* **1976**, *21*, 661.

[92] V. Gutmann, G. Resch, *Lecture Notes on Solution Chemistry*, World Scientific Publishing Company **1995**.

[93] W. Linert, R. F. Jameson, *J. Chem. Soc., Perkin Trans. 2* **1993**, 1415.

[94] N. Chapman, J. Shorter, *Advances in linear free energy relationships*, Plenum Press **1972**.

[95] A. G. Burden, G. Collier, J. Shorter, *J. Chem. Soc., Perkin Trans. 2* **1976**, 1627.

[96] A. J. Parker, U. Mayer, R. Schmid, V. Gutmann, *The Journal of Organic Chemistry* **1978**, *43*, 1843.

[97] P. M. Spaziante, V. Gutmann, *Inorganica Chimica Acta* **1971**, *5*, 273 .

[98] C. Reichardt, *Solvent effects in organic chemistry*, Verlag Chemie, Weinheim/New York **1979**.

[99] E. M. Kosower, *Journal of the American Chemical Society* **1958**, *80*, 3253.

[100] E. S. Dodsworth, M. Hasegawa, M. Bridge, W. Linert, *Compr. Coord. Chem. II*, vol. 2, 351–365.

[101] R. W. Soukup, R. Schmid, *Journal of Chemical Education* **1985**, *62*, 459.

[102] W. Linert, R. F. Jameson, A. Taha, *J. Chem. Soc., Dalton Trans.* **1993**, 3181.

[103] W. Linert, R. F. Jameson, G. Bauer, A. Taha, *J. Coord. Chem.* **1997**, *42*, 211.

[104] W. Linert, Y. Fukuda, A. Camard, *Coordination Chemistry Reviews* **2001**, *218*, 113 .

[105] V. Gutmann, *Coordination Chemistry Reviews* **1976**, *18*, 225 .

[106] W. Linert, A. Camard, M. Armand, C. Michot, *Coordination Chemistry Reviews* **2002**, *226*, 137 .

[107] S. Spange, D. Keutel, *Liebigs Annalen der Chemie* **1992**, *1992*, 423.

[108] M. P. Seah, *Surf. Interface Anal.* **2007**, *39*, 634.

[109] M. P. Seah, I. S. Gilmore, *Surf. Interface Anal.* **2011**, *43*, 228.

[110] J. J. D. Fitzgerald, P. Kunnath, A. V. Walker, *Anal. Chem. (Washington, DC, U. S.)* **2010**, *82*, 4413.

[111] G. Nagy, L. D. Gelb, A. V. Walker, *J. Am. Soc. Mass Spectrom.* **2005**, *16*, 733.

[112] M. P. Seah, *J. Surf. Anal.* **2008**, *14*, 305.

[113] M. P. Seah, F. M. Green, I. S. Gilmore, *J. Phys. Chem. C* **2010**, *114*, 5351.

[114] M. V. Kosevich, V. S. Shelkovsky, O. A. Boryak, V. V. Orlov, *Rapid Commun. Mass Spectrom.* **2003**, *17*, 1781.

[115] C. Reichardt, *Organic Process Research & Development* **2007**, *11*, 105.

[116] B. R. Mellein, S. N. V. K. Aki, R. L. Ladewski, J. F. Brennecke, *J. Phys. Chem. B* **2007**, *111*, 131.

[117] R. Lungwitz, M. Friedrich, W. Linert, S. Spange, *New J. Chem.* **2008**, *32*, 1493.

[118] H. Tokuda, S. Tsuzuki, M. A. B. H. Susan, K. Hayamizu, M. Watanabe, *The Journal of Physical Chemistry B* **2006**, *110*, 19593.

[119] K. Ueno, S. Imaizumi, K. Hata, M. Watanabe, *Langmuir* **2009**, *25*, 825.

[120] M. J. Muldoon, C. M. Gordon, I. R. Dunkin, *J. Chem. Soc., Perkin Trans. 2* **2001**, 433.

[121] P. Wasserscheid, C. Hilgers, C. M. Gordon, M. J. Muldoon, I. R. Dunkin, *Chem. Commun. (Cambridge, U. K.)* **2001**, 1186.

[122] R. Lungwitz, *Ionic Liquids - Polarity and Interaction with Silicious Surfaces*, Ph.D. thesis, Chemnitz University of Technology, Faculty of Natural Science **2011**.

[123] L. Crowhurst, P. R. Mawdsley, J. M. Perez-Arlandis, P. A. Salter, T. Welton, *Phys. Chem. Chem. Phys.* **2003**, *5*, 2790.

[124] T. Fujisawa, M. Fukuda, M. Terazima, Y. Kimura, *The Journal of Physical Chemistry A* **2006**, *110*, 6164.

[125] T. A. Zawodzinski, R. A. Osteryoung, *Inorganic Chemistry* **1989**, *28*, 1710.

[126] J. Estager, A. A. Oliferenko, K. R. Seddon, M. Swadzba-Kwasny, *Dalton Trans.* **2010**, *39*, 11375.

[127] C. Reichardt, *Green Chem.* **2005**, *7*, 339.

[128] L. Crowhurst, R. Falcone, N. L. Lancaster, V. Llopis-Mestre, T. Welton, *The Journal of Organic Chemistry* **2006**, *71*, 8847, pMID: 17081015.

[129] M. Y. Lui, L. Crowhurst, J. P. Hallett, P. A. Hunt, H. Niedermeyer, T. Welton, *Chem. Sci.* **2011**, *2*, 1491.

[130] J. Dupont, *J. Braz. Chem. Soc.* **2004**, *15*, 341.

[131] P. Bonhote, A.-P. Dias, N. Papageorgiou, K. Kalyanasundaram, M. Graetzel, *Inorg. Chem.* **1996**, *35*, 1168.

[132] K. M. Dieter, J. Dymek, Chester J., N. E. Heimer, J. W. Rovang, J. S. Wilkes, *J. Am. Chem. Soc.* **1988**, *110*, 2722.

[133] P. Koelle, R. Dronskowski, *Inorg. Chem.* **2004**, *43*, 2803.

[134] Z. Meng, A. Dolle, W. R. Carper, *THEOCHEM* **2002**, *585*, 119.

[135] S. Kossmann, J. Thar, B. Kirchner, P. A. Hunt, T. Welton, *J. Chem. Phys.* **2006**, *124*, 174506/1.

[136] P. A. Hunt, I. R. Gould, *J. Phys. Chem. A* **2006**, *110*, 2269.

[137] M. G. Del Popolo, R. M. Lynden-Bell, J. Kohanoff, *J. Phys. Chem. B* **2005**, *109*, 5895.

[138] Y. Wang, H. Li, S. Han, *J. Chem. Phys.* **2005**, *123*, 174501/1.

[139] F. C. Gozzo, L. S. Santos, R. Augusti, C. S. Consorti, J. Dupont, M. N. Eberlin, *Chem.–Eur. J.* **2004**, *10*, 6187.

[140] N. Martinez, K. Isa, R. Nakata, K. Endo, *J. Mass Spectrom. Soc. Jpn.* **2001**, *49*, 51.

[141] R. V. Ham, A. Adriaens, L. V. Vaeck, R. Gijbels, F. Adams, *Nuclear Instruments and Methods in Physics Research Section B: Beam Interactions with Materials and Atoms* **2000**, *161-163*, 245 .

[142] G. Wang, R. B. Cole, *Analytical Chemistry* **1998**, *70*, 873.

[143] R. Bini, O. Bortolini, C. Chiappe, D. Pieraccini, T. Siciliano, *J. Phys. Chem. B* **2007**, *111*, 598.

[144] A. M. Fernandes, M. A. A. Rocha, M. G. Freire, I. M. Marrucho, J. A. P. Coutinho, L. M. N. B. F. Santos, *J. Phys. Chem. B* **2011**, *115*, 4033.

[145] A. K. Abdul-Sada, A. E. Elaiwi, A. M. Greenway, K. R. Seddon, *Eur. Mass Spectrom.* **1997**, *3*, 245.

[146] R. M. Fuoss, C. A. Kraus, *Journal of the American Chemical Society* **1933**, *55*, 476.

[147] P. Rechberger, W. Linert, *Computers & Chemistry* **1980**, *4*, 61 .

[148] P. Rechberger, W. Linert, *Journal of Chemical Education* **1981**, *58*, 245.

[149] C. J. Straif, H. Hutter, *Anal. Bioanal. Chem.* **2009**, *393*, 1889.

Curriculum Vitae

LEBENSLAUF

Angaben zur Person

Name	Markus Holzweber
Adresse	Hießgasse 11/9, 1030 Wien
Geburtsort, -datum	Wien, 17. Feb. 1978
Familienstand	Ledig
Staatsbürgerschaft	Österreich
Email	markus.holzweber@tuwien.ac.at
Telefonnummer	+43 (699) 121 50 439

Schul- und Berufsbildung

seit Nov. 2006	Doktoratsstudium der technischen Wissenschaften an der Technischen Universität Wien
Jul. 2006	Abschluss des Studiums mit ausgezeichnetem Erfolg
Aug. 2003 - Feb. 2004	Auslandssemester in Göteborg, Schweden (Chalmers University of Technology)
1997 - 2006	Studium der Technischen Chemie an der Technischen Universität Wien, Studienzweig Organische Chemie und Technologie
Jun. 1997	Matura mit gutem Erfolg
1992 - 1997	HTL, Technologisches Gewerbemuseum Wien, 1200 Wien Ausbildungszweig Maschinenbau – Kraftfahrzeugtechnik
1988 - 1992	Akademisches Gymnasium, 1010 Wien
1984 - 1988	Volksschule, Lycée Français de Vienne, 1090 Wien
1983 - 1984	Vorschule, Lycée Français de Vienne, 1090 Wien

Berufserfahrung

Mai 2010 – Mai 2011	Bildungskarenz
Juni 2011 – August 2011 und Dez. 2009 – April 2010	Projektassistent am Institut für Chemische Technologien und Analytik, Christian Doppler Labor für Diffusions- und Segregationsvorgänge bei der Produktion hochfesten Stahlbands
Sept. 2007 – Nov. 2009	Projektassistent am Institut für Chemische Technologien und Analytik, Christian Doppler Labor für Oberflächen- und Grenzflächenanalytik

Dezember 2011   Markus Holzweber

Curriculum Vitae

Nov. 2006 - Jul. 2007	Anstellung auf Werkvertragsbasis am Institut für Angewandte Synthesechemie, Bereich organische Synthese (Prof. Stanetty)
Mai 2007	Betreuung Laborkurs organische Chemie der FH-Tulln (Biotechnische Verfahren)
Mai 2006	Betreuung Laborkurs organische Chemie der FH-Tulln (Biotechnische Verfahren)
Sonstige Tätigkeiten	
Jul. 2006	Mitarbeit am FIGIPAS - Kongress
Jun. 2003	Vorbereitungen zum 10. BDSHC - Kongress
Jul. - Aug. 2002	Institut für Angewandte Synthesechemie, Ferialpraktikum FG Stanetty
Jul. - Aug. 2001	Institut für Angewandte Synthesechemie, Ferialpraktikum FG Stanetty
Aug. - Sept. 2000	Institut für Angewandte Synthesechemie, Ferialpraktikum FG Stanetty
Feb. 1998 - Jan. 1999	Zivildienst Arbeiter-Samariter-Bund (Krankentransport, Rettungsdienst), Ausbildung zum Hilfssanitäter
Jul. - Aug. 1997	Österreichische Post AG (Urlaubsersatzkraft)
Jul. 1996	Steyr Bus Ges.m.b.H. (Ferialpraktikum, Konstruktionsbüro)
Jul. 1994	Fa. Duhan (Ferialpraktikum, KFZ-Werkstatt)
Persönliche Fähigkeiten und Kompetenzen	
Muttersprache	Deutsch
Fremdsprachen	Englisch (fließend in Wort und Schrift) Französisch (Maturaniveau) Schwedisch (Grundkenntnisse)
PC Kenntnisse	MS Windows, MS Office 2003, Win NMR, Chemoffice, ISIS Draw, Chemische Datenbanken (SciFinder, Crossfire), Latex, Origin
Tätigkeiten in der ÖH	1997 - 2006 ehrenamtliche Mitarbeit in der Studienvertretung Technische Chemie (Institutskonferenzen, Habilitationskommissionen, Berufungskommission, Studienkommission) 2007 - 2011 ehrenamtliche Mitarbeit in der Studienvertretung Doktorat (gewählter Studierendenvertreter, Studienkommission) 2007 - 2009 Vorsitzender der Studienvertretung Doktorat
Organisatorische Tätigkeit	Organisation und Abhaltung einer Informationsveranstaltung über den 2. Studienabschnitt (1999)
Persönliche Interessen	Sport (Aikido, gesundheitsorientiertes Krafttraining (Kieser), Ausdauer, Ski fahren), Film, Lesen, Kochen, Bildungspolitik
Sonstiges	Führerschein A, B, Kranführer (flurgesteuerte Kräne), Staplerführer, Erfahrungen mit GC-MS, MPLC, IR, ToF-SIMS

Dezember 2011   Markus Holzweber

Curriculum Vitae

Wissenschaftliche Veröffentlichungen		
Publikationen		Holzweber, Markus; Kriegl, Markus ; Schintlmeister, Arno; Paesold, Dieter; Danninger, Herbert; Hutter, Herbert. **Oxygen diffusion in grain boundaries: a ToF-SIMS investigation on hot-rolled steel sheets.** Analytical and Bioanalytical Chemistry (2011), 400, 659-663 Holzweber, Markus; Pittenauer, Ernst; Hutter, Herbert. **Investigation of Ionic Liquids under Bi-Ion and Bi-Cluster Ions bombardment by ToF-SIMS.** Journal of Mass Spectrometry (2010), 45, 1104-1110 Holzweber, Markus; Hutter, Herbert. **Investigation of 1-butyl-3-methylimidazolium bis(trifluoromethylsulfonyl)-imide under Bi_n^{x+} cluster ion bombardment.** Surface and Interface Analysis (2010), 42 (6), 1025-1029 Hula, Robert; Edtmaier, Christian; Holzweber, Markus; Hutter, Herbert; Eisenmenger-Sittner, Christoph. **The wetting behaviour of silver on carbon, pure and carburized nickel, cobalt and molybdenum substrates.** Applied Surface Science (2010), 256 (14), 4697-4701 Schnürch, Michael; Holzweber, Markus; Mihovilovic, Marko D.; Stanetty, Peter. **A facile and green synthetic route to boronic acid esters utilizing mechanochemistry.** Green Chemistry (2007), 9 (2), 139-145 Holzweber, Markus; Schnürch, Michael; Stanetty, Peter. **Polysubstituted thiazole derivatives *via* the halogen-dance reaction.** Synlett (2007), 19, 3016-3018
Vorträge		European Workshop on Secondary Ion Mass Spectrometry (SIMS Europe), 2010, Münster, Deutschland **Interaction of Bi Cluster Ions with Room Temperature Ionic Liquids** International Symposium on Solubility Phenomena and Related Equilibrium Processes (ISSP), 2010, Leoben, Österreich **ToF-SIMS Analysis of Ionic Liquids** European Conference on Applications of Surface and Interface Analysis (ECASIA) 2009, Antalya, Türkei **ToF-SIMS Analysis of Room Temperature Ionic Liquids under Bi-Cluster Bombardment**
Poster		Angewandte Oberflächenanalytik (AOFA), 2010, Kaiserslautern, Deutschland **Oxygen Diffusion on Grain Boudaries: A ToF-SIMS Investigation on Hot Rolled Steel Sheets** Blue Danube Symposium of Heterocyclic Chemistry (BDSHC) 2007, Tihany, Ungarn **Boronic Acid Esters via Mechanochemistry**

Dezember 2011   Markus Holzweber